
FACULTY OF INFORMATION TECHNOLOGY AND ELECTRICAL ENGINEERING

DEGREE PROGRAMME IN ELECTRONICS AND COMMUNICATIONS ENGINEERING

# MASTER'S THESIS

# Isolation and Unwanted Emissions in OTA Co-location Conformance Testing for New Radio Massive MIMO Transceivers

| | |
|---|---|
| Author | Toni Kotikumpu |
| Supervisor | Risto Vuohtoniemi |
| Second Examiner | Juha-Pekka Mäkelä |
| Technical Advisor | Tuomas Jääskö/Jukka Sutinen |

June 2022

**Kotikumpu T. (2022) Isolation and Unwanted Emissions in OTA Co-location Conformance Testing for New Radio Massive MIMO Transceivers.** University of Oulu, Faculty of Information Technology and Electrical Engineering, Degree Programme in Electronics and Communications Engineering. Master's Thesis, 104 p.

# ABSTRACT

**As new frequency bands have been taken into use in the fifth generation (5G) of base stations, mobile network sites especially in urban areas are becoming crowded with antennas and radios. With the New Radio (NR) design having highly integrated antennas, there is high potential for interference from these Active Antenna Systems (AAS) to other co-located equipment. To ensure performance of existing equipment is not impeded by deployment of NR base stations, the level of interference is to be measured through Over The Air (OTA) measurements. For this purpose, the Third Generation Partnership Project (3GPP) specifies a set of co-location test cases and requirements for future NR base stations.**

**The goal of this thesis is to evaluate and implement the 3GPP co-location test case for OTA measurement of spurious emissions. This is done through practical measurements using a multi-band base station antenna as a Co-location Test Antennas (CLTA). A preliminary isolation measurement is done followed by co-location spurious emissions measurements. The aim is to assess how fit for purpose the 3GPP test case is, find any practical challenges in implementing the test case and potentially comment on how the 3GPP definitions could be improved. Findings in this work will be used to develop methods for implementing the co-location test cases in the future.**

**The isolation measurement is done to see what factors affect the isolation of two base station antennas in proximity of each other. The measurement data is statistically analysed in different subsets to find the parameters which affect the isolation the most. The OTA spurious emissions measurement is done afterwards two times: first according to the 3GPP specifications, then a second time according to a "worst-case" scenario based on the isolation measurement results and considering beamforming. The results are analysed against the 3GPP requirements for each frequency band. The analysed results are then presented and discussed.**

**The results show that spurious emissions could be measured successfully. Yet there were some things that could not be considered, improvements that should be made for future implementations of these measurements and further studies that could be done.**

**Key words: 5G, AAS, base station, 3GPP, out-of-band emissions, OTA test environment, CLTA**

**Kotikumpu T. (2022) 5G NR mMIMO -lähetin-vastaanottimien isolaation ja ei-toivottujen emissioiden OTA-mittaukset.** Oulun yliopisto, tieto- ja sähkötekniikan tiedekunta, elektroniikan ja tietoliikennetekniikan tutkinto-ohjelma. Diplomityö, 104 p.

# TIIVISTELMÄ

**Viidennen sukupolven matkapuhelinverkkojen (5G) uusien taajuusalueiden käyttöönoton myötä etenkin kaupunkialueiden tukiasemissa on runsaasti radioita ja antenneja. New Radio (NR) -arkkitehtuurien integroitujen antennien myötä riski on suuri, että aktiiviset antennijärjestelmät (AAS) aiheuttavat häiriötä saman maston (co-located) laitteisiin. Varmistukseksi ettei NR-tukiasemien asennus heikennä olemassa olevien laitteiden suorituskykyä, häiriöiden tasot tulee mitata OTA (Over The Air) -mittauksilla. Tätä varten 3GPP (3rd Generation Partnership Project) määrittelee ryhmän co-location -testimenetelmiä ja vaatimuksia tulevaisuuden NR-tukiasemille.**

**Työssä toteutetaan ja arvioidaan 3GPP:n määrittelemä co-location harhalähete OTA-mittaus. Tämä toteutetaan käytännön mittauksien avulla käyttäen Co-location Test Antenneina (CLTA) monitaajuuskaistaisia tukiasema-antenneja. Ensimmäisenä on alustava isolaatiomittaus, jonka jälkeen tehdään saman maston tukiasemien harhalähetteiden mittauksia. Tavoitteena on määrittää kuinka tarkoituksenmukainen 3GPP testi on, löytää käytännön haasteita testin toteutuksesta ja mahdollisesti kommentoida kuinka 3GPP määritelmiä voitaisiin kehittää. Työn tulosten avulla tullaan kehittämään co-location -mittausmenetelmiä tulevaisuudessa.**

**Isolaatiomittauksessa selvitetään mitkä tekijät vaikuttavat kahden lähekkäin olevan tukiasema-antennin väliseen isolaatioon. Mittausdata analysoidaan tilastollisesti erilaisissa osajoukoissa isolaatiolle merkittävimpien parametrien löytämiseksi. Sen jälkeen harhalähetteiden OTA-mittaus tehdään kahteen kertaan: ensin 3GPP määritelmien mukaisesti ja toisen kerran isolaatiomittauksiin perustuvan pahimman tapauksen mukaan ottaen myös huomioon antennin suuntakuvion. Tulokset analysoidaan jokaisen taajuuskaistan 3GPP vaatimuksia vasten. Analysoidut tulokset esitetään ja niistä keskustellaan.**

**Tuloksista nähdään, että harhalähetteet mitattiin onnistuneesti. On kuitenkin tekijöitä, joita ei voitu mittauksissa ottaa huomioon. Työssä esitetään parannusehdotuksia, jotka tulisi tehdä tulevien mittausten toteutuksiin ja esitetty uusia jatkotutkimusaiheita.**

**Avainsanat: 5G, AAS, tukiasema, 3GPP, kanavan ulkopuoliset emissiot, OTA testiympäristö, CLTA**

# TABLE OF CONTENTS

# FOREWORD

Four years into my studies it had become almost impossible to stay motivated and have hope for the future, since the only summer work I was able to find was as a roofer instead of something in my own field. Due to this two-to-three-year slump and the loneliness resulting from friends who I studied with quitting university, I started to fall behind in my studies and bachelor's thesis progress. I have my dear friend Niklas Siipola to thank for motivating me to finish my bachelor's degree and assisting me in applying for summer work in 2016. That year I finally got my chance, as Timo Juntunen hired me to work at Nokia in the BTS Conformance team he was leading at the time. I got a lot of recognition for my work ethic and ability to learn quickly, which gave me confidence in myself and rekindled my passion for master's studies in the years after.

I want to thank everyone I've worked with at Nokia for providing a welcoming environment and helping me develop myself over the years following my first summer job there. Thank you to Marko Honkalampi for being patient and understanding in enabling me to focus on my thesis when I needed it. Special thanks also to Tuomas Jääskö and Jukka Sutinen for providing me with this chance and for all the guidance along the way.

At University of Oulu, I would like to thank my main supervisor Risto Vuohtoniemi and Juha-Pekka Mäkelä for their encouragement, feedback, and advice during the final months of this process. Thank you to all the teachers who have given me personal guidance over the years, as I strive to not only pass courses but understand the subjects covered.

I also want to thank my loving parents for being understanding and supportive through the years. Lastly, thanks from the bottom of my heart go to my loving friends in Finland and outside of it. I wouldn't have made it through these 10 agonizing years without you all as the wind in my sails.

Oulu, June, 16, 2022

Toni Kotikumpu

# LIST OF ABBREVIATIONS AND SYMBOLS

| | |
|---|---|
| 3GPP | 3rd Generation Partnership Project |
| AE | Antenna Element |
| BS | Base Station |
| BW | Bandwidth |
| CA | Carrier Aggregation |
| CATR | Compact Antenna Test Range |
| CLRA | Co-location Reference Antenna |
| CLTA | Co-location Test Antenna |
| CW | Continuous Wave |
| DAS | Distributed Antenna System |
| DL | Downlink |
| DUT | Device Under Testing |
| E-UTRAN | Evolved Universal Terrestrial Access Network |
| EIRP | Effective Isotropic Radiated Power |
| EIS | Equivalent Isotropic Sensitivity |
| EPS | Evolved Packet System |
| FR | Frequency Range |
| GSM | Global System for Mobile Communications |
| HPBW | Half Power Beam Width |
| IM | Intermodulation |
| IoT | Internet of Things |
| LA BS | Local Area Base Station |
| LMI | Local Management Interface |
| LO | Local Oscillator |
| LOS | Line of Sight |
| LTE | Long Term Evolution |
| MIMO | Multiple-Input and Multiple-Output |
| mMIMO | Massive Multiple-Input and Multiple-Output |
| mmWave | Millimetre Wave |
| MU-MIMO | Multi-User Multiple-Input and Multiple-Output |
| MR BS | Medium Range Base Station |
| NF | Noise Figure |
| NLOS | Non-Line of Sight |
| NR | New Radio |
| OBUE | Operating Band Unwanted Emissions |
| OTA | Over The Air |
| RAT | Radio Access Technology |
| RET | Remote Electrical Tilt |
| R&D | Research & Development |
| RDN | Radio Distribution Network |
| RoAoA | Range of Angles of Arrival |
| SCS | Subcarrier Spacing |
| SMS | Short Message Service |
| SNR | Signal-to-Noise Ratio |
| TDD | Time Division Duplex |
| TRP | Total Radiated Power |

| | |
|---|---|
| UE | User Equipment |
| UL | Uplink |
| VNA | Vector Network Analyzer |
| WA BS | Wide Area Base Station |
| QoS | Quality of Service |
| | |
| $B$ | Bandwidth |
| dB | Decibel |
| $F$ | Noise Figure |
| $f$ | Frequency |
| $f_{high}$ | BS operating band upper edge frequency |
| $f_{low}$ | BS operating band lower edge frequency |
| $\Delta f_{OBUE}$ | Operating band unwanted emissions mask offset from the operating band edge |
| Hz | Hertz |
| $k$ | Boltzmann constant |
| $K$ | Kurtosis |
| kbps | kilobits per second |
| $L$ | Loss |
| $M_{RFBW}$ | Middle of the supported frequency range in the operating band |
| $P_0$ | Thermal noise |
| $S$ | Skewness |
| $SD$ | Standard Deviation |
| $T$ | Temperature |
| | |
| $\Delta$ | Delta |
| $\mu$ | Mean isolation |
| $\Gamma_{ANT}$ | Reflection coefficient at antenna port |

# 1 INTRODUCTION

The development of mobile networks has been one of the main stages and enablers for technological innovation and advancement in the last 40 years. Since the launch of the first mobile network generation, 1G, the industry has entered a new generation in approximately 10-year intervals. Once 1G enabled wireless analogue voice services in 1980s, 2G made communication more efficient through digitalization and introduced the short message service (SMS). This 2nd generation of mobile networks technology is referred to as Global System for Mobile Communications (GSM) and the data rates were in the scale of kilobits per second (kbps). In 3G, the mobile network gained access to the internet and the first multimedia services became available through features like sharing pictures through SMS messages, email, and video calls. The focus of the mobile network started shifting drastically from voice communication to more data centric applications. The old circuit switching method of the first two generations was slowly being replaced by packet switching method and data rates increased to megabits per second (Mbps). Development of 4G, commonly known as Long Term Evolution (LTE), focused on further developing the groundwork that was done in 3G for bringing the internet to users' mobile devices. This helped enable services like video streaming, cloud services and social media.

In recent years with ever increasing daily reliance on mobile devices like smartphones, mobile networks have become an essential section of infrastructure. At the same time, increasing demand for streaming high-quality video, virtual reality applications and autonomous robotics set high requirements for data rate, latency, and quality of service (QoS). In the 5th generation (5G), some of the key ways of tackling these requirements are utilizing higher frequencies, wider bandwidths, massive multiple-input multiple-output (mMIMO) systems as well as multi-user MIMO (MU-MIMO). MIMO techniques were already utilized in previous generations for increased network capacity and reliability through diversity combining with for example eight (8) antennas. In 5G, with mMIMO it is done at a much larger scale, as a single New Radio (NR) base station (BS) can have an array of 32, 64, 128 or more antennas. In addition to capacity these large arrays enable the use of precise beamforming which through user tracking allows high data rates and QoS for multiple users at a time.

While some limited 5G capabilities can be realized through software changes with existing hardware from previous generations, even just the antennas alone have limited beamforming capability and were not designed for 5G frequency bands above 6 GHz. A significant amount of new hardware deployment is required to existing network sites in the form of NR base stations to truly enable the vision for 5G. While many US and European network operators have been or plan to ramp down their 2G and 3G networks [1][2], there is still a significant amount of hardware from previous generations deployed on sites. Therefore, it should be ensured by the manufacturer that the NR radios do not cause any interference to existing co-located BS equipment that the same or another operator sharing the same site has deployed. A significant part of research and development (R&D) for base station radios is measuring for unwanted effects or emissions that could deteriorate the performance of the radio itself or co-located equipment close to it.

In any kind of product performance measurements, the methods and circumstances of testing must adhere to certain specifications agreed upon within the given industry. These specifications establish a baseline that enables measurements done for different Devices Under Testing (DUT) and in different R&D sites to be comparable. They also often define the measurement environment and setup in a way that accurately mimics key conditions in the real world so that the test results reflect expected performance in the field. For cellular

telecommunication technologies the main standardization organization is the 3rd Generation Partnership Project (3GPP) which unites seven different standard development partners [3] and their standards. Companies manufacturing base station equipment must be able to prove that their products conform with the 3GPP requirements as well as any regional requirements that may apply in the country their customer operates in.

For products of previous generations most of the 3GPP defined performance testing has been done by so called conducted testing. These measurements are done by attaching measurement cables directly to the antenna ports of the radio and measuring the signal that would be fed into the BS antenna. With the number of antennas increasing substantially in NR base stations, it is no longer a sufficient measure of system performance to measure single antenna ports. The development of the radios themselves are also going towards antennas that are integrated into the radio, whereas in previous generations it was common for the radio and BS antenna to be separated. Integrated antennas provide fewer conducted interfaces for conducted measurements and it becomes more important to consider the effect of the antenna for these kinds of BS products. As a result, the development of 3GPP specifications has been steering away from conducted testing and towards full Over The Air (OTA) verification for future NR products. At the time of writing NR radios are still subject to a mixture of conducted and OTA requirements, but in 3GPP [4] there is already a definition for a BS type which is exclusively verified through OTA measurements. As a result, many R&D sites will need to investigate how to implement both the conducted test cases and new test cases in OTA test environments.

OTA testing refers to testing of radio frequency (RF) devices done in conditions where the transmitted RF signal is subject to free space propagation and the effect of the antenna is considered. For 3GPP defined tests, this is done in anechoic chambers where the space is isolated from interference from the outside world and reflections are minimized. This allows for accurate performance and emission measurements, as noise is minimized and only RF signals from the Device Under Testing (DUT) and measurement equipment are present.

The main purpose of this thesis is to study the 3GPP defined co-location test cases and investigate the feasibility of implementing the test cases in an OTA environment. For this purpose, modifications to an existing OTA environment were designed and implemented based on current specifications within 3GPP standards and previously established methods. The modified OTA environment was then verified by planning and executing one of 3GPP defined the co-location test cases in the environment. The main sources of complications are the introduction of the Co-location Test Antenna (CLTA) to the test setup, wide range of frequencies to be measured and strict dynamic range requirements for the measurement system. The goal of the thesis is to investigate and provide solutions to the complications introduced by these required changes to the existing OTA test environment. The findings in this thesis will be used as a reference for future development of OTA testing methods, in the development of OTA test environments and to comment on 3GPP co-location specifications.

In the second chapter, a brief overview of 4G is given followed by discussion of developments in 5G in contrast to 4G. In the third chapter, the 3GPP OTA Co-location requirements and the motivations behind them will be discussed. The fourth chapter presents the planning and design of the practical measurements in this research. The progression of the measurement process along with the results are presented in the fifth chapter. In chapter six, the findings from this research are discussed. A summary of this thesis is given in chapter seven.

# 2 FROM 4G TO 5G

There are very high expectations from a variety of technology industries regarding what the 5th generation of mobile networks (5G) will enable. Increased data rates per user, minimal latency, high reliability, increased mobility, and increased number of not only users but connected devices are some of the main requirements [8][9]. Fulfilling these requirements will provide the mobile network infrastructure necessary for 4K video streaming, virtual reality, Internet of Things (IoT), autonomous vehicles, and other applications of the next technological era. This chapter gives a brief overview of the advances and changes between 4G and 5G relevant to this thesis.

## 2.1 Long Term Evolution

The 4th generation (4G) of mobile networks dubbed Long Term Evolution (LTE) or the Evolved Universal Terrestrial Access Network (E-UTRAN) was motivated by ensuring the 3G system would stay competitive for the future. With the continued rise of the internet and its integration into mobile networks, user demand for higher data rates and QoS needed to be met. To accommodate this, high spectral efficiency, high peak data rates, short round trip time and flexibility in frequency and bandwidth were required. This was to be done by building on the networks of previous generations, but there was also a need to reduce complexity in the network solutions. The access networks of previous generations were using a mix of circuit switched and packet switched connections depending on the service. The transition to the Evolved Packet System (EPS) brought all services under IP based packet switched connection, simplifying the network design, and better facilitating data services. Using modulations up to 64QAM, bandwidths up to 20 MHz and up to 4x4 downlink multiplexing enabled higher data rates. Release 8 of the 3GPP specification provided the basis for the first wave of LTE equipment in 2008. Theoretical peak data rates were 75 Mbps in the uplink and as high as 300 Mbps in the downlink using spatial multiplexing. [5]

In Figure 1, a generic model of a typical LTE base station (BS) is presented. The hardware configuration consists typically of a passive 2x2 or 4x4 Multiple-Input Multiple Output (MIMO) antenna which is transmitting signals generated and fed by the radio unit (RU) through RF cables. In some cases the LTE BS antenna can also be integrated into the RU. The RU is connected through a fiber connection to the Base Band Unit (BBU) that connects to the core network. LTE base station antennas typically service for example a 120° sector, making three antennas distributed around the radio tower cover the full 360° area of the cell. Utilizing Single-User MIMO (SU-MIMO) the BS can establish a link with a single User Equipment (UE) using multiple antennas [6]. Having more than one channel available between BS and UE allows for more data transmission, but also sending the same data through multiple channels. If the Signal-to-Noise ratio (SNR) in one or more of the channels drops, by applying combining techniques the data can be restored even in challenging radio channel conditions. These spatial multiplexing and diversity techniques allow for increased data rate towards a single user and increases reliability of communication.

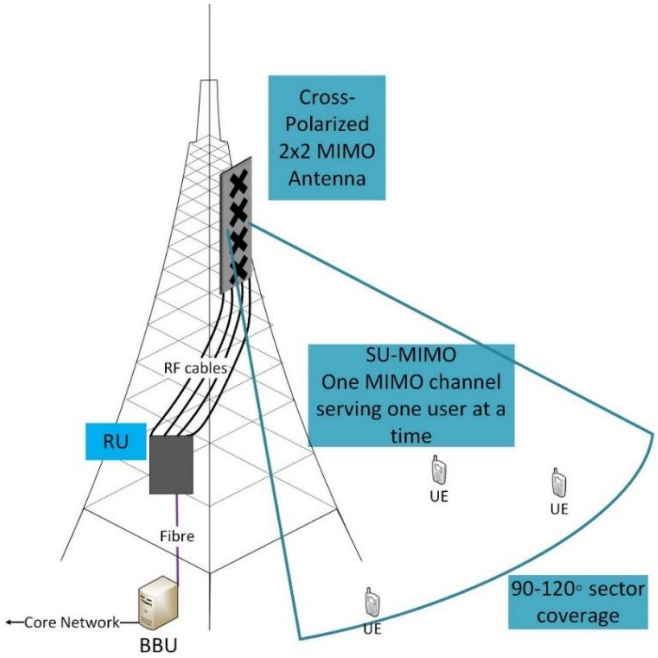


Figure 1. LTE base station.

### 2.2 5G and New Radio base stations

Like in 4G, when the transition to 5G started in 2020 it was important to not fully replace existing networks but build upon them. For this purpose, 3GPP defines two separate architectures for 5G systems: standalone (SA) and non-standalone (NSA) [7]. The principle of NSA 5G deployment is to enable some 5G functionality within the existing LTE networks by adding 5G capable radio nodes. This way network operators don't have to completely replace their existing networks with SA deployments where the 5G network is built from the ground-up.

Some main performance requirements for 5G networks compared to the performance of 4G networks are given in Table 1 [8][9]. There have been significant improvements to the 4G network performance compared to what is discussed in [5]. Regardless, the targets for 5G are to multiply the data rate by a factor of 20 and many other metrics tenfold. One of the main enablers is the expansion of licensed frequency bands. The frequency bands specified for LTE range from hundreds of megahertz up to 6 GHz [10]. These frequency bands are not licensed for carrier bandwidths wider than 100 MHz for 5G. They are also very crowded and originally designed for maximum carrier bandwidth of 20 MHz, so they cannot fit very many wide 5G carriers. In [11], two frequency ranges are defined for 5G New Radio (NR). Frequency range 1 (FR1) contains the LTE bands and expands above it, ranging from 410 MHz to 7.125 GHz. Frequency range 2 (FR2) covers millimetre wavelength (mmWave) frequencies from 24.25 GHz to 52.6 GHz. Frequencies in FR1 enable 5G deployments where existing UEs and BS equipment designed for LTE frequencies can be utilized. FR1 frequencies also provide wider cell coverage compared to FR2 due to lower frequencies experiencing less attenuation in the radio channel. FR2 enables usage of a completely new spectrum and as such allows for wider frequency bands and carrier bandwidths. It is planned to be densely deployed into areas such as city centres where high data rates are needed. This way the network efficiency is high between lower FR1 frequencies providing network coverage with minimal stress and FR2 delivering the bulk of required capacity.

Table 1. 4G vs 5G performance comparison

| **Performance Requirement** | **4G** | **5G** |
|---|---|---|
| Peak Data Rate | 1 Gbit/s | 20 Gbit/s |
| Area Traffic Capacity | 0.1 Mbit/s/$m^2$ | 10 Mbit/s/$m^2$ |
| User Experienced Data Rate | 10 Mbit/s | 100 Mbit/s |
| Latency | 10 ms | <1 ms |
| Mobility | 350 km/h | 500 km/h |
| Connection Density | $10^5$ devices/$km^2$ | $10^6$ devices/$km^2$ |
| Carrier Bandwidth | Up to 20 MHz | FR1: Up to 100 MHz<br>FR2: Up to 400 MHz |

An example of a 5G base station is shown in Figure 2. In contrast to Figure 1, the massive MIMO (mMIMO) antenna array can have dozens of antennas and is now integrated into the RU. The size of single antennas is inversely proportional to operating frequency, so especially in FR2 frequencies the mMIMO arrays are expected to have hundreds of antennas. These arrays enable precise beamforming and Multi-User MIMO (MU-MIMO) techniques. In MU-MIMO multiple UEs can be serviced simultaneously which increases cell capacity compared to SU-MIMO. Due to the nature of urban environments, Line of Sight (LOS) links between the UE and BS can be blocked by structures, vehicles, or people. In these cases NLOS links are utilized, where best reception between BS and UE might be from the signal reflecting from walls. As users move around within the cell, the NR BS will continuously adjust the beam direction to guarantee maximum throughput and QoS.

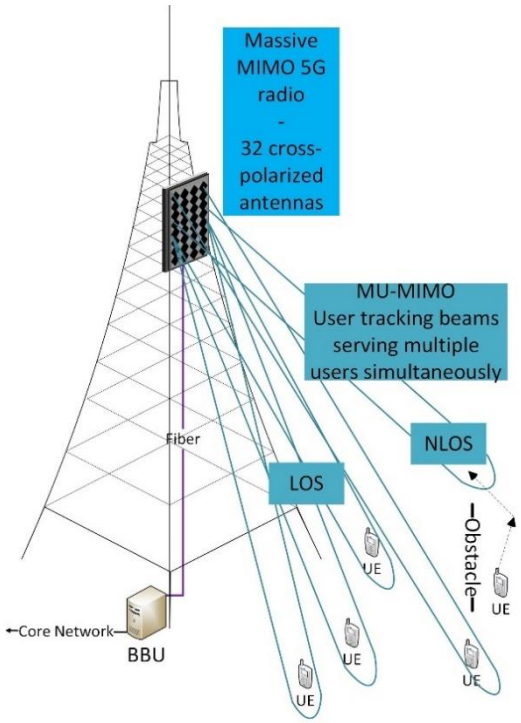


Figure 2. 5G base station.

# 3 OTA CO-LOCATION TESTING

In most cases, mobile network sites are being utilized by multiple operators and the BS equipment deployed are using multiple Radio Access Technologies (RAT), different frequency bands and configurations. 5G mobile network sites consist mostly of urban environments like the rooftops or walls of buildings, which can lead to more potential for interference between co-located BS equipment. Therefore, it is important from a regulatory and functionality standpoint to ensure no operator's network is being hindered by interference from another operator's co-located equipment.

Testing BS products according to standardized specifications is key in minimizing the potential interference between co-located systems. There are multiple telecommunication standard development organizations around the world with the major one being 3GPP that unites multiple standards into one technical specification for mobile systems. In 3GPP co-location interference is addressed in co-location requirements where the purpose is to ensure two co-located systems can operate with minimal degradation to each other. This chapter describes the motivations from a mobile network site perspective for co-location testing of BS products. The chapter also gives an introduction into international and national regulations. In the last section, the 3GPP Co-location requirements are presented in detail.

## 3.1 Site considerations

In previous generations of the mobile communication systems, outdoor sites have been a mix of macro cells and micro cells [13]. Macro cells refer to cells where the coverage is the largest and obstructions should be minimal. To achieve this, the antennas are mounted above the average rooftop height for the area on structures like radio towers or rooftops to ensure maximum likelihood for Line of Sight (LOS) between user and base station (BS) antenna. Micro cells have approximately 10% of a macro cell's coverage area yet they provide additional coverage and capacity in areas where macro cells could at best provide Non-Line of Sight (NLOS) coverage. Urban areas have high data traffic needs due to industry, commercial spaces and population density and a high density of obstructions, so deployment of micro cells in such areas is essential. In these sites, the antennas are below average rooftop height mounted on building walls, lamp posts or other fixtures. For coverage inside buildings that outdoor cells cannot reach without considerable drop in Quality of Service (QoS) so called small cells are used, which can range from relays and Distributed Antenna Systems (DAS) to pico- and femtocells [13].

Macro cell sizes in 2G/3G/4G or pre-5G technologies are usually in the scale of several to tens of kilometres [13] and the RF signals at those frequencies have decent penetration through walls of buildings. Macro cells on the edges of urban areas have been able to service much of said area through penetration or NLOS links. However, obstructions like tall buildings and varying terrain elevations attenuate, scatter, and block the signal which results in significant performance degradation or complete blind spots. In radio tower sites like in Figure 3, there are usually more deployment options, established methods and available space for several base station systems compared to urban sites. As depicted on the right side of Figure 3 the antennas on the long vertical sides of the victim antenna are considered to have the most potential to cause interference. While interference between co-located antennas in the radio tower can still be an issue it can be mitigated by intelligent deployment of BS equipment. Examples of such methods would be spacing out the antennas as much as possible through additional rigging and avoiding adjacent deployment of antennas operating on the same or adjacent frequency band.

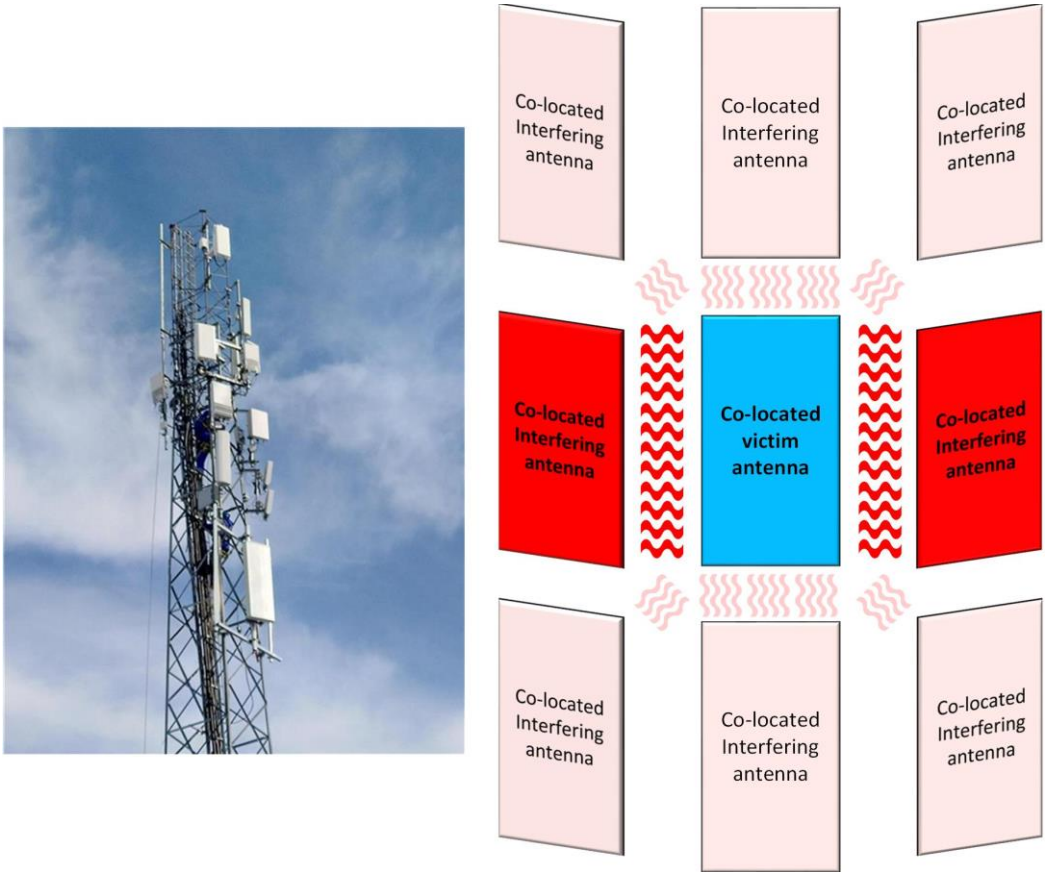


Figure 3. Radio mast with several co-located BS antennas and radios potentially causing interference.

With the transition to 5G and NR, cell sizes of networks are shrinking with mid-band frequencies of 2.5 – 3.7 GHz allowing coverage of a few kilometres and mmWave frequencies having a range in the scale of a few hundred meters [14]. The decrease in cell size and signal penetration will mean urban areas will be relying more on micro cells for 5G signal coverage compared to previous generations of mobile communication networks. The urban environment is quite "hostile" to wireless communication due to the high amount of traffic and sources of interference present from density of communication equipment, users, and networks. The signal levels from user equipment (UE) can be low due to high path loss at 5G frequencies and increased reliance on reflections from surfaces for tracking moving UEs as opposed to a LOS link. As demonstrated in Figure 4, the deployment of antennas on urban sites is not always as organized as in radio towers. There are many appearance and size criteria set by urban zoning regulations that can vary from city to city and the areas within the cities. Available space can therefore be limited and the mechanical structures supporting the antennas might not provide as many options for deployment compared to radio towers. In addition, the NR BS equipment is being added alongside existing pre-5G BS equipment. This can result in antennas being very close to one another and it becomes more challenging to prevent interference between antennas through deployment techniques alone. As NR BS products are primarily deployed on micro cell sites it sets high sensitivity requirements for the radio due to the realities of the environment and low signal levels, but also said equipment should not interfere with existing networks. This justifies an increased focus on unwanted emissions towards co-located antennas generated by NR BS equipment, since a noisy radio from one operator will directly affect the sensitivity of co-located radios of another operator sharing the same site and affect the QoS of their network.

Figure 4. Examples of urban mobile network sites.

Previously, the beamforming of BS transceivers has been mostly static or certain beam sets are being utilized depending on the needs of the network operator for a given site. In 5G, the introduction of user tracking via beam steering produces more potential ways for co-located base stations to interfere with each other. In Figure 5, it is illustrated how the magnitude and direction of side lobes, back lobes, and potential grating lobes are also changing when utilizing beam steering to change the main lobe direction. While there are other types of interference that can be radiated by the BS equipment, the interference transmitted from one co-located BS antenna to another is directly linked to the beamforming patterns of both antennas. For a 5G BS said pattern will be constantly changing as mobile users are being tracked. Therefore, it is fair to assume the amount of interference will also be constantly changing due to beam steering and it should be considered when regulating and measuring co-location interference for 5G BS transceivers.

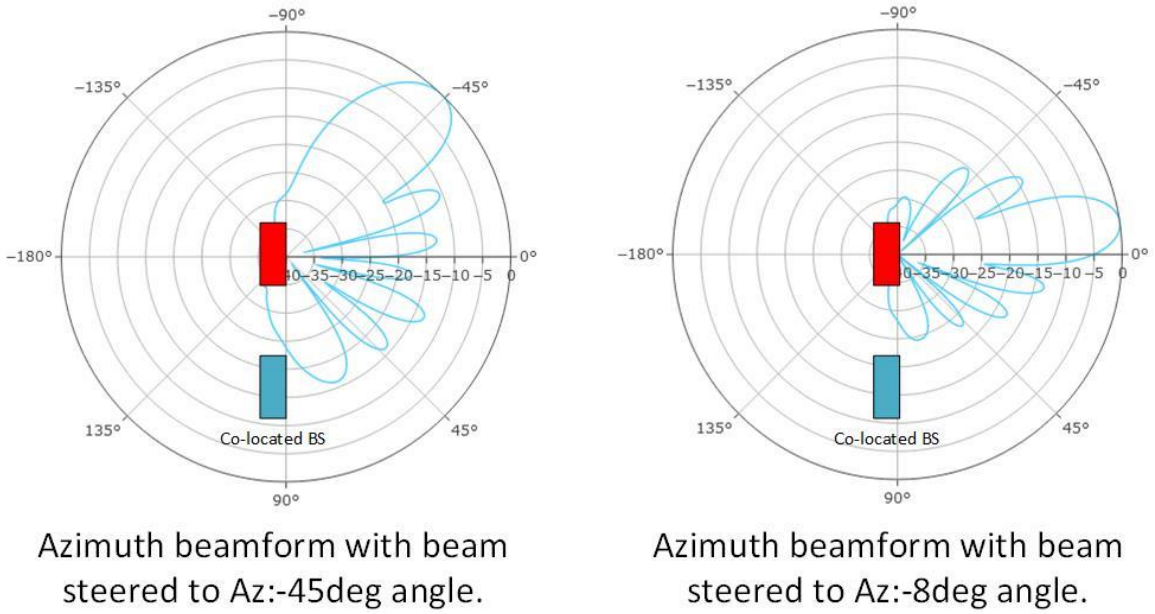


Figure 5. Example of beamform behaviour due to beam steering.

## 3.2 3GPP Co-location requirements

The co-location requirements in 3GPP aim to ensure that the BS under testing has minimal potential for degrading the operation of any BS of the same base station class operating in the same location i.e., radio tower, roof, or other fixture. 3GPP categorizes NR base stations into BS type 1-C, 1-H, 1-O, and 2-O based on their general architecture in terms of reference points. BS type 1-C only has a set of conducted requirements defined at individual antenna connectors. BS types 1-O and 2-O have only over the air (OTA) requirements defined at Radiated Interface Boundary (RIB). BS type 1-H has a hybrid mix of both conducted and OTA requirements. To mimic the base station to base station co-location scenario the measurements rely on proximity measurements done with a co-location test antenna (CLTA) which is a practical passive antenna that is required to have certain characteristics. The CLTA and co-location reference antenna will be discussed more in Chapter 5. The co-location requirements are defined as power levels going into or out of the conducted interface of the CLTA. These requirements are defined only BS type 1-O, where the BS transceiver operates at FR1 frequencies. There are no conducted interfaces available in the antenna architecture and the transceiver unit array has at least 8 transmitters and receivers. [4][15]

The following subsections summarize the different test cases for 3GPP co-location requirements [4] shown in Table 2. Reader should note that requirements and methods for BS Type 2-O are outside the scope for this thesis and only BS Type 1-O will be discussed. For details on BS Type 2-O refer to the 3GPP specifications referenced in the following subsections.

Table 2. 3GPP 38.141-2 co-location requirements

| Requirement | Co-location reference antenna operation | Requirement type |
|---|---|---|
| OTA transmit ON/OFF power for FR1 | Measure emission | Mandatory |
| OTA spurious emission: Protecting of the BS receiver of own or different BS | Measure emission | Optional based on declaration |
| OTA transmitter intermodulation | Inject the interferer signal | Mandatory |
| OTA out-of-band blocking: Co-location with other base stations | Inject the interferer signal | Optional based on declaration |

### *3.2.1 OTA spurious emission*

According to ITU definitions [16] OTA unwanted emissions is split into two categories: out-of-band emissions and spurious emissions. The two categories are depicted in frequency domain in Figure 6 [16]. Out-of-band emissions are described as unwanted emissions immediately outside the BS channel bandwidth resulting from modulation and non-linearities in the transmitter not including spurious emissions. Spurious emissions are emissions caused by unwanted transmitter effects such as harmonics, parasitics, intermodulation and frequency conversion, but excluding out-of-band emissions. By measuring DUT spurious emissions via OTA co-location measurements, it can be determined if they are on a low enough level to not interfere with the operation of a co-located BS operating on a different band.

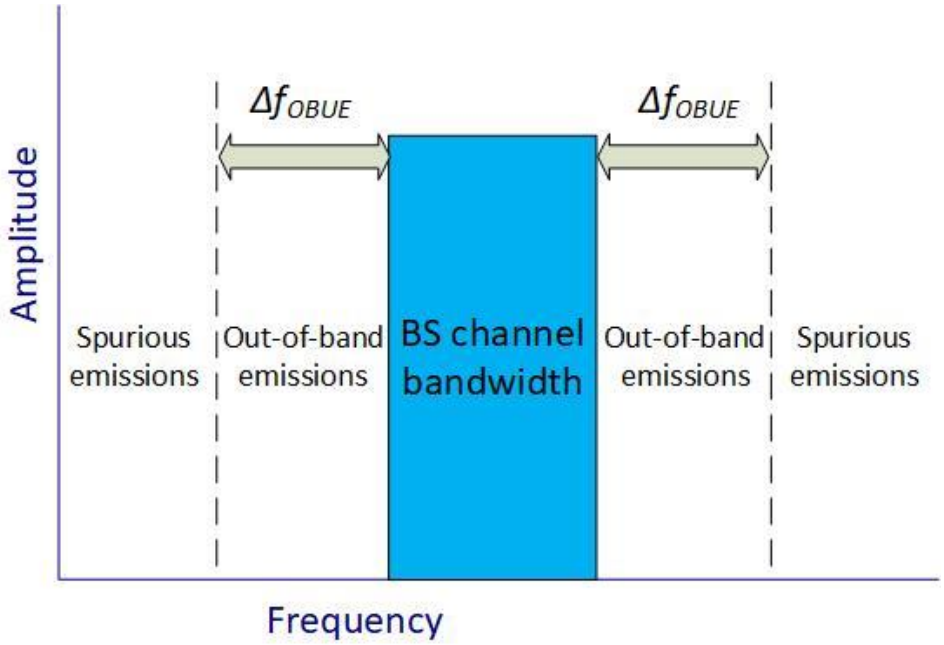


Figure 6. Out-of-band emissions of spurious emissions in the frequency domain.

In 3GPP, these two categories of OTA unwanted emissions are defined by the frequency range they occupy outside of the BS channel bandwidth. The distinction is done utilizing the definition of the maximum offset of the operating band unwanted emission (OBUE) mask from the operating band edge $\Delta f_{\mathrm{OBUE}}$ expressed in Table 3 [4]. OTA spurious emissions requirements apply to unwanted emissions that are in frequency ranges beyond $\Delta f_{\mathrm{OBUE}}$ from the operating band edges $f_{\mathrm{low}}$ and $f_{\mathrm{high}}$.

Table 3. The maximum offset of the operating band unwanted emissions mask from the operating band edge $\Delta f_{\mathrm{OBUE}}$

| **BS type** | Operating band characteristics | $\Delta f_{\mathrm{OBUE}}$**(MHz)** |
|---|---|---|
| BS type 1-O | $f_{\mathrm{high}} - f_{\mathrm{low}} < 100$ MHz | 10 |
| | $100$ MHz $\leq f_{\mathrm{high}} - f_{\mathrm{low}} \leq 900$ MHz | 40 |
| BS type 2-O | $f_{\mathrm{high}} - f_{\mathrm{low}} \leq 4000$ MHz | 1500 |

The requirements for OTA spurious emission levels per BS operating band are given in [4] as power levels determined at the CLTA physical interface while the CLTA is in proximity of the DUT. The spurious emissions are to be measured as the power sum over all supported polarizations of the CLTA antenna. The requirement to be applied for each frequency band is dependent on whether the DUT base station class is Wide Area (WA BS), Medium Range (MR BS) or Local Area (LA BS). For BS type 1-O these classes are defined in 3GPP by the BS to user equipment minimum distance so that for WA BS it is 35 m, for MR BS it is 5 m and for LA BS it is 2 m. The manufacturer shall declare the intended class of the DUT BS, and this thesis focuses on the WA BS class. As mentioned in [4], frequency ranges from $\Delta f_{\mathrm{OBUE}}$ below the DUT BS operating band lower edge $f_{\mathrm{low}}$ to $\Delta f_{\mathrm{OBUE}}$ above the DUT BS operating band upper edge $f_{\mathrm{high}}$ are not included in OTA spurious emission requirements. Therefore, frequencies $f$ for which $(f_{\mathrm{low}} - \Delta f_{\mathrm{OBUE}}) < f < (f_{\mathrm{high}} + \Delta f_{\mathrm{OBUE}})$ are excluded from the OTA spurious emission requirements. [4] Theory and test cases of spurious emissions are further elaborated in Chapters 4 and 5 respectively.

### *3.2.2 OTA transmit ON/OFF power*

The 3GPP OTA transmit ON/OFF power requirements apply only to TDD operation of a NR base station. The purpose of the OTA transmit ON/OFF power requirements is to verify the power transmitted by a NR BS during the transmitter OFF period is low enough to not interfere with the receiver of a co-located BS. As illustrated in Figure 7 [4] the transmitted power needs to drop below a certain threshold during the transmitter transient period to not spread over to the uplink (UL) period. After the transient period, the power needs to stay below the required level, so it does not interfere with UL transmission. [4]

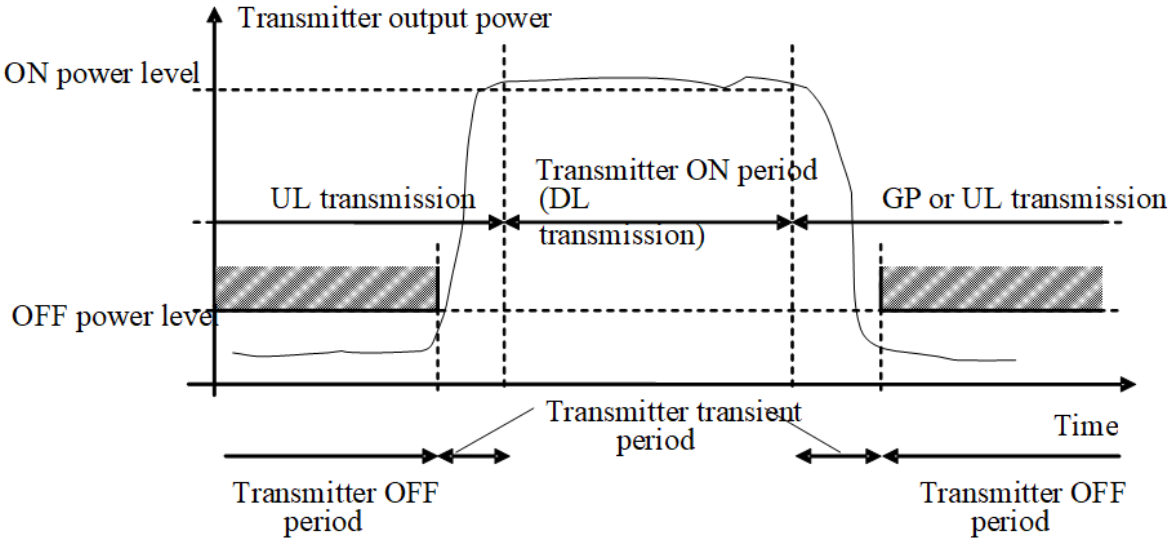


Figure 7. Illustration of the relations of transmitter ON period, transmitter OFF period and transmitter transient period.

The transmitter OFF power is defined as the output power at the co-location test antenna conducted output(s). In the measurement, the mean power is measured over $70/N$ µs and filtered with a square filter of bandwidth equal to the transmission bandwidth configuration of the BS $BW_{Config}$ centred on the assigned channel frequency during the transmitter OFF period. The parameter $N$ is calculated from Sub Carrier Spacing (SCS) in kHz as $N$=SCS/15. For BS supporting intra-band contiguous carrier aggregation (CA) the square filter of bandwidth is equal to the aggregated BS channel bandwidth $BW_{Channel\_CA}$ centred on $(F_{edge\_high}+F_{edge\_low})/2$ and SCS in this case is the smallest supported Sub Carrier Spacing in kHz in the aggregated BS channel bandwidth. The total power measured from all co-location reference antenna output(s) shall be less than -106 dBm/MHz and the maximum length of the transmitter transient period is shown in Table 4. [4][15]

Table 4. Maximum lengths for the OTA transmitter transient period

| **Transition type** | **Transient period length [µs]** |
|---|---|
| OFF to ON | 10 |
| ON to OFF | 10 |

### *3.2.3 OTA transmitter intermodulation*

If an interfering signal from a co-located BS reaches the transmitter unit of another BS through the antenna array and Radio Distribution Network (RDN) the transmitter unit may generate intermodulation products. This is due to the non-linear elements within the transmitter generating intermodulation products from the wanted signal of the victim BS and the interfering signal. These intermodulation products if not restricted may then be transmitted by the transmitter unit of the victim BS and interfere with other co-located base stations. The purpose of the OTA transmitter intermodulation test is to verify the transmitter unit of the DUT BS can reject or suppress the intermodulation products so that they are not transmitted at a level where they would interfere with co-located base stations.

In the measurement the DUT BS is set to transmit, the interfering signal is injected into the CLTA, and the total radiated power (TRP) transmitted by the DUT BS is measured with a test antenna. The characteristics of the wanted signal and interfering signal are given in Table 5 [4]. The measured TRP is subject to several different limits specified for OTA transmitter spurious emissions, OTA operating band unwanted emissions and OTA Adjacent Channel Leakage Ratio. These limits are applicable depending on the BS type and operating band. For example, the total frequency range for which the OTA transmitter spurious emissions requirements are defined range from 9 kHz up to 26 GHz, but for a BS type 1-O it is from 30 MHz up to the 5$^{th}$ harmonic frequency of the downlink (DL) operating band upper edge or 26 GHz if operating on band n46 or n96. There are also different categories of limits which are chosen by the manufacturer and BS products may be required to meet a certain category of limits by regional regulations. Further details on the OTA transmitter intermodulation requirements are outside the scope of this thesis, but they can be found in [4] and [15].

Table 5. Interfering and wanted signals for the OTA transmitter intermodulation test

| **Signal parameter** | **Value** |
|---|---|
| Wanted signal | NR single or multi-carrier, or multiple intra-band contiguously or non-contiguously aggregated carriers |
| Interfering signal | NR signal, the minimum BS channel bandwidth with 15 kHz SCS of the frequency band |
| Interfering signal level | Same power level as the BS, fed into a CLTA |
| Interfering signal centre frequency offset from the lower (upper) edge of the wanted signal or edge of the sub-block inside a gap | $f_{\text{offset}} = \pm BW_{\text{channel}}\left(n - \frac{1}{2}\right)$, for n = 1, 2 and 3 |

### *3.2.4 OTA out-of-band blocking*

Whereas the previous co-location test cases measure the BS transmitter, the purpose of OTA out-of-band blocking is to assess the receiver's ability to receive a wanted signal in the presence of an unwanted interferer signal. In the related clause of [4], a general OTA out-of-band blocking measurement and an additional co-location measurement are defined. The latter's requirement can be applied for protection of BS receivers when NR, E-UTRA BS, UTRA BS, CDMA BS or GSM/EDGE BS operating in a different frequency band are co-located with a BS. In both measurements, the requirement for the receiver is that the throughput shall be ≥ 95% of the maximum throughput in the presence of the interferer signal.

The main difference between the two measurements is that in the general measurement a test antenna will be used to generate the interferer signal according to Table 6 and in the co-location case the CLTA will transmit the interferer signal according to Table 7. In both measurements, the wanted signal mean power is defined to be 6 dB above the Equivalent Isotropic Sensitivity (EIS) declared for the minimum sensitivity Range of Angles of Arrival (RoAoA). The interfering signal to be used is a continuous wave (CW) for which in the general case test antenna Effective Isotropic Radiated Power (EIRP) needs to be adjusted according [4] so that interferer RMS field-strength at the DUT receiver is 0.36 V/m. In the co-location requirements, the interferer power is defined as mean power at the CLTA physical interface per DUT BS type. As stated in [4], interfering signal should be placed in each of the bands that are to be operated in by co-located base stations excluding bands that are within the DUT BS uplink operating bands or within $\Delta f_{\mathrm{OOB}}$ of the uplink operating band edges. [4][15]

Table 6. OTA out-of-band blocking performance requirement

| **Wanted signal mean power [dBm]** | **Interfering signal RMS field-strength [V/m]** | **Interfering signal type** |
|---|---|---|
| $\mathrm{EIS}_{\mathrm{minSENS}}$ + 6dB | 0.36 | CW carrier |

Table 7. OTA blocking requirement for co-location with BS in other frequency bands

| **Interfering signal frequency range** | **Wanted signal mean power [dBm]** | **Interfering signal mean power** | | | **Interfering signal type** |
|---|---|---|---|---|---|
| | | **WA BS [dBm]** | **MR BS [dBm]** | **LA BS [dBm]** | |
| Frequency range of co-located downlink operating band | $\mathrm{EIS}_{\mathrm{minSENS}}$ + 6dB | +46 | +38 | +24 | CW carrier |

# 4 TEST SETUP AND PLANNING

In this chapter the design, planning and choices made for implementing the practical measurements for this thesis are discussed. The testing was done in two parts: first a preliminary isolation measurement using a Vivaldi antenna followed by carrying out the 3GPP OTA spurious emission co-location measurement. In the first section, the Compact Antenna Test Range (CATR) measurement environment and chosen DUT are presented and the motivations behind choosing them for this study are given. The second section presents the 3GPP requirements for a Co-location Test Antenna (CLTA) and how the two chosen CLTAs match these requirements. Third section presents the two measurement setups used in the study along with power budget calculations for them.

## 4.1 Measurement environment and DUT

Anechoic chambers are commonly used for OTA measurements in laboratory environments. Their purpose is to minimize outside interference, noise from the measurement environment and reflections. This way the dynamic range of the measurements is maximized, and results are repeatable. An anechoic chamber is an enclosed space where the walls have high electromagnetic isolation for keeping interference from e.g. commercial mobile networks propagating into the chamber. To prevent reflections within the chamber the roof, walls, floor, and other surfaces are covered with absorber material. Any inlets for cables from outside the chamber are carefully designed and appropriately filtered to prevent interference or noise entering the chamber.

Part of this work was to develop the means of utilizing existing anechoic chambers, so the measurements were designed specifically for a Compact Antenna Test Range (CATR) shown in Figure 8. The CATR test environment is used to measure the whole 3D far field radiation pattern of an antenna. This is enabled by the parabolic reflector transforming spherical waves into a plane wave form, thus forming a far field test environment in relatively small space. Even though the 3D positioner was kept stationary, and the feed antenna was not needed for the measurements of this thesis it was part of the work to develop methods for utilizing the CATR environment for 3GPP co-location testing. In [4], the OTA transmitter intermodulation test case is an example of a co-location requirement that requires rotating both the NR BS and CLTA around the same axis, so it is beneficial for future test implementation studies to explore how both the DUT and CLTA can be attached to the existing 3D positioners utilized in CATRs.

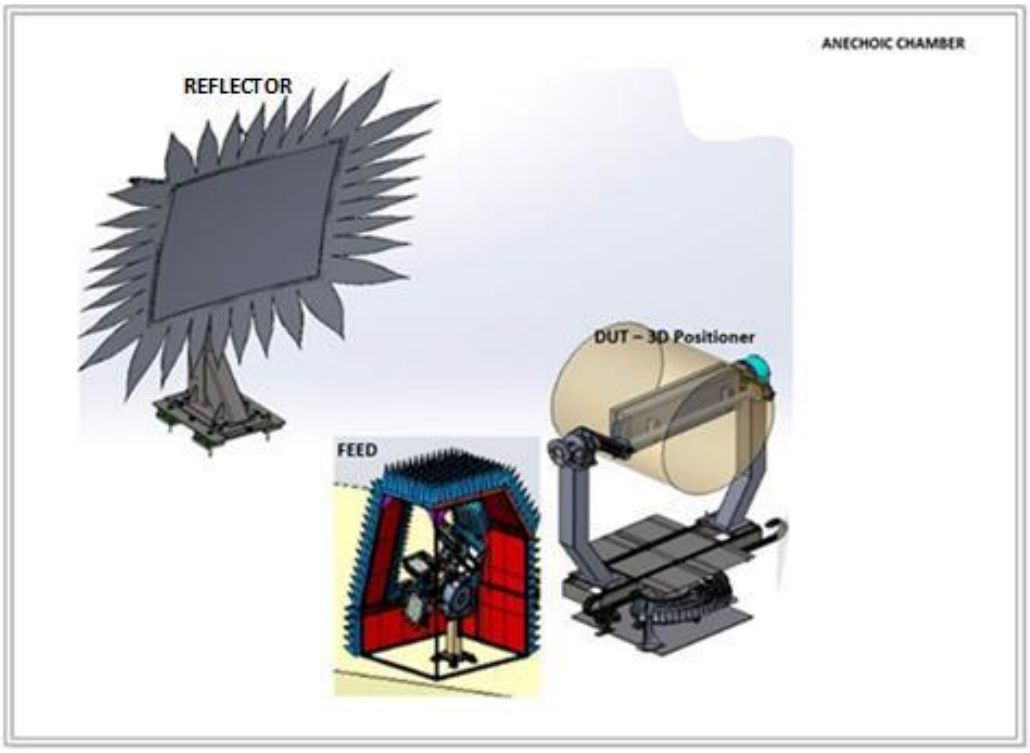


Figure 8. Concept picture of a CATR chamber.

The DUT chosen was a mMiMo 64T64R 192AE TDD base station radio operating on FR1 band n41 (2496 – 2690 MHz). It was chosen since the DUT has been thoroughly tested and usage is well documented. It should be noted that of the BS types described in Section 3.4 this DUT is of 3GPP BS type 1-H. This is due to no BS type 1-O or 2-O BS equipment being available at the time of planning these tests. The chosen carrier configuration 2xNR40 where the two carriers were placed at bottom and top of the n41 band. This was the dual carrier configuration with narrowest carriers that still have the BS transmitting at full power. Placing the carriers on the edges of the band was assumed to maximize potential for interference towards a co-located BS. The narrowest intended vertical Half Power Beam Width (HPBW) declared for the DUT is 8°, which will be relevant for choosing the CLTA to be used for co-location testing in the next section.

### 4.2 Co-location test antenna

In the co-location test case, the CLTA is a passive antenna that acts as a victim antenna for any unwanted emissions the DUT generates around it. In Figure 9 [4], it is depicted how the NR BS under testing and CLTA should be physically aligned. The figure shows how radome surfaces and centres of the radiators should be lined up. This is an important distinction since in NR radios the device centre and antenna array centre are not always the same point. The edge-to-edge separation $d$ is defined as being 10 cm and all these requirements have a 1 cm margin for error as can be seen from the table at the bottom of the figure. The potential asymmetry in the placement of radiating elements within the DUT is addressed in required manufacturer declarations [4]. The manufacturer should declare the side of the DUT where the radiating elements are the closest to the edge of the DUT when applicable and place the CLTA on said side during co-location testing.

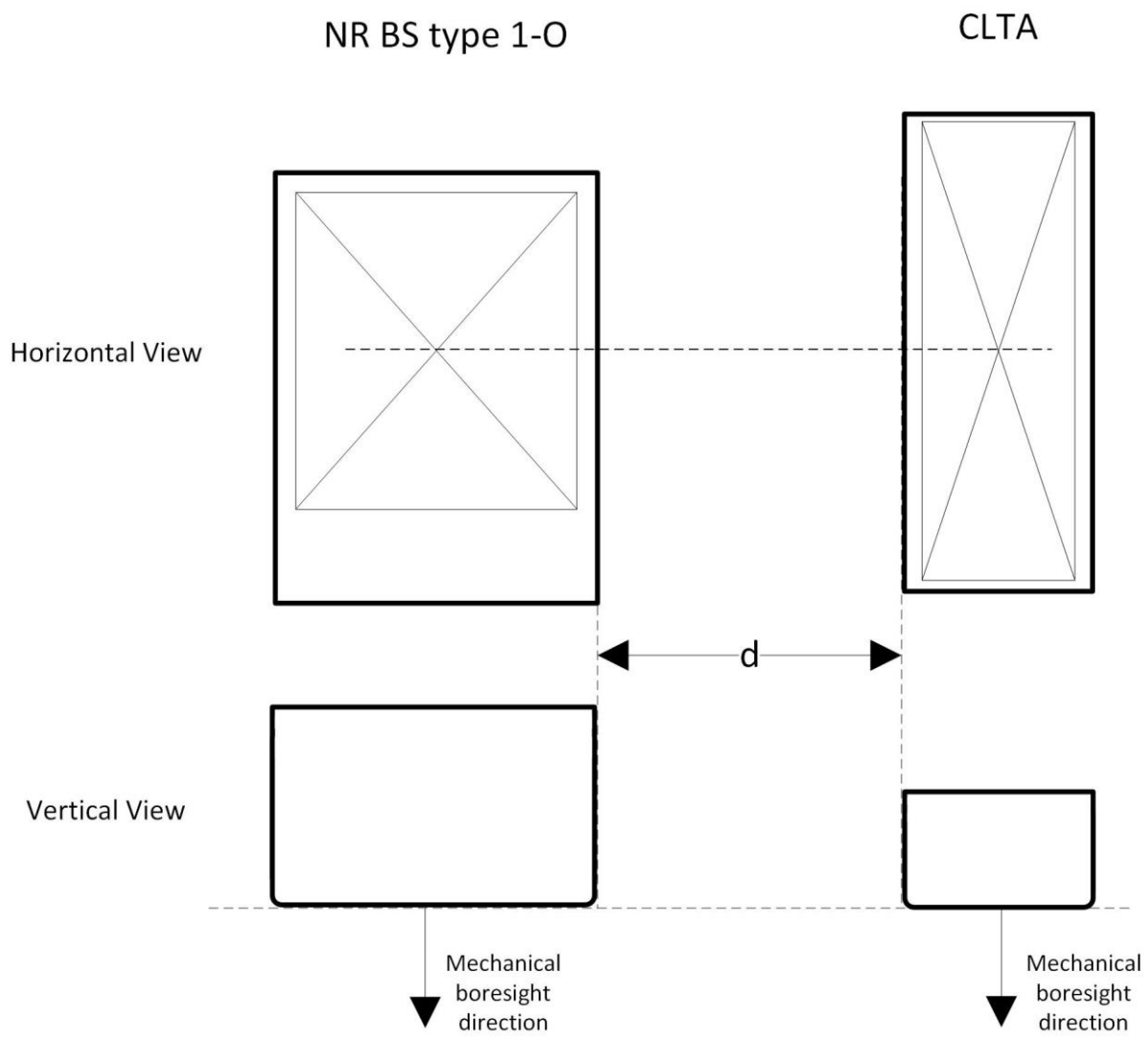


| Parameter | |
|---|---|
| Edge-to-edge separation between the NR BS and the CLTA, d | 0.1 m ± 0.01 m |
| Vertical alignment | Centre ± 0.01 m |
| Front alignment | Radome front ± 0.01 m |

Figure 9. Physical orientation requirements for NR BS DUT and CLTA.

### *4.2.1 Co-location test antenna requirements*

A co-location test antenna is defined in [4] as a practical passive antenna that can be used in the conformance testing of co-location requirements and is based on the definition of the co-location reference antenna (CLRA) in [15]. According to the CLRA definitions the antenna used for in-band measurements shall be a single column antenna with an equal vertical radiation dimension $h$, frequency range, polarization to the DUT's and a 65° horizontal HPBW which is typical for 3-sector deployment. If the frequency range of the CLRA is different to that of the DUT, it is stated that any CLRA suitable for the frequency range can be used.

The characteristic requirements of the CLTA are defined in Table 8 [4]. The requirements are different depending on if the CLTA is used for in-band or out-of-band measurements.

Compared to the CLRA definitions there are added margins for deviations as well as additional requirements listed. Addition of tolerances is intuitive, as in practise it is unreasonable to find a CLTA for every DUT with equal $h$ and a horizontal HPBW of exactly 65°. For out-of-band CLTAs the requirement for $h$ is removed all together, as antenna size is typically inversely proportional to frequency i.e., a CLTA operating on a lower frequency than the DUT will naturally be larger in size. The additions not covered in CLRA definitions are the vertical HPBW and return loss of the conducted interface. Choosing the narrowest declared vertical HPBW intuitively means that the transmitted power will be spread more widely in the horizontal plane of the beam both in terms of the main lobe and the side lobes. It is not entirely clear from [4] whether the "narrowest declared vertical beamwidth" refers to that of the DUT or CLTA, but in this thesis it was assumed it is referring to the DUT's beamwidth. The return loss requirement makes sure that less than 10% of the power fed to or measured from the CLTA conducted interface is lost due to e.g., antenna port impedance mismatching. The note at the bottom of Table 8 is important to point out as a multi-band antenna will cut down the number of CLTAs needed to measure all out-of-band frequencies and such antennas were chosen for the practical portion of this thesis. Each antenna within the multi-band antenna that is used for co-location test cases must meet the CLTA requirements.

Table 8. Characteristic requirements for a CLTA

| **Parameter** | **In-band CLTA** | **Out-of-band CLTAs** |
|---|---|---|
| Vertical radiating dimension (h) | DUT vertical radiating length ± 30% | N/A |
| Horizontal beam width | 65° ± 10° | 65° ± 10° |
| Vertical beam width | N/A | The HPBW of the CLTA equals the narrowest declared DUT HPBW ± 3° |
| Polarization | Match | Match to in-band |
| Conducted interface return loss | > 10 dB | > 10 dB |
| NOTE: For multi-column or multi-band antennas, column closest to DUT shall be selected while other columns are terminated during testing. | | |

### *4.2.2 Selected co-location test antenna*

Based on the requirements listed above, two CLTAs were chosen for use in the practical measurements of this thesis. Both are multi-band antennas, as it was not possible in practise to find separate passive antennas to cover the entire frequency range. It was also deemed more practical to swap between ports of a multi-band antenna instead of swapping between different CLTAs for each frequency range. For these technical and practical reasons, the choice was to study feasibility of multi-band antennas for co-location measurements. The characteristics of the two multi-band antennas relevant to CLTA requirements are listed in Figure 10 per antenna. The cells in red have values or ranges of values that exceed the CLTA requirements in Table 8 before considering the antenna manufacturer's tolerances. Values in yellow cells exceed the requirements once the tolerances are considered. The antennas that were chosen to be used in the co-location measurement are shown in green text, while the ones not utilized are in white text.

CLTA A

| Radiating element | Lr1/Rr2 | Ry3 | Lb1 | Ly1 | p1 | Rb2 | Cy2 |
|---|---|---|---|---|---|---|---|
| Frequency band [MHz] | 690-960 | 1427-2609 | 1695-2200 | 2490-2690 | 2300-3800 | 1695-2200 | 2490-2690 |
| Horizontal HPBW [deg]* | 60 - 65 ± 5 | 58 - 70 ± 5 | 66 - 67 ± 5 | 58 ± 5 | 70-90*** | 61 - 62 ± 5 | 58 ± 5 |
| Vertical HPBW [deg]* | 8.9 - 10.9 ± 0.5 | 5.1 - 8.7 ± 0.5 | 6.8 - 7.5 ± 0.5 | 5.3 ± 0.5 | 5.5 - 8.0*** | 6.8 - 7.6 ± 0.5 | 5.3 ± 0.5 |
| Return Loss [dB] | >14.0 | >14.0 | >14.0 | >14.0 | >14.0 | >14.0 | >14.0 |
| Vertical radiation dimension [cm]** | 209.9 | 104.95 | 104.95 | 104.95 | 104.95 | 104.95 | 104.95 |

CLTA B

| Radiating element | R1/R2 | B1/B2 | Y1/Y4 | Y2/Y3 |
|---|---|---|---|---|
| Frequency band [MHz] | 694-960 | 1695-2180 | 2490-2690 | 1427-2690 |
| Horizontal HPBW [deg]* | 63 - 68 ± 6.2 | 68 ± 6.2 | 55 ± 6.2 | 56 - 68 ± 6.2 |
| Vertical HPBW [deg]* | 10 - 11.7 ± (1.0 - 1.1) | 7.2 ± 0.8 | 5.7 ± 0.6 | 5.7 - 9.6 ± (0.7 - 0.9) |
| Return Loss [dB] | 14 | 14 | 14 | 14 |
| Vertical radiation dimension [cm]** | 209.0 | 104.5 | 104.5 | 104.5 |

Value range outside CLTA requirement

Tolerance can put value range outside of CLTA requirement

*Antenna datasheet shows different values for different frequency ranges within the frequency band, so range of values across the element frequency band are given.

**Estimated size based on antenna dimensions, as there is no mention of radiating element dimensions in datasheet. Real element sizes are likely smaller.

*** p1 HPBW values are for "Single column beam"

Figure 10. Comparison of the chosen CLTAs.

In Figure 11 the layout of antenna arrays within the multi-band antennas are presented. The colouring of each antenna indicates the upper band edge range [17]. The antennas that were used in the co-location measurement are highlighted. Note that in CLTA A there are four p1 antennas each with an antenna port per polarity and of them both polarities of Ant4 would be used in the measurements. In the datasheets for both antennas no dimensions were given for the elements themselves nor how they are positioned within the antenna beyond what is shown in the figure. As a result, it was estimated that the large low band arrays are the length of the entire antenna and higher frequency arrays are half as long. Figure 11 would suggest that the higher frequency antennas are shorter than what was estimated, but there was no real way to know without taking apart the entire multi-band antenna.

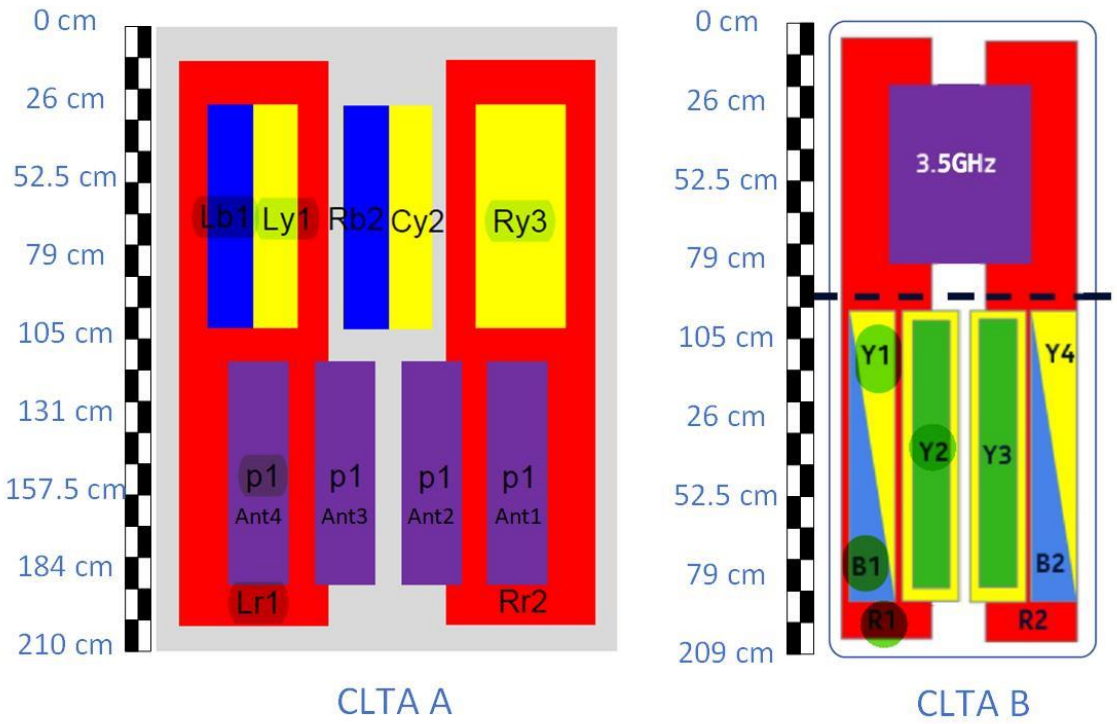


Figure 11. Array layouts and measurement points for chose CLTAs.

## 4.3 Power budget

The 3GPP spurious emission limits shown in [4] set strict requirements not only for the DUT but also the dynamic range of the test environment. For example, on the GSM900 band the DUT emissions should be below -115.9 dBm at the physical interface of the CLTA. This also means the noise floor of the measurement environment should have enough margin to the requirement so that random noise in the environment itself isn't causing fail -results. Achieving a low noise floor means careful selection of components but also sets limits on the length of RF cables, which can be limiting in the practical implementation of the measurement setup. Power budget and noise calculations are a useful tool for narrowing down the requirements for components of the measurement setup. In the following subsections, the measurement setup used for the co-location measurement is shown and the power budget and noise calculations are presented. Lastly the components selected for the measurement are shown along with their characteristics.

### *4.3.1 CLTA & Vivaldi isolation measurement setup*

The measurement setup in Figure 12 was designed for measuring how the isolation between the CLTA and a test antenna changes at different positions and orientations of the test antenna. A Vivaldi type test antenna was used for this measurement and the isolation between the port of the CLTA and Vivaldi antenna port measured by a S21 measurement with the chosen network analyzer. The Vivaldi antenna is discussed more in Section 5.4.1.

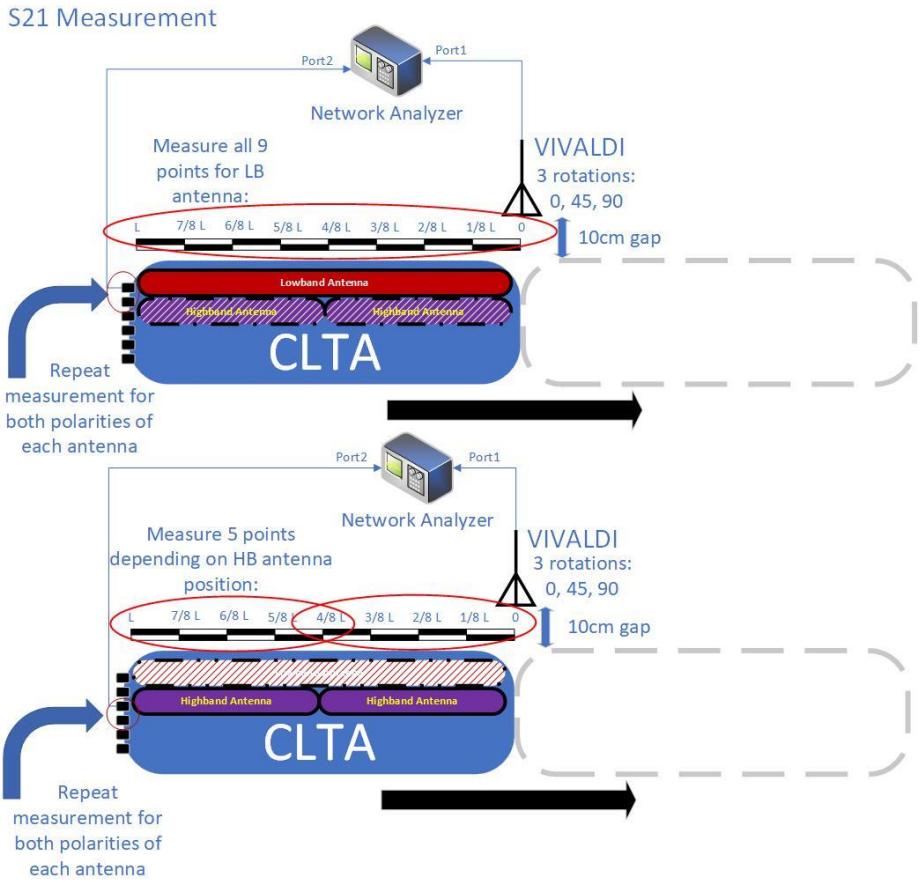


Figure 12. Depiction of isolation measurement setup.

For power budget considerations the route from network analyzer Port 1 to Port 2 consists of cabling and the isolation between the Vivaldi antenna and CLTA antenna under test. This is depicted in Figure 13 where the minimum isolation is 30 dB as is the assumption in 3GPP [18] based on results in [19]. The isolation defined from one antenna's port to another consists of many components including free-space path loss, insertion loss at the antenna port, both antenna gains in the incident direction and radiation efficiency. However, not enough was known about the near-field properties of the antennas to take all these factors into account. Instead of approximating all the components of the isolation the focus was instead on the practical isolation between the antennas.

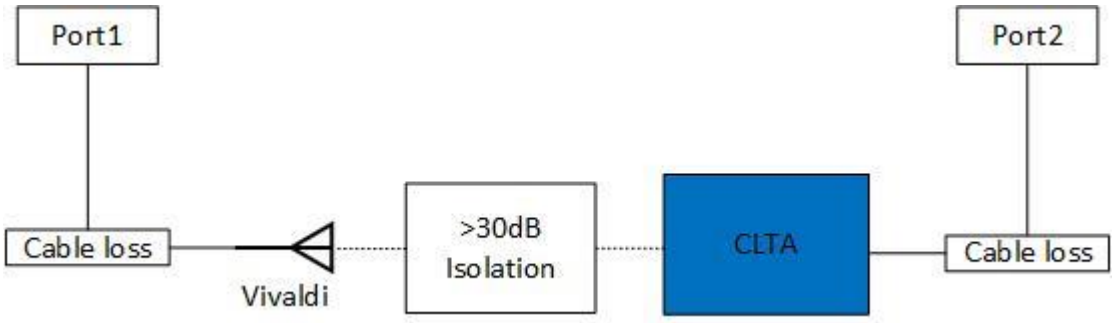


Figure 13. Simplified schematic of isolation measurement setup.

For considering input thermal noise $P_0 = kTB$, the Boltzmann coefficient equals to $k = 1.380649 * 10^{-23}\ \frac{\mathrm{J}}{\mathrm{K}}$, the temperature within the test environment is assumed to be equal to $T = 293$ K and the measurement bandwidth $B = 1$ kHz. This gives a thermal noise of $P_0 =$ -143.9 dBm. The specification RMS noise level of the R&S ZNL6 vector network analyzer (VNA) according to datasheet [22] is $P_{VNA} = B * \left(\text{-}125 \frac{\mathrm{dBm}}{\mathrm{Hz}}\right) =$ -95 dBm. Assuming only thermal noise, port noise and a 1 kHz continuous wave wanted signal with power $P_i = 0$ dBm at Port1 the input signal-to-noise ratio becomes

$$SNR_1 = \frac{P_i}{P_0 + P_{VNA}} = P_i[\mathrm{dBm}] - (P_0[\mathrm{dBm}] + P_{VNA}[\mathrm{dBm}])$$
$$= 0\ \mathrm{dBm} - \left(\text{-}143.9\ \mathrm{dBm} + (\text{-}95\ \mathrm{dBm})\right) = 94.999 \ldots \mathrm{dB} \approx 95\ \mathrm{dB}$$

Before radiating through the Vivaldi antenna, the wanted signal is attenuated by the cable loss $L_C = 0.4$ dB and return loss of the Vivaldi antenna port $L_V = 0.37$ dB. It is then assumed that the radiation properties of both the transmitting and receiving antenna equal to a minimum attenuation of $L_{iso} = 30$ dB and the signal will enter Port2 after being attenuated by the return loss $P_0$ of CLTA port $L_{CLTA} = 0.18$ dB and another cable. Assuming the same level of thermal noise is present in the CLTA side of the setup the signal-to-noise ratio in Port2 is

$$SNR_2 = SNR_1 - 2L_c - L_V - L_{iso} - L_{CLTA} = 63.65\ \mathrm{dB}$$

This result suggests a good margin for additional noise and dynamic range for measuring the behaviour of isolation. It should be possible to measure isolations up to 90 dB or more, as this calculation was done with specification values instead of typical ones. Lower isolations are more interesting from finding the worst-case for the co-location scenario. However, being able to also measure high isolations is important for understanding how the isolation behaves overall.

### *4.3.2 Co-location measurement setup*

The measurement setup for the co-location spurious emissions measurement includes external components shown in Figure 14 which serve to both improve the dynamic range of the measurement and filtering out the transmission band of the DUT. These components were proven to provide the required dynamic range in previous unwanted emission measurements during the first months of this thesis. The schematic has three components that contribute to the power budget and noise calculations between the CLTA antenna port and spectrum analyzer input port: the diplex filter (DPF), low-noise amplifier (LNA) and the RF cabling used.

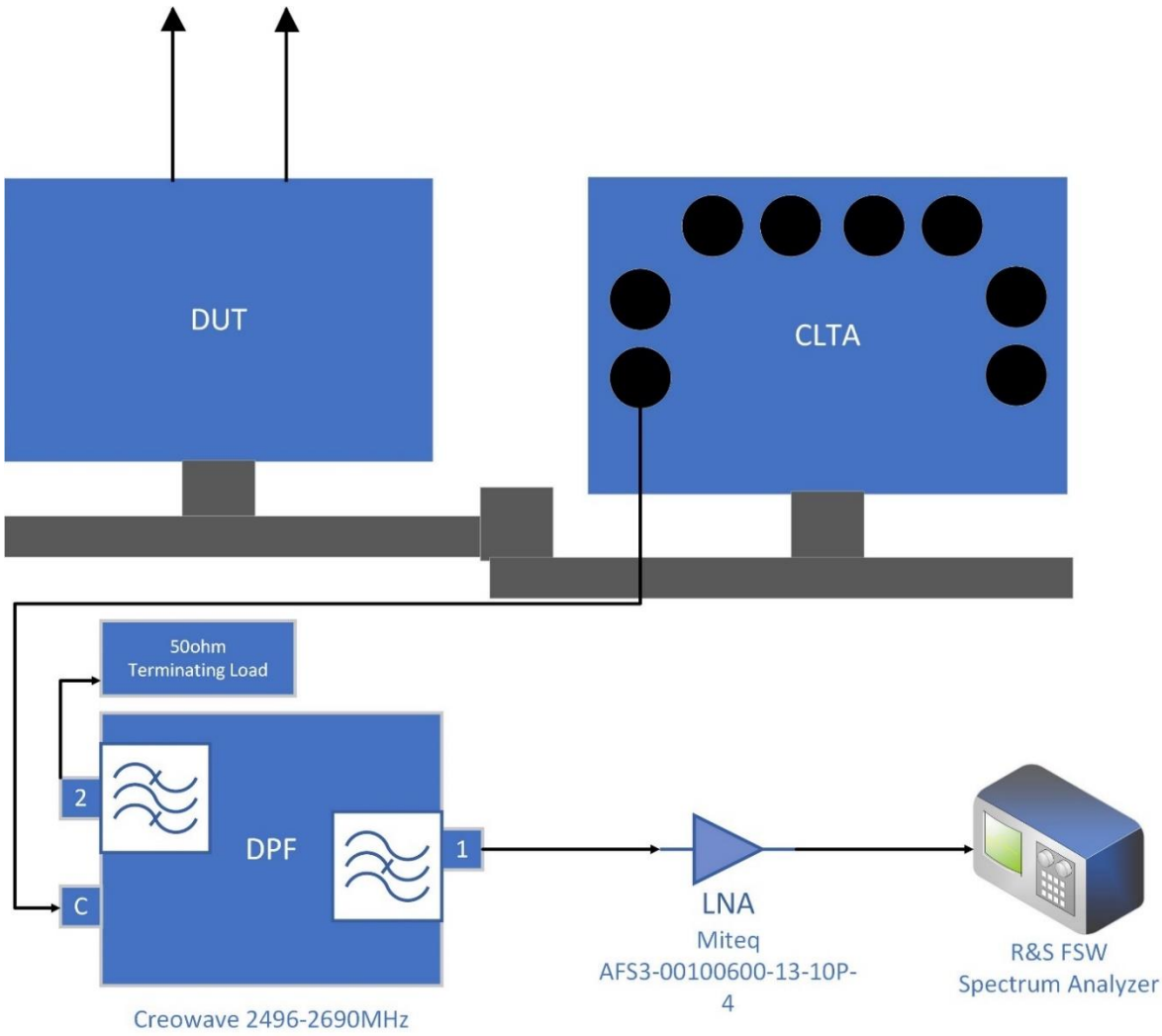


Figure 14. Co-location measurement setup schematic.

For the co-location test the weakest emission that needs to be detected according to [4] is $-115.9$ dBm, so for power budget calculations it will be used as input signal level $P_i$. The measurement bandwidth for all frequency ranges in [4] is $B = 100$ kHz. To be able to distinguish such an emission from noise at the spectrum analyzer input, the signal-to-noise ratio should be in the order of several decibels at said input. By assuming the input signal and thermal noise at the CLTA port the input signal-to-noise ratio $SNR_{CLTA}$ becomes

$$SNR_{CLTA} = \frac{P_i}{P_0} = \frac{P_i}{kTB} == \text{-115.9 dBm} - (\text{-123.9 dBm}) = 8 \text{ dB}. \quad (1)$$

The filter and amplifier stages in Figure 15 add not only gain and loss to the input signal and noise, but also generate noise which degrades the SNR at the output of each stage. This degradation of SNR between the input and output of a component is quantified by noise figure $F$ [20].

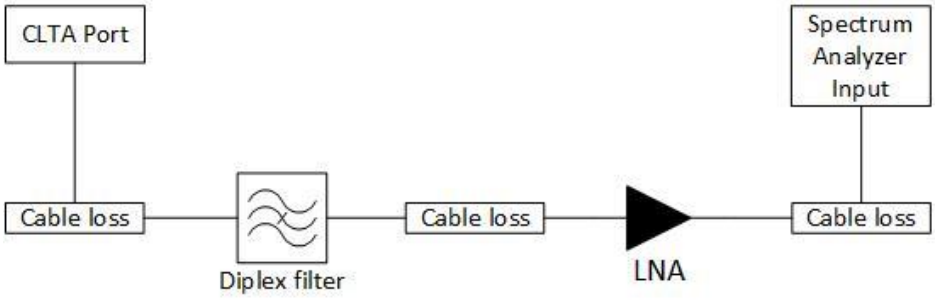


Figure 15. Simplified depiction of the co-location measurement setup.

The decibel and linear values for gain and noise figure for each contributing component are given in Table 9. The total loss of the cabling was measured to be 1.2 dB so it was assumed each cable has a loss of 0.4 dB, while the values for the diplexer and LNA [21] are from their respective datasheets. Since temperature is assumed to be $T = 293$ Kacross the setup, the noise figure of passive stages is set to be equal to the loss of said stage [20].

Table 9. LNA, diplexer and cabling characteristics for power budget calculations

| | **Creowave diplexer** | **Miteq LNA** | **Cabling** |
|---|---|---|---|
| Noise figure $F$ | $F_{DPF} = -G_{DPF} \leq$ 4 dB ($\approx 2.51$) | $F_{LNA} = 1.3$ dB ($\approx 1.35$) | $F_C = -G_C = 0.4$ dB ($\approx$ 1.10) |
| Gain $G$ | $G_{DPF} \geq -4$ dB ($\approx$ 0.40) | $G_{LNA} = 30$ dB ($= 10^3$) | $G_C = -0.4$ dB ($\approx 0.91$) |

It is assumed that the diplexer noise figure and loss are at their worst-case value given in datasheet. Using the linear values from Table 9 the noise figure of the five-stage cascade can be calculated according to [20] as

$$F = F_1 + \frac{F_2 - 1}{G_1} + \frac{F_3 - 1}{G_1 G_2} + \cdots \quad (2)$$

$$= F_C + \frac{(F_{DPF} - 1)}{G_C} + \frac{(F_C - 1)}{G_C G_{DPF}} + \frac{(F_{LNA} - 1)}{G_C^2 G_{DPF}} + \frac{(F_C - 1)}{G_C^2 G_{DPF} G_{LNA}}$$

$$= 1.10 + \frac{(2.51 - 1)}{0.91} + \frac{(1.10 - 1)}{0.91 * 0.4} + \frac{(1.35 - 1)}{0.91^2 * 0.4} + \frac{(1.10 - 1)}{0.91^2 * 0.4 * 10^3} = 4.09 \ldots \approx 6.1 \text{ dB},$$

which results in an output signal-to-noise ratio of $SNR_{out} = 1.9$ dB. This gives very little margin between the input signal and the noise floor of the measurement and demonstrates the difficulty of implementing such a setup. However, this calculation was done with worst-case values instead of typical values and practical results presented in Chapter 6 show that the SNR is higher in practise.

## 4.4 Test plan

The purpose of this test plan is to provide the background motivations, approaches, methods, and goals for the two measurements of this thesis. The focus in this work is on the 3GPP defined OTA spurious emissions test case. However, many parts of the measurements are also applicable for future implementation of other co-location test cases. Similar measurements were done for the first time during the first few months of this thesis work, so some reference data and lessons learned were available.

The purposes behind the measurements are as follows:

- Investigate how coupling or isolation between two antennas in the near-field changes depending on at least the following factors:
  - Antenna polarity
  - Antenna orientation and polarity alignment
  - Antenna position relative to each other
  - Antenna remote electrical tilt (RET) angle
  - Frequency
- Through investigating the isolation phenomena define a "worst-case coupling scenario" for two base station antennas. Compare said worst-case scenario to the 3GPP defined co-location scenario.
- Study and investigate the common practicalities of the 3GPP co-location test cases for a typical 5G mMiMo radio and how well they can be executed in practise.
  - The usability of chosen CLTA candidates and how fit for purpose they are.
  - Feasibility of achieving the required frequency coverage.
  - Work effort and test duration considerations.
- Study and investigate the possible limitations of the CATR environment for implementing the 3GPP co-location test cases.
- Find methods for implementation of the chosen testcase and improving it for future Nokia use.

### *4.4.1 CLTA & Vivaldi isolation measurement*

The purpose of the preliminary isolation measurement is to gain an understanding on how the isolation between two antennas changes depending on their physical orientation. The goal is to find key factors that increase or decrease isolation between two antennas in the near-field and establish a worst-case scenario. The established worst-case scenario can then be compared to the 3GPP defined co-location scenario and assess whether the 3GPP definitions are comprehensive. Observations from this measurement could potentially be used to explain measurement results in the OTA spurious emissions tests.

Figure 16 and Figure 17 depict the measurement setup for isolation measurement of a low-band antenna and a high-band antenna respectively. For both cases the measurement setup is calibrated to the antenna port of the Vivaldi and CLTA antenna under test. In each measurement point along the edge of the CLTA's length, the S21 measurement is done with three different rotations of the Vivaldi measurement antenna. The gap between the CLTA and Vivaldi was kept at 10 cm with a 1 cm margin for error in the vein of Figure 9 definition for edge-to-edge separation $d$. For the chosen multi-band CLTAs the low-band antenna spans the entire length $L$ of the CLTA, so the isolation is measured in nine different points as illustrated in Figure 16.

The high-band antennas are estimated to span half the length of the CLTA based on pictures in the multi-band antenna's datasheet. As depicted in Figure 17, the isolation is measured at five different points depending on which half of the CLTA is antenna is located. Exact locations or sizes for the different antennas within one CLTA were not available from manufacturer's datasheets. Due to time constraints, it was not considered feasible to measure the effect of RET on the isolation at every measurement point as it would triple the number of measurements required. As a compromise, two additional measurements are done at the middle measurement point *4/8L*. In these two measurements, the isolation is measured with CLTA RET angle at its maximum and minimum value for the given CLTA antenna. The amount of data from the minimum and maximum RET angles would be small compared to other subsets and likely insufficient to draw any comprehensive conclusions on the effect of RET angle. However, the goal was to at least see if the RET angle has a notable effect on isolation at the middle point of the antenna.

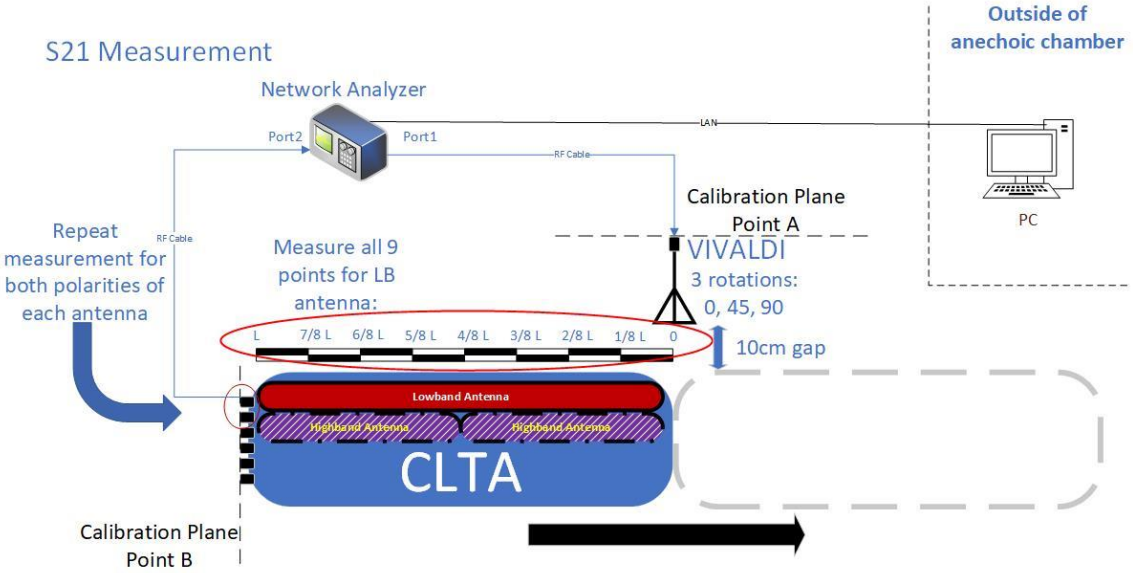


Figure 16. Setup with calibration plane for low-band antenna isolation measurement.

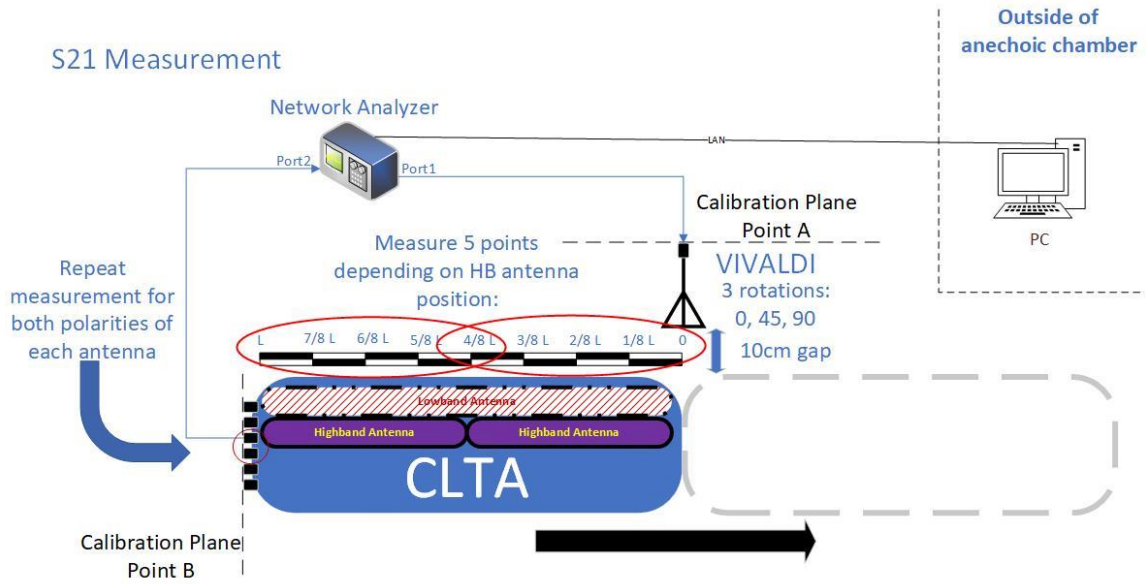


Figure 17. Setup with calibration plane for high-band antenna isolation measurement.

The Vivaldi antenna consists of two radiating elements perpendicular to one another as shown in Figure 18. The elements are named with physical markings as K-polarity and N-polarity. Only one of these elements is needed for the measurement, though it is an option to switch between the measured element instead of physically rotating the Vivaldi from rotation 0° to 90°. However, physical rotation of the Vivaldi is still required to measure the rotation 45° and there are some minor differences between elements.

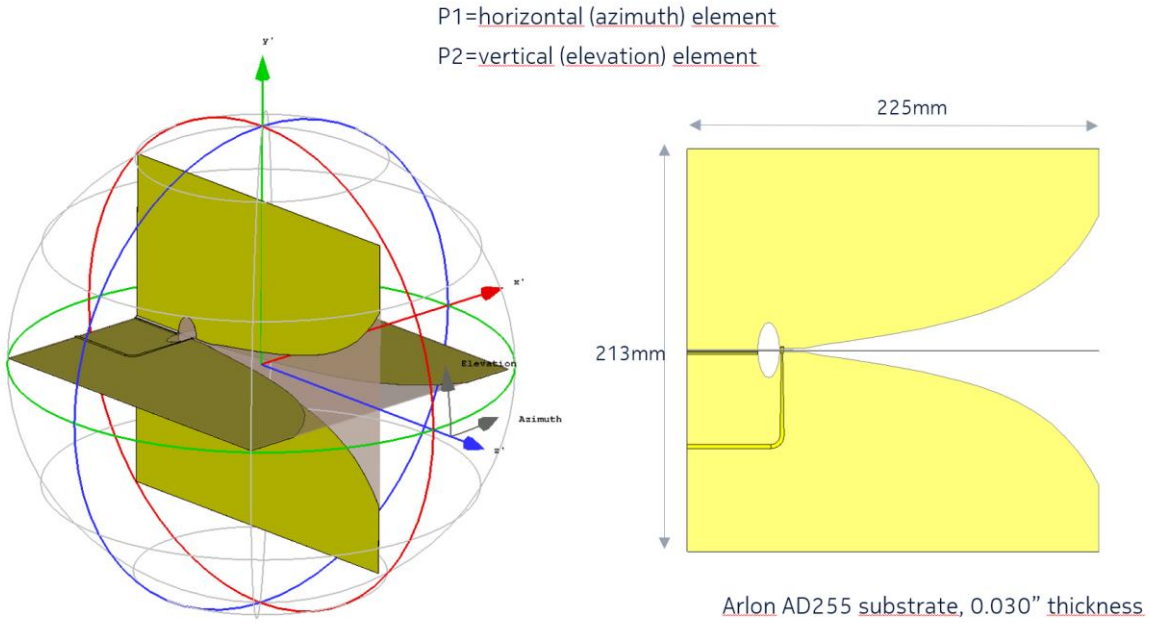


Figure 18. 3D model of the Vivaldi antenna.

This Vivaldi antenna was designed primarily for the frequency range 1.7 – 6 GHz, but as seen in Figure 19 the VSWR stays at an acceptable level even down to 1 GHz. Most of the frequencies in [4] are within the 1 – 6 GHz range, so the frequency coverage was the main reason for choosing the Vivaldi. Other option would be to have several test antennas to also cover the lower frequencies, but that will increase testing time and complicate comparability of the results.

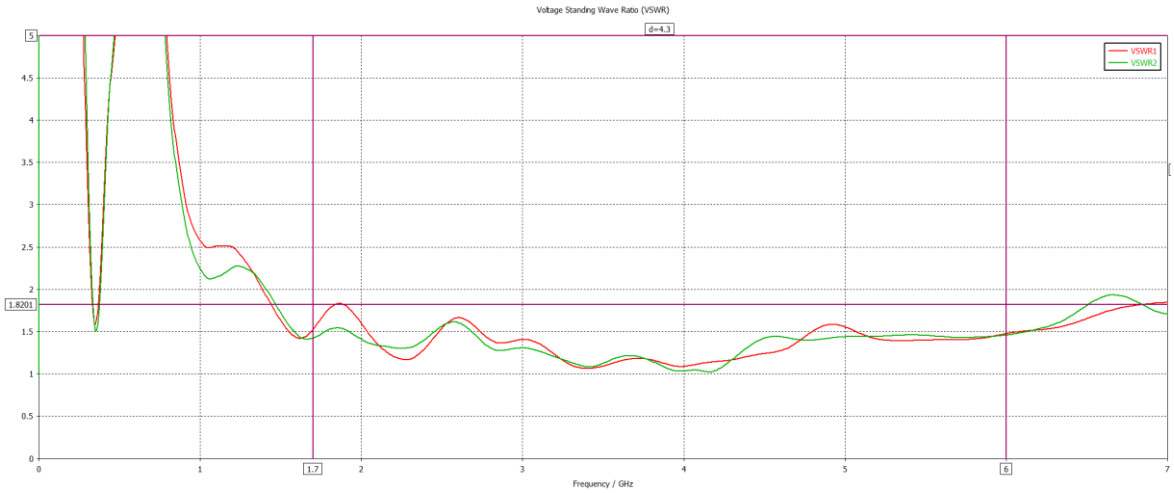


Figure 19. The VSWR of the Vivaldi antenna for both radiating elements.

Rohde & Schwarz ZNL6 vector network analyzer was chosen for measuring the S21 from Vivaldi antenna port to CLTA antenna port. The frequency range of the Vivaldi was the main factor for choosing the VNA and ZNL6 was the only available VNA that can measure up to 6 GHz. There were also some automation scripts available for the ZNL6 from a previous S-parameter study. The scripts were determined to be helpful with exporting the measurement results for later analysis, decrease chance for human error and lessen or even remove need for manually operating the VNA.

### *4.4.2 Co-location measurement*

In the second measurement the OTA spurious emission test case defined in Section 4.1 is carried out in practise. The goal is to form and develop the methods for implementation of this test case in the future at similar test environments across Nokia. The practical feasibility of multi-band passive antennas as CLTAs for co-location tests is to be studied. The purpose is also to evaluate the practical solutions used for the mechanical attachment of the DUT and CLTA to the test range positioner. The analysed results are to be reflected against the theory and results of the first measurement to further understanding of interference in the co-location scenario. The lessons learned can potentially help comment on the 3GPP definitions for the co-location test cases in terms of the practicality of implementation, fit for purpose and coverage.

The measurement setup is shown in Figure 20 along with the mechanical supports and brackets used. The supports and brackets were designed at Nokia so that a variety of DUTs and CLTAs could be aligned according to the 3GPP definitions that were discussed in Section 5.2. Attachment points of the supports into the main pole need to be measured beforehand and adjusted so that the DUT antenna panel and CLTA centres are aligned. As depicted in the figure the height of the brackets is adjustable to align the radomes and they slide along the length of the supports so the 10 cm gap can be realised.

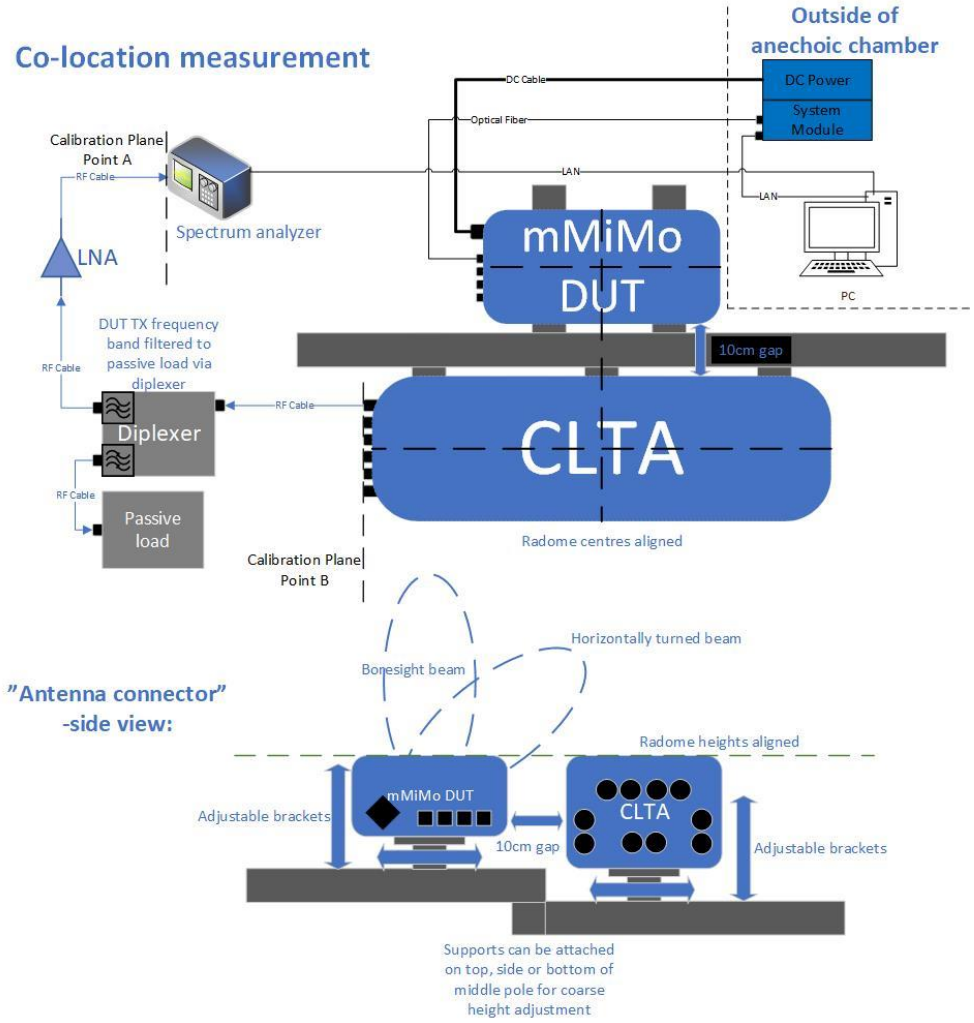


Figure 20. Setup with calibration plane for OTA spurious emissions measurement.

The wanted 2xNR40 carrier configuration is configured through the system module GUI accessible via the measurement PC. The two carriers are placed on the edges of the n41 operating band so that the centre frequency for Carrier 1 is 2516.01 MHz and for Carrier 2 it is 2670 MHz. The NR BS would be running in Test Dedicated State (TDS) to enable the selection and usage of test models per carrier as required by 3GPP [4]. Both carriers would be configured according to FR1 test model NR-FR1-TM1.1, which is defined in detail in 3GPP TS 38.141-1 [23]. In terms of DUT operation, the measurements will be repeated for three different configurations. First, a reference measurement where the DUT is powered down. The purpose is to establish a point of reference and find any potential sources of interference within the test environment that could be falsely attributed to the DUT otherwise. In the second measurement, the DUT will be transmitting a boresight beam in azimuth direction of 0° and elevation direction of 6°. As [4] does not address what kind of beamform the DUT is transmitting during the OTA spurious emission measurement, this would be chosen as the default. The third measurement has the DUT transmitting a beam that is turned in the azimuth direction 50 degrees towards the CLTA as depicted in Figure 20. This is the manufacturer specified maximum turn in the azimuth direction for the chosen DUT and it serves to demonstrate the effect of beamforming on spurious emissions. Additional measurement rounds could be done where the beam is for example turned 50 degrees away from the CLTA or steered in elevation direction. However, due to time constraints they were left out of the test plan's scope. It is important to note that

only the second measurement is necessary for fulfilling the 3GPP defined test case. The reference measurement is important for verifying the test environment if such a measurement has not been done before in the chosen test environment. The measurement rounds for steered beams can potentially reveal additional emissions transmitted through the DUT antenna. In a real site scenario mMIMO radios are steering beams continuously, so it is intuitive to explore effect of beam steering on interference towards co-located BS equipment.

The CLTA antenna port is measured for any unwanted emissions coupling from the DUT. A diplex filter depicted in Figure 20 is used to filter out the n41 operating band of the DUT and route those frequencies into a passive load. The rest of the frequencies are amplified with an LNA and fed to the FSW spectrum analyzer. The FSW is controlled by test automation software running on the measurement PC. Test automation will measure all frequencies that are applicable according to Section 3.4.1 and within the current CLTA antenna's frequency range. The frequencies in [4] that aren't applicable for the DUT or that the chosen CLTAs don't support are listed in Table 10. The measurement data for each measured frequency range will be saved as a CSV file containing the measurement result in dBm for each frequency point. A screenshot of the FSW GUI will also be taken automatically for each frequency sweep.

Table 10. Frequency ranges excluded from the measurement

| **Type of co-located BS** | **Frequency range for co-location requirement** | **Reason for exclusion** |
|---|---|---|
| UTRA FDD Band VII or E-UTRA Band 7 or NR Band n7 | 2500 – 2570 MHz | Frequencies are within OBUE mask: $(f_{low} - \Delta f_{OBUE}) < f < (f_{high} + \Delta f_{OBUE})$ |
| UTRA TDD Band d) or E-UTRA Band 38 or NR Band n38 | 2570 – 2620 MHz | Frequencies are within OBUE mask: $(f_{low} - \Delta f_{OBUE}) < f < (f_{high} + \Delta f_{OBUE})$ |
| E-UTRA Band 41 or NR Band n41 | 2496 – 2690 MHz | Frequencies are within OBUE mask: $(f_{low} - \Delta f_{OBUE}) < f < (f_{high} + \Delta f_{OBUE})$ |
| E-UTRA Band 46 | 5150 – 5925 MHz | Not applicable for WA BS. |
| E-UTRA Band 51 or NR Band n51 | 1427 – 1432 MHz | Not applicable for WA BS. |
| E-UTRA Band 53 or NR Band n53 | 2483.5 – 2495 MHz | Frequencies are within OBUE mask: $(f_{low} - \Delta f_{OBUE}) < f < (f_{high} + \Delta f_{OBUE})$ |
| E-UTRA Band 71 or NR Band n71 | 663 – 698 MHz | Not supported by chosen CLTAs. |
| E-UTRA Band 72 | 451 – 456 MHz | Not supported by chosen CLTAs. |
| NR Band n77 | 3.3 – 4.2 GHz | Not supported by chosen CLTAs. |
| NR Band n79 | 4.4 – 5.0 GHz | Not supported by chosen CLTAs. |

## 4.5 Test management and execution

In this section the planned steps of executing the measurements outlined in Section 5.4 are discussed. Originally the plan was to have two weeks to conduct the two measurements, but it turned out due to other R&D needs that the CATR chamber could only be booked for one week. This meant the content of the test plan needed to be reviewed to fit it into seven (7) days. To achieve this, not all the antennas in each CLTA could be measured and measurements at different RET angles could not be done in either of the two measurements. Instead, only antennas required for frequency coverage in the co-location spurious emissions highlighted in Figure 11 would be measured. In addition, studying the effect of RET angles was reduced to only the middle point of each antenna in the isolation measurement and all spurious emission measurements would be done with the default RET angle. The planned measurement schedule is shown in Table 11. The preparations include building the measurement setup inside of the chamber, calibration of the measurement setup and configuring the test automation software. Software preparations for both test automation and the DUT along with gathering all the required equipment is done as much as possible beforehand.

Table 11. Planned schedule for the measurement

| Time | Day1 | Day2 | Day3 | Day4 | Day5 | Day6 | Day7 |
|---|---|---|---|---|---|---|---|
| 8-12 | Isolation measurement preparations | CLTA A 8/14 ports | CLTA A 14/14 ports - Switch to CLTA B | CLTA B 8/12 ports | Check data - Potential re-tests | Co-loc measurements | Check data - Potential re-tests |
| 12-13 | Lunch | Lunch | Lunch | Lunch | Lunch | Lunch | Lunch |
| 13-17 | CLTA A 4/14 ports | CLTA A 12/14 ports | CLTA B 4/12 ports | CLTA B 12/12 ports | Co-loc measurement preparations | Co-loc measurements | Tear down setup |

### *4.5.1 Calibration*

In both measurements the power at the CLTA antenna port is to be measured, so the reference plane needs to be moved from the measurement device port to the CLTA antenna port. In the isolation measurement, the port 1 reference plane also needs to be moved to the Vivaldi antenna port. To move the reference plane, the losses, and gains of the components between said ports need to be measured across the frequency range of the measurement. This calibration of the measurement setup is done with a VNA through measurement, where both ends of the calibration plane are connected to different VNA ports.

The calibration plane ends are shown for the isolation measurement and co-location measurement in Figure 16, Figure 17 and Figure 20, respectively. In the isolation measurement, this calibration data is stored on the ZNL6 VNA and all measurement results will have the cable losses compensated for. This way the measurement result will be the S21 between the Vivaldi antenna port and CLTA antenna port. In the co-location measurement, the calibration data is measured by the test automation software using a ZVL VNA. A different VNA was used for this calibration due to the automation software not supporting the ZNL6. The calibration data

is then used by the automation software to compensate for the cable losses, losses in the diplex filter and LNA, and the gain of the LNA.

### *4.5.2 CLTA & Vivaldi isolation measurement*

The setup phase for the isolation measurement was estimated to take up to 4 hours based on previous experiences of building similar measurement setups. The preparation steps were planned as follows:

1) Verify that control of the VNA within the CATR chamber from the measurement PC is up and running and that all required connections from inside the chamber to the outside are functional.
    a. Run VNA self-alignment/self-calibration
2) Move CLTA into chamber radome facing upwards on a surface where it is practical to orient the Vivaldi antenna next to it.
    a. for example, two tables with wheels.
3) Prepare markings for the different measurement points along the length of the CLTA.
4) Prepare necessary connections between CLTA and VNA port 2.
    a. For multi-band CLTA, terminate all ports except the one connected to VNA.
5) Orient the Vivaldi against the first measurement point so that
    a. It is orthogonal to the vertical edge of the CLTA
    b. The centre is approximately on the same plane as CLTA radiators
        i. Orienting to radome plane can be easier option if knowledge of CLTA radiator plane is insufficient.
6) Prepare necessary connections between Vivaldi and VNA port 1.
    a. If VNA has more than 2 ports, connect both polarities of the Vivaldi to separate VNA ports
7) Calibrate the VNA reference plane to CLTA and Vivaldi antenna ports by performing through measurement.
    a. S11 and S22 calibration should also be done if calibration kit is available.
8) Setup S21 measurement on the VNA.
    a. Frequencies from 1 GHz to 6 GHz (Vivaldi frequency range)
9) Run a few test measurements while adjusting measurement settings to find best possible accuracy, dynamic range, and reasonable sweep for the VNA.

The first measurement point will be at either end of the CLTA. The measurement phase itself consists of the following steps:

1) Measure S21 between CLTA antenna port and Vivaldi antenna port
    a. S11 and S22 should also be measured, if possible
    b. If VNA has more than 2 ports, measure both polarities of Vivaldi at the same time
        i. Result from Vivaldi element orthogonal to CLTA length $L$ will be the 0° rotation result, the other 90° rotation result.
2) If measurement position is at the approximate centre of the antenna element, run S-parameter measurement for minimum and maximum RET angles for the given CLTA antenna. Otherwise skip to next step.
3) Rotate Vivaldi to next offset angle.

4) Repeat from step 1) until all Vivaldi offset angles have been measured.
5) Move Vivaldi to next measurement point along the length of the CLTA.
6) Repeat from step 1) until all measurement points along the length of the CLTA antenna have been measured.
7) Change CLTA antenna port:
    a. to the cross-polarity port for the same CLTA antenna.
    b. if both polarities of current CLTA antenna already measured, switch to a port of an unmeasured CLTA antenna.
8) Repeat from step 1) until all antenna ports of the CLTA have been measured.
9) Change to next CLTA.
10) Repeat from step 1) until all CLTAs have been measured.

The measurement data is carefully categorized according to CLTA, CLTA antenna, per RET angle and per polarity using file naming conventions and folder structures on the measurement PC. This is important so that the MATLAB analysis script in Appendix 1 can find the correct files for categorizing and parsing the data. The MATLAB script is introduced and discussed in Section 5.6. The data is saved in s1p file format, which contains the S21 magnitude in dB and phase in degrees for each frequency point.

### *4.5.3 Co-location measurement*

The preparation phase of the co-location measurement was also estimated to take around 4 hours, but as this is the first time the mechanical supports are used it is possible it will take longer. Preparations regarding test automation software installation and configuration are done beforehand. Dimensions of the DUT and CLTA should be measured prior to preparations as well. This is for adjusting the brackets to offset their height difference and brackets can be attached to correct points along the side supports. CLTA B consists of two modules with different dimensions, so adjustments offsets for both modules need to be done separately. CLTA B also requires two side supports and adjustable brackets per module, so installing it will take a more effort compared to CLTA A. The preparation steps are as follows:

1) Compensate for height difference of the DUT and CLTA from radome surface to the adjustable bracket attachment point behind the DUT/CLTA.
    a. In addition to adjustable brackets, by attaching the side supports of the CLTA and DUT to different sides of the main pole (top, side or bottom) additional 80mm or 160mm offset is possible. Therefore, in calculations below the required offset is given in format:
        i. <offset with main pole attachment> + <offset with adjustable bracket>
        ii. Negative offset implies CLTA needs to be lowered compared to DUT
    b. DUT height: 18 cm
    c. CLTA A height: 34.5 cm
        i. (18 – 34.5) cm = -16.5 cm -> 16 cm + 0.5 cm
    d. CLTA B
        i. top module height: 45.5 cm
            1. (18 – 45.5) cm = -27.5 cm -> 16 cm + 11.5 cm
        ii. base module height: 27 cm
            1. (18 – 27) cm = -9 cm -> 8 cm + 1 cm

2) Attach side supports to the positioner main pole accounting for the offsets required in step 1).
3) Attach adjusted brackets on to the side supports in points determined by the radome width of the DUT and CLTA, so that the physical gap between them is (10 ± 1) cm
    a. Distances from radome centre to vertical edge:
        i. DUT: 27.3 cm
        ii. CLTA A: 25 cm
        iii. CLTA B: 22.5 cm
    b. DUT and CLTA bracket middle point distance required:
        i. DUT & CLTA A: 52.3 cm + 10 cm = 62.3 cm
        ii. DUT & CLTA B: 49.8 cm + 10 cm = 59.8 cm
4) Use chamber crane to lift the CLTA on top of the adjustable brackets and attach CLTA to them.
5) Use chamber crane to lift the DUT on top of adjustable brackets and attach the DUT to them.
6) Check that radomes of the CLTA and DUT are aligned within ± 1 cm of each other, adjust with help of chamber crane if necessary.
7) Check that the gap between CLTA and DUT is (10 ± 1) cm, adjust with help of chamber crane if necessary.
8) Prepare necessary RF connections between first CLTA port to be tested, diplexer, LNA and spectrum analyzer.
9) Terminate all other CLTA antenna ports.
10) On the measurement PC, commission the DUT to transmit 2xNR40 and place one carrier at the bottom and the top of the $M_{RFBW}$ as defined in subclause 4.9.1 of [4].

The preparation phase steps need to be done separately for each CLTA. However, it will take a shorter time after the first CLTA has been measured, as the setup will not need to be built from the ground up. The measurement steps:

1) Activate downlink test model NR-FR1-TM1.1 and uplink test model G-FR1-A1-5 RB0.
    a. UL testmodel activation is needed purely for beamforming calibration cycle to start running on the DUT.
2) Run spurious emissions testcase in test automation for all frequency ranges within the operating frequency range of the connected CLTA antenna port.
3) Deactivate DL&UL test models. Switch RF cable to the xpol antenna port and terminate the already measured copol port. Repeat step 1) and 2) for xpol antenna port.
4) Deactivate DL&UL test models. Switch RF cable to the next CLTA copol antenna port. Repeat from step 1) until all required CLTA antenna ports have been measured.
5) Deactivate DL&UL test models. Remove the current CLTA and go through the preparation phase for the next CLTA. Repeat from step 1) until all CLTAs have been measured.

For the 3GPP defined test case step 5) would only be repeated until all frequency ranges required in [4] have been measured. For this thesis it was important to compare the two chosen

CLTAs and thus the same frequency ranges are measured with both. As mentioned in Section 5.4, the measurement would be done three times per CLTA. First a reference measurement with the DUT depowered, then with a boresight beam and finally a horizontally steered beam. The results are saved by test automation in CSV format on the measurement PC along with a screenshot of the frequency sweep.

## 4.6 Result analysis

As is evident from the previous sections, both measurements would provide a large amount of data for analysis. Both measurements would require their own analysis methods as both the quantity being measured, and the parameters used to group data are not completely the same. For the isolation measurement the goal was to find what parameters the isolation between the two antennas is most sensitive to. A statistical analysis approach was chosen where the data is categorized into different subsets. These subsets would then be compared, and findings would be used to split them into finer subsets and iterate on the analysis further. For the co-location measurement the results failing to meet the requirements in [4] would be highlighted and inspected. The reference measurements are to be used as a baseline for analysis and comparison of the two DUT beam steering configurations. Results between CLTAs and antennas within the CLTA would also be compared.

### *4.6.1 CLTA and Vivaldi isolation analysis*

Categorizing the data into subsets was determined as the key to determining what parameters have the most effect when it comes to the isolation between the Vivaldi and CLTA antennas listed in Figure 11. The data for CLTA A and CLTA B would be analysed separately and compared. The parameters used for categorizing the data and the number of subsets it splits the data into are shown in Table 12.

Table 12. Parameters used for grouping isolation measurement data and data subset count

| Parameter | Number of data subsets | |
|---|---|---|
| | **CLTA A** | **CLTA B** |
| CLTA Antenna | 5<br>(Lr1, Ry3, Lb1, Ly1, p1) | 4<br>(R1, B1, Y1, Y2) |
| Antenna polarity | 2 per antenna | |
| Vivaldi position | 9 for LB antenna Lr1<br>5 for Ry3, Lb1, Ly1, p1 | 9 for LB antenna R1<br>6 for B1, Y1, Y2 |
| RET Angle | 3 per middle measurement point of antenna. | |
| Vivaldi rotation | 3 per measurement point of antenna. | |
| Frequency | 1-6 GHz range split into 5 parts of equal width. | |

In practise the parameters in Table 12 are reflected in the folder structure and filenames for each measurement data file shown in Figure 21. The folder structure will allow the MATLAB script used for analysis shown in Appendix 1 to find the files specific to a CLTA, CLTA antenna and polarity of said antenna. From the filename the script can parse the rest of the parameter values to further categorize the data into subsets. The RET angle parameter is only included in

file name when middle point of the antenna is being measured. The information at the end of the file name is ignored by the script but can be useful if manual sorting of data is required.

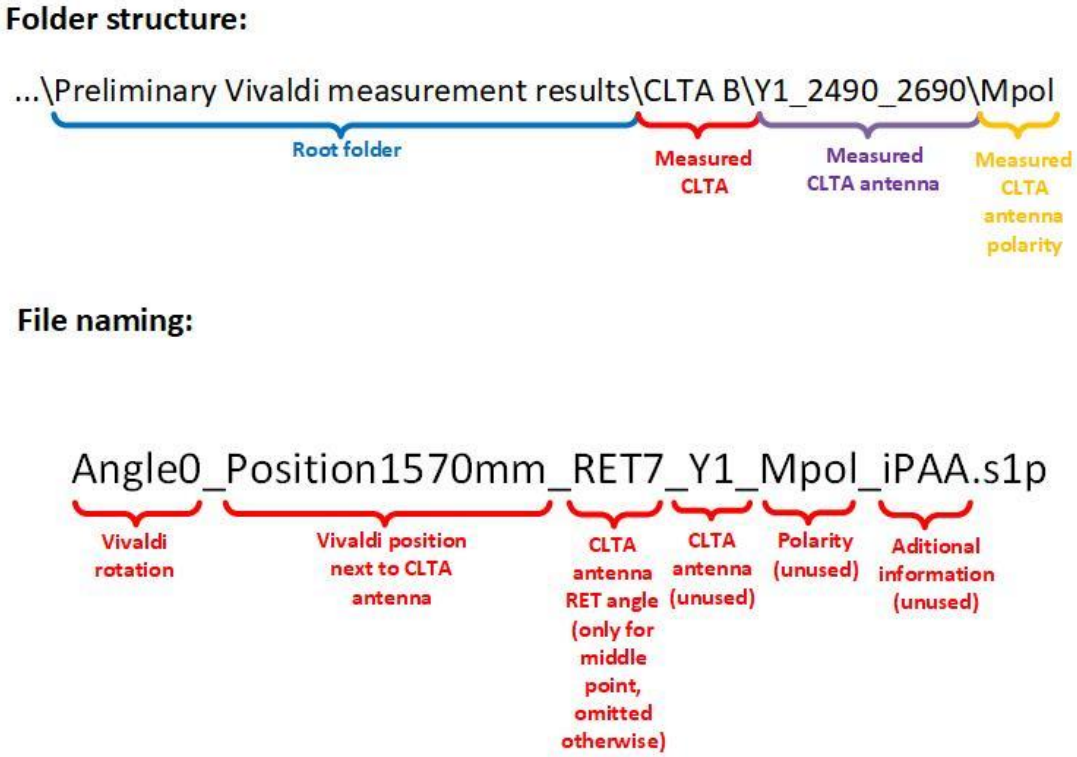


Figure 21. File path and naming conventions used for isolation measurement data.

Once the data has been grouped according to the above parameters the formed subsets of data need to be analysed and displayed graphically. The characteristics that are inspected per subset of data were chosen as:

- Mean isolation ($\mu$)
- Maximum isolation (omitted)
- Minimum isolation
- Standard deviation ($SD$)
- Median isolation
- Kurtosis ($K$) of the distribution:

$$K = \frac{E(x-\mu)^4}{\mathrm{SD}^4} \tag{3}$$

- Skewness (S) of the distribution:

$$S = \frac{E(x-\mu)^3}{SD^3} \tag{4}$$

- Percentage of isolation values above 30 dB.

The maximum isolation was later deemed to not be an interesting characteristic for the data, as the focus of this measurement was on finding the worst-case isolation. For this reason, it was omitted from the analysis and the focus was on average and minimum isolation. Comparing to

the 30 dB minimum isolation assumed in 3GPP [18] in reference to results in [19] is deemed relevant for studying the validity of the assumption. Different solutions for graphically displaying these characteristics of the data subsets were studied and iterated on. For the Vivaldi position a set of line graphs shown in Figure 22 was chosen to represent how the isolation changes at different positions along the length of the CLTA per element. Separate plots were done for both polarities and each Vivaldi rotation. The markings "Element Top", "Element Middle" and "Element Bottom" refer to the orientation of the CLTA antenna being measured. "Bottom" refers to the end of the antenna closest to the antenna connectors and "Top" to the opposite end of the antenna. The Vivaldi position on the x-axis has been normalized with the approximated CLTA antenna size so it is easier to plot and compare the results of different sized antennas in the same graph.

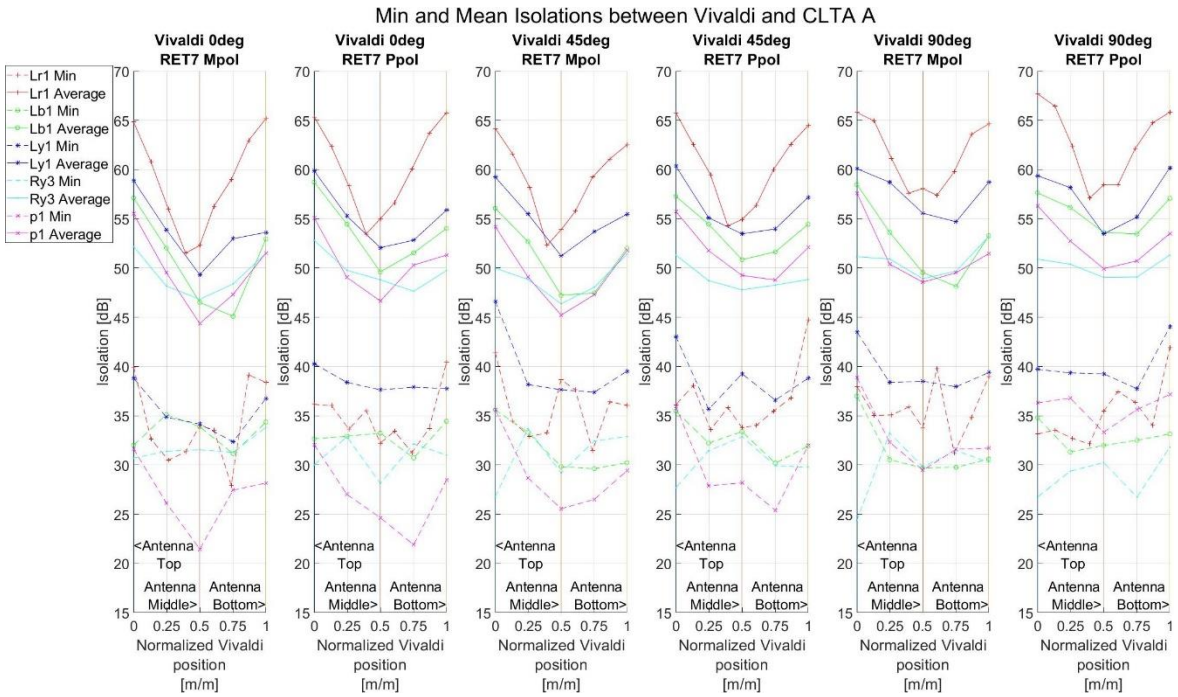


Figure 22. Example plot for minimum and mean isolation behaviour as a function of Vivaldi position.

Already in the planning phase for this measurement it was known that the amount of data for different CLTA RET angles was going to be small compared to other parameters. Thoroughly analysing the statistical characteristics of such a small subset of data could prove misleading, so a simplified bar graph presentation was chosen. In Figure 23, the data is split by polarities to different plots and two 2-part bars are plotted for each RET angle. The smallest RET angle is denoted as "minRET", the default RET angle as "defaultRET" and the largest RET angle as "maxRET". The numerical minimum, default and maximum RET angle values depend on the CLTA antenna in question, so this denotation is used for generalization. The left bar denoted as "MIN" is analysed from the minimum isolation values for each S21 measurement done for the given RET angle. The right bar denoted as "MEAN" is analysed from the mean isolations of each S21 measurement done for the given RET angle. The smallest and largest values from the data subset are shown in the orange and blue part of the bar, respectively. This is to depict the range in which the minimum isolation or mean isolation can vary between elements and across frequency for the given RET angle. If the RET angle has a significant effect on isolation, it should be visible in the ratio of the blue and orange portions or

the height between the bar graphs for different RET angles. The data was split by polarities to see if one polarity is more susceptible to any potential effect of RET angle.

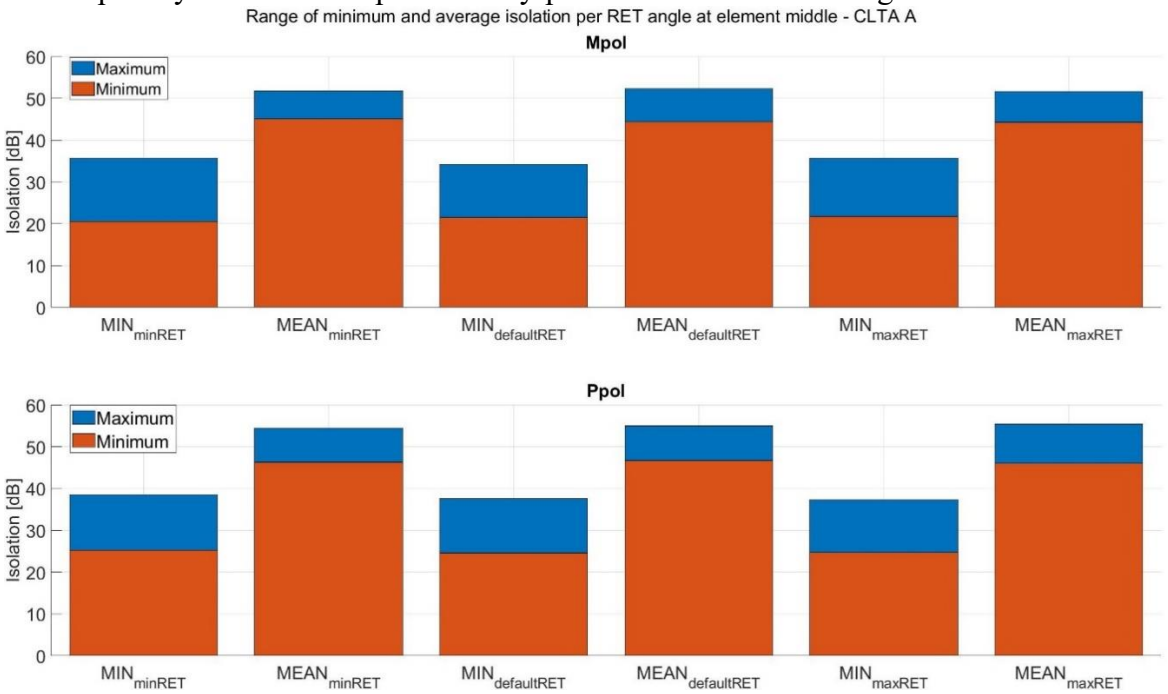


Figure 23. Example of bar graph for comparing isolation at different RET angles.

For the larger subsets of data, the isolation values will be distributed across a wide range of values. The characteristics of said distributions is analysed like shown in Figure 24 to be able to compare the subsets. The entire dataset for a given CLTA is inspected first and from there different subsets are analysed and compared to the entire dataset but also to each other. Any outlier subsets found are used for establishing which parameters the isolation is most sensitive to.

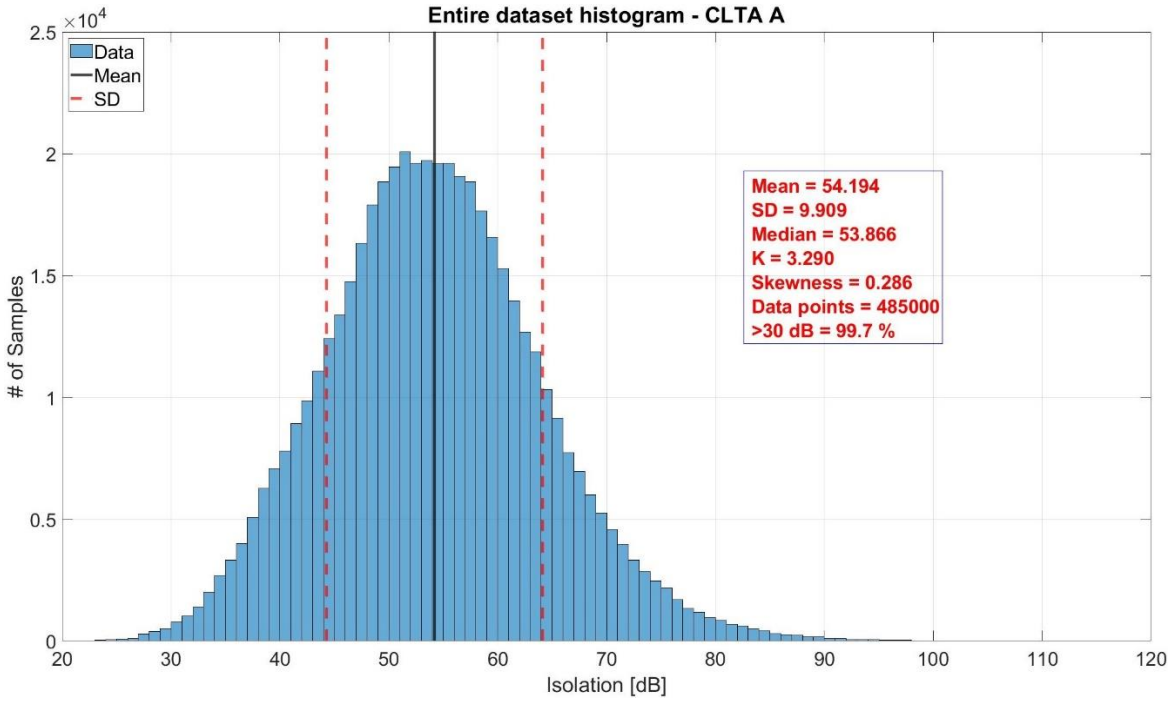


Figure 24. Example of histogram for analysing data subsets.

### *4.6.2 Co-location measurement*

The co-location measurement results are analysed in a less thorough and more selective manner compared to the isolation results. The focus is on any failing test cases, inconsistencies, or outliers in the test results. There are also less parameters that are changing between measurements compared to the isolation measurement.

In the measurement process described in Sections 5.4.2 and 5.5.3 each CLTA antenna port is measured separately. As mentioned in Section 3.4.1, the final measurement result will be the sum of all supported polarities of the CLTA antenna. For this purpose, the Python script in Appendix 2 was written based on the flow chart shown in Figure 25. From test automation the data will be gathered in folders per CLTA antenna and in separate folders for each polarity. The data from each frequency sweep applicable for the CLTA antenna is stored in a separate .csv file. The files include trace data for the frequency sweep consisting of power and frequency. The Python script extracts the frequency range from a co-polarity data file's name and uses it to pair the file with an equivalent cross-polarity data file. The results in both files are converted from dBm to Watts, added together, and converted back to dBm. From the summed values the maximum power sum is saved along with the measurement frequency point. The polarity sum maximums per frequency sweep are gathered and written into a .csv file which contains the frequency range, the maximum power result and frequency point. These per CLTA antenna results are then analysed against the requirements in [4] with Excel.

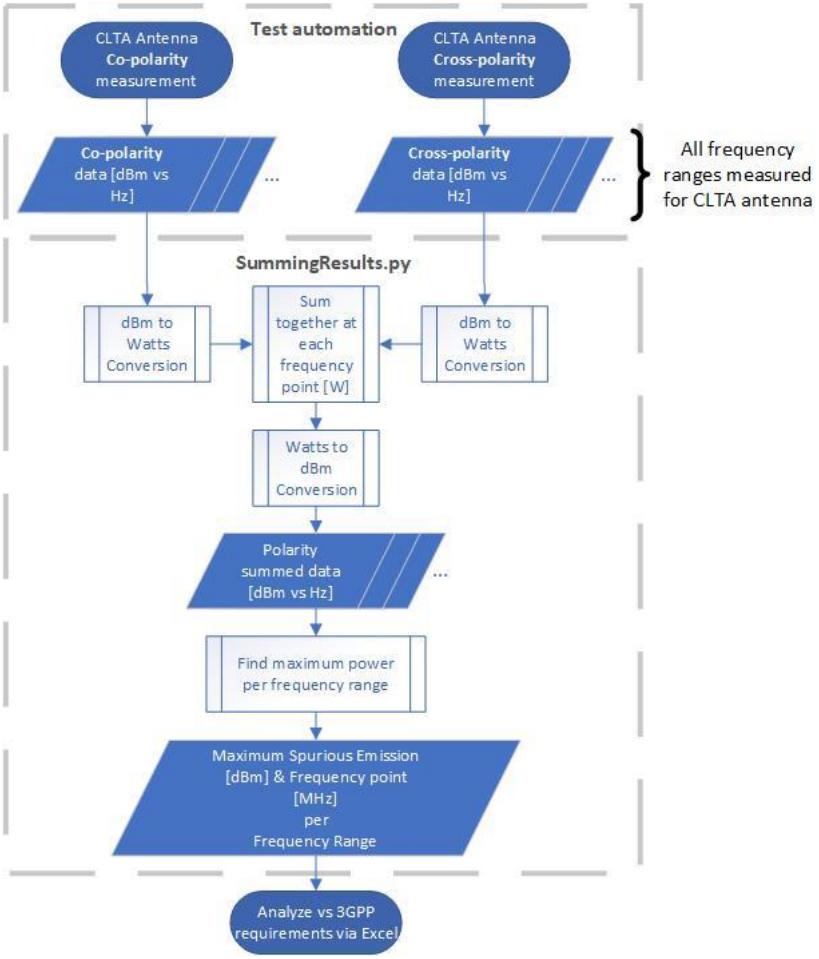


Figure 25. Flow chart for spurious emission result analysis.

# 5 TEST PROGRESS AND RESULTS

This chapter describes the realisation of the planned measurements and presents the highlights of the results. In practise, the measurements took a total of 8 days with two days of rest after the first 5 days, which was made possible by changes in R&D schedule during the first week. The overall preparations made leading up to the measurements are described in Section 6.1. The isolation measurement discussed in Section 6.2 was done first so that any findings from it could be accounted for in the spurious emission measurement or for additional measurements. Lastly, in Section 6.3 the co-location spurious emissions measurement progression and results are presented.

## 5.1 Measurement preparations

Most of the preparations were down during weeks 33-34 leading up to the start of the measurements. Significant amount of time was spent gathering and transporting the required hardware components, cabling, terminations and CLTAs to the chosen CATR chamber. The automation scripts available from a previous study for the ZNL6 were studied, but it turned out they would have required significant additions to be beneficial. It was evaluated that there was not enough time for the required modifications, so configuration and control of the ZNL6 was done manually through remote desktop instead. Settings for the ZNL6 for S-parameter measurement were set as:

- Start frequency: 600 MHz
- Stop frequency: 6 GHz
- Signal power: 0 dBm
- Measurement bandwidth: 1 kHz
- Number of measurement points: 2700
    - Frequency step: ~2 MHz

The start frequency was 600 MHz because of faulty information that the Vivaldi operation frequency range started from 600 MHz instead of 1 GHz. This would be corrected in MATLAB analysis by excluding the measurement data below 1 GHz from analysis. The signal power was set to its maximum to retain dynamic range of the measurement since the isolation was expected to be high especially at the far ends of the antennas. The measurement bandwidth and number of measurement points were iterated on until a suitable compromise between accuracy and measurement time was reached.

Due to lacking documentation by the manufacturer of CLTA A regarding the four p1 antenna positions, an initial isolation measurement shown in Figure 26 was done. The p1 antennas are named Ant1, Ant2, Ant3 and Ant4 based on the labels on their respective connectors. It was known from previous users of CLTA A that Ant1 and Ant4 are the ones closest to the edge, but it would need to be measured which one is on which edge. The Vivaldi was moved do different edges on the radome surface and isolation between it and the p1 antennas Ant1 and Ant 4 was measured in 2.3 – 3.8 GHz frequency range.

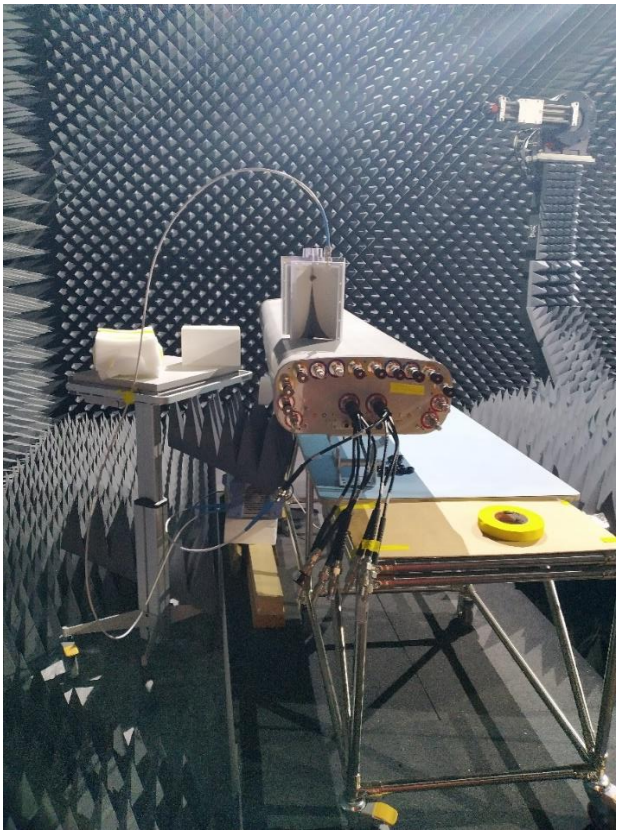

Figure 26. Initial CLTA A measurement for finding p1 antenna positions.

When the Vivaldi was placed on the left side of the radome as in Figure 26, the isolations for both polarities of p1 Ant1 were 5-10 dB higher compared to both polarities of p1 Ant4. Likewise, when the Vivaldi was placed on the right side the isolations for both polarities of p1 Ant4 were 5-10dB higher compared to both polarities of p1 Ant1. It was thus concluded that Ant4 is on the left side from the radome front perspective, and it would be the p1 antenna measured.

Preparations for the spurious emissions measurement were done as well in the weeks leading up to the isolation measurement. As much of the CLTA support assembly as possible was done beforehand, so that attachment to the main pole of the positioner would be easier when the spurious emission measurements are started. This included removing the main pole from the positioner to insert extra T-slot nuts into the tracks for attaching the CLTA supports. Frequency ranges to be measured needed to be mapped to specific CLTA antennas so that there is no overlap and test automation configuration files could be prepared.

### 5.2 CLTA and Vivaldi isolation measurement

The measurements were started on schedule starting on Monday 30.8.2021. During the planned 4hour preparation phase calibrating the test environment was done and the physical preparations were done for the setup of Figure 12. No calibration kit was available at the time for the ZNL6, so phase calibration for the measurement instrument could not be done. However, it wasn't deemed a necessity for S21 measurements. Calibration of the ZNL6 vector network analyzer was done with the following settings:

- Channels to be calibrated: Ch1, Ch2
- Ports: P1, P2
- Type of calibration: Trans Norm Both
- Connector: N 50 Ω
- Gender: Female
- Cal Kit: N 50 Ω Ideal

Physical measurement points were marked with tape along the length of both CLTAs with the top of the antenna chosen as the zero point. The measurements were started with CLTA A low-band antenna Lr1 with measurement points from the top end of the antenna being: 0cm, 27.5 cm, 55.0 cm, 82.5 cm, 105.0 cm, 127.5 cm, 155.0 cm, 182.5 cm and 210.0 cm. In each of these measurement points the isolation was measured at Vivaldi rotations 0°, 45° and 90°. Based on initial results it was determined that Vivaldi rotation 0° seemed to have the lowest isolation for Lr1, so it was chosen for the RET measurements at the middle point of the antennas. This was to further cut down the test content so that measurements could be carried out on schedule and reduce complexity of the already limited RET related data. Measurement of the first polarity for Lr1 antenna took approximately three (3) hours, but the second polarity took only 1 h 20 min as the methods became more familiar and adjusted.

During Lr1 antenna measurements it was noticed that the measurement points were not evenly distributed, so for the rest of the antennas they were adjusted to: 0 cm, 26.0 cm, 52.5 cm, 79.0 cm, 105.0 cm, 131.0 cm, 157.5 cm, 184.0 cm and 210.0 cm. The measured antennas and corrected measurement points for both CLTAs are shown in Figure 11. For the shorter antennas of CLTA A the five (5) measurement points closest to the antenna were measured. For CLTA B the 79 cm point was also measured for a total of six (6) measurement points. It was included to better see how the joint between base and top module at 83 cm unique to the CLTA B affects isolation.

The following p1 antenna Ant4 measurement was done in three (3) hours. However, during the testing the soldering on the Vivaldi antenna's K-polarity SMA connector started breaking. This was due to the stress inflicted on the connector when rotating the Vivaldi with the RF cable attached. As a result the rest of the measurements were done with the Vivaldi's N-polarity element and the RF cable was disconnected when changing the Vivaldi rotation. As both radiating elements of the Vivaldi are identically manufactured, this should not cause significant deviation in results before and after this change. When adjusting the RET of the CLTA with the Kathrein PCA module, the Windows operating system on the attached laptop would crash when the PCA USB connection was disconnected. This was likely due to the old Kathrein PCA software not being compatible with Win10 operating systems or drivers. The workaround was to close the software before disconnecting the PCA USB cable from the laptop.

While MATLAB analysis script was not yet complete during the testing, the results were analysed briefly by hand during the measurements to try and pick up on any notable observations. One such observation was when Ry3 antenna Mpol measurement was done with Vivaldi angle 45° instead of 0° at the 52.5 cm middle point with RET angle set to 12°. From the S21 results in Figure 27 its seen that the isolation drops to 26 dB just below 1.4 GHz.

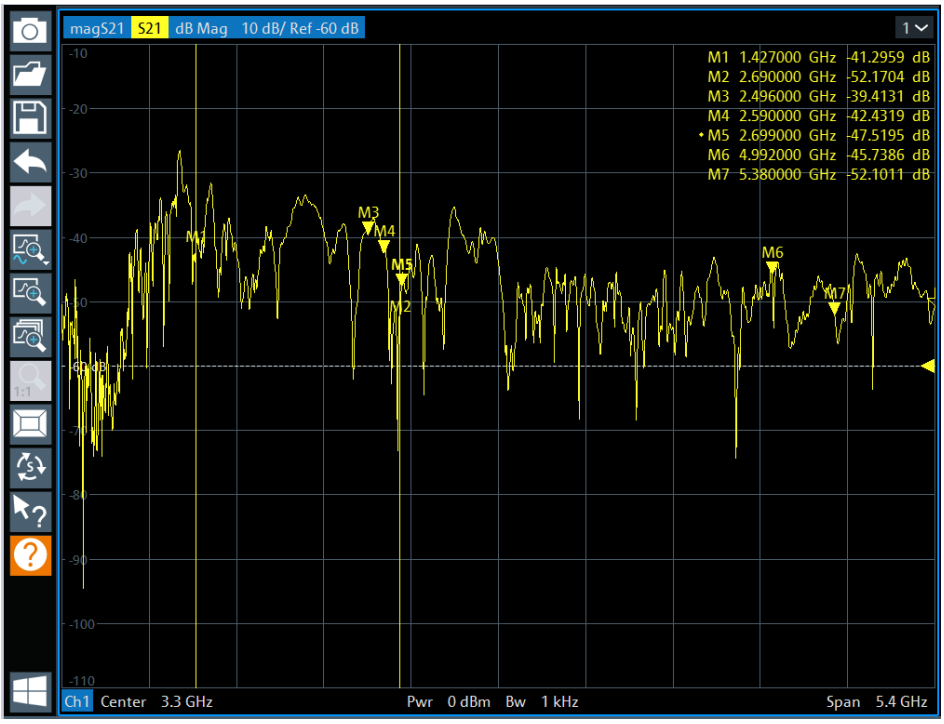


Figure 27. S21 measurement result for Ry3 antenna Mpol measurement point 52.5 cm at Vivaldi angle 45° and RET angle 12°.

Compared to the same measurement done with Vivaldi angle 0° shown in Figure 28 at the lower half of the measurement frequency several isolation points are 3-4 dB higher in Figure 27. Outlier results like this could suggest that the effect of RET angles on the isolation would be worth studying more thoroughly than was possible in the schedule and scope of this thesis.

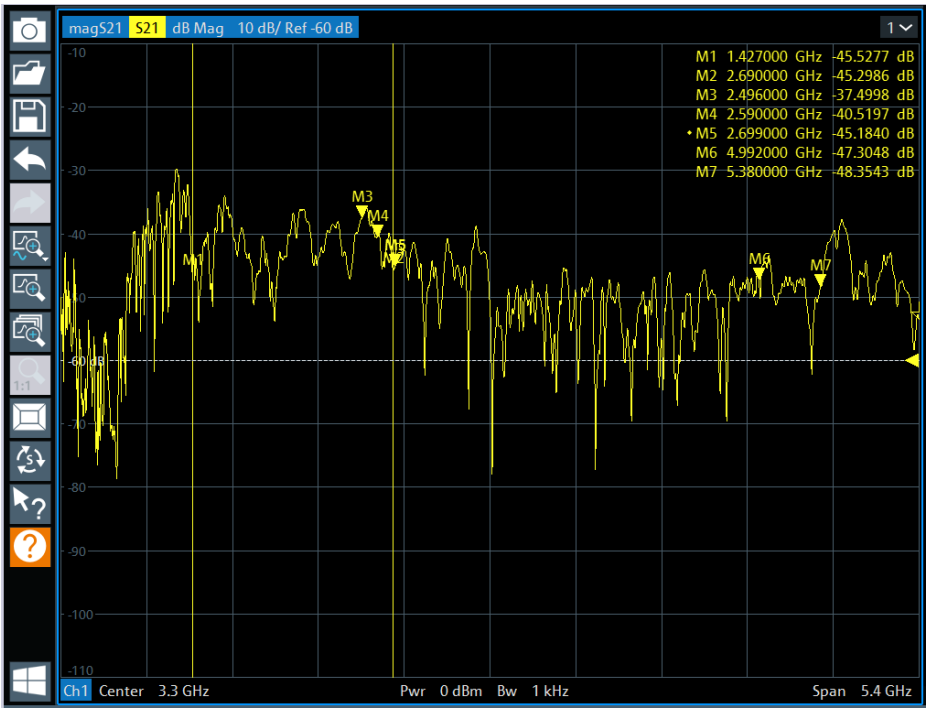


Figure 28. S21 measurement result for Ry3 antenna Mpol measurement point 52.5 cm at Vivaldi angle 0° and RET angle 12°.

At the start of CLTA B measurements required some time-consuming mechanical work to modify the brackets so that both modules are at the same level on the measurement table. Shortly after measuring the low-band antenna R1 the Vivaldi N-polarity SMA connector was also starting to break off. Some measurement time was lost to soldering it back by hand. For CLTA B there were no outlier results seen during testing, but in general the lowest isolations were observed to be below 2 GHz.

The s1p -format measurement data files for different RET angles were analysed with WinCal XE 4.5.1 during testing to try and determine the worst-case RET angles for each CLTA antenna. The RET angle that gives the most consistently low isolation across frequency band was chosen to be the worst-case RET. As the spurious emissions are only measured within each CLTA antenna's frequency range, the data RET angle analysis was also limited to the frequency range of the antenna in question. An example of analysis is shown in Figure 29 where for CLTA A antenna Ly1 RET angles 7° and 12° were showing the lowest isolation within Ly1 frequency range. The RET angle 12° was chosen out of the two as it gives a flatter behaviour. This analysis would be done for each CLTA antenna separately and chosen RET angles would then be used during the co-location spurious emission measurements.

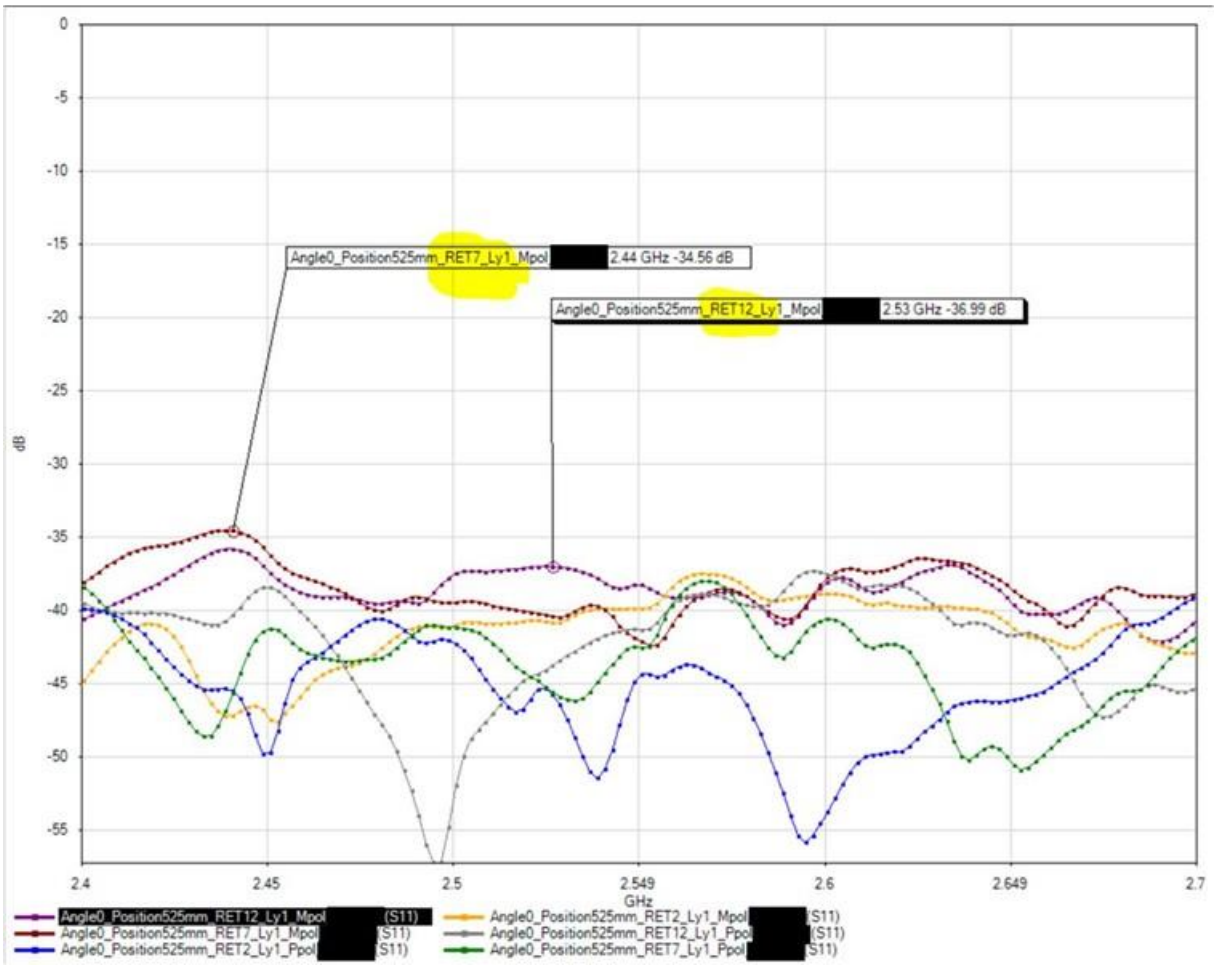


Figure 29. Isolation behaviour at different RET angles for CLTA A antenna Ly1.

### *5.2.1 Results*

The isolation measurement results were analysed using a MATLAB script discussed in Section 5.6 that was developed after the completion of both measurements. The script was exclusively developed for analysis of this measurement's results and continuously iterated on based on analysis results, so it better fits the purpose. Due to the large amount of data, statistical analysis was deemed the best approach to finding the key factors affecting antenna-to-antenna isolation.

The first approach is to illustrate how the isolation changes as a function of the position of the Vivaldi antenna. In Figure 22, these results are presented for CLTA A. At the middle point of each antenna the isolation is at minimum due to the Vivaldi antenna having the maximum amount of the CLTA antenna within its beam width. The average isolation minimums are not always at the middle point of the antenna. This can be due to the imperfect knowledge of the antenna middle points mentioned in Section 5.4.1. or some asymmetry in the placement of the CLTA antennas. The overall trend for the average isolation of all elements suggests that rotating the Vivaldi from angle 0° to 45° and 90° results in higher average isolation. A moderate exception is antenna Ry3 where this trend is not so clear, but when comparing angles 0° and 90° there is still a difference of several decibels. Another general observation is regarding polarity, since Mpol results tend to have lower isolation compared to the Ppol results. When comparing the antennas, Lr1 exhibits the deepest change in isolation from the ends of the antenna to the middle point while also having the highest overall isolation. The deep change is likely due to larger antenna size having more area for the Vivaldi to couple with and the Vivaldi having a wider HPBW at lower frequencies. The shorter high-band antennas are very similar, yet antenna Ly1 has the highest isolation overall while Ry3 and p1 exhibit the lowest isolation overall. The minimum curves are drawn from single data points and serve to give an indication on how low the isolation can go in each element and position.

The same analysis for CLTA B is shown in Figure 30. As mentioned in the previous section, there is an extra measurement point for the shorter antennas past the joint of the top and base modules. Compared to CLTA A there is no clear trend regarding Vivaldi rotation or polarity. The average isolation is more symmetrical across the length of CLTA B, whereas with CLTA A there can be a 4-5 dB difference between opposite ends of the antenna. The low-band antenna R1 has the highest isolation overall similarly to CLTA A antenna Lr1, but the change in isolation is the largest from the ends of the antenna to the middle. The higher frequency antennas are more in line with each other with antenna Y2 exhibiting lower isolation at its top half.

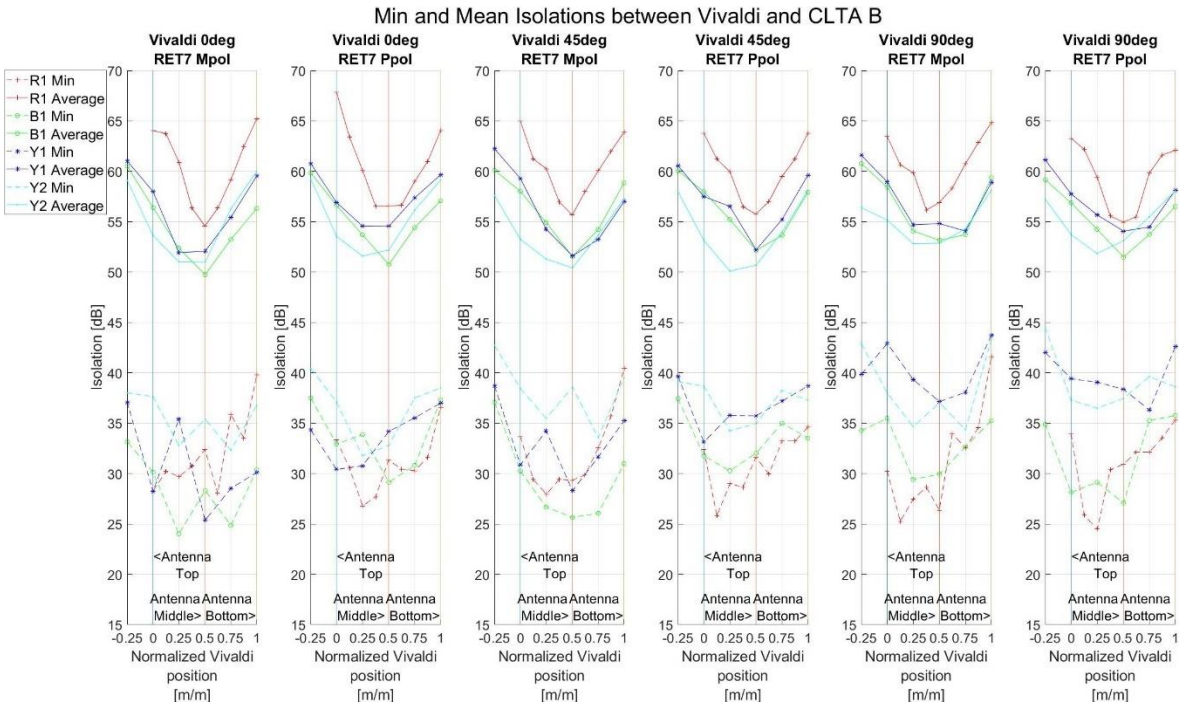


Figure 30. Isolation as a function of Vivaldi position for CLTA B.

Even though the data for different RET angles was limited a simple analysis of the data for CLTA A is shown in Figure 23. Within the same polarity the results are nearly identical. The Mpol results show lower isolation overall which is in line with observations from the previous line graphs. The RET angle data for CLTA B is analysed in Figure 31. Same as with CLTA A, the differences between RET angles within the same polarity's data are negligible. On the Mpol data there seems to be more variance in the minimum isolation for each RET angle. With more data from different measurement points along the CLTAs a more exhaustive conclusion could be made regarding the effect RET angle has on isolation.

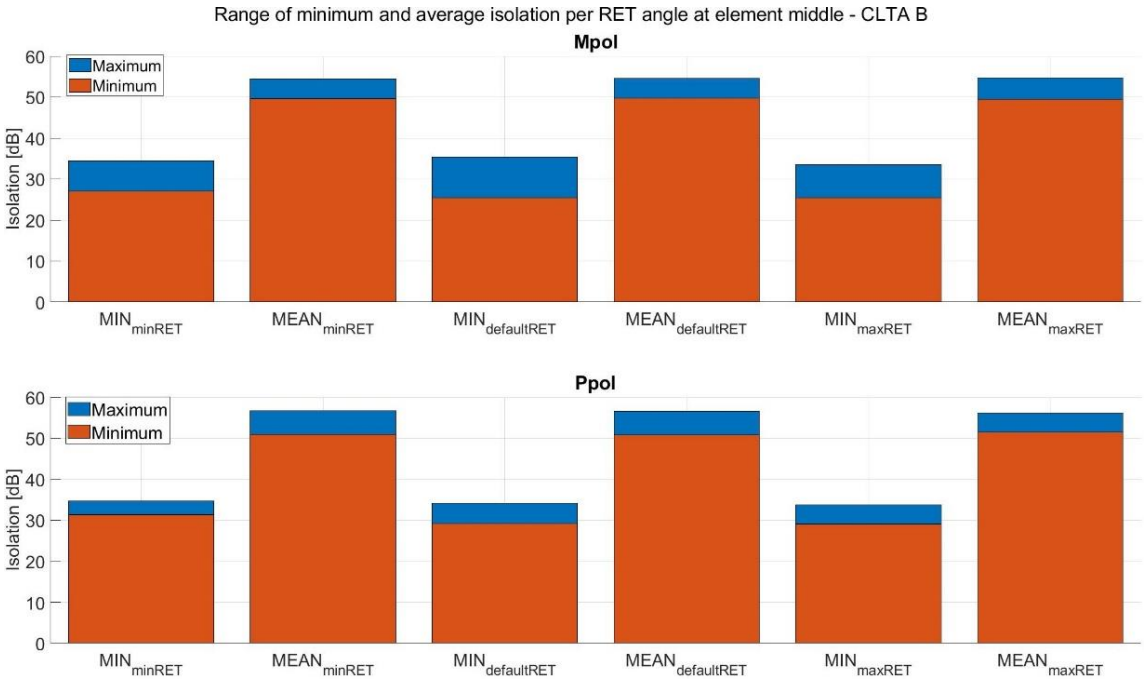


Figure 31. Isolation ranges of different RET angles for CLTA B.

The whole dataset histograms of CLTA A in Figure 24 and CLTA B in Figure 32 show that the data for both CLTAs follow normal distribution evident by kurtosis (K) close to three (3). CLTA B exhibits 2.5 dB higher mean and 3.1 dB higher Median along with zero skewness, but otherwise the distributions are very similar. The amount of data points is not the same because a total of five (5) CLTA A antennas were measured and compared to the four (4) CLTA B antennas. The shorter CLTA B antennas had six (6) physical measurement points while the shorter CLTA A antennas were measured at five (5) points.

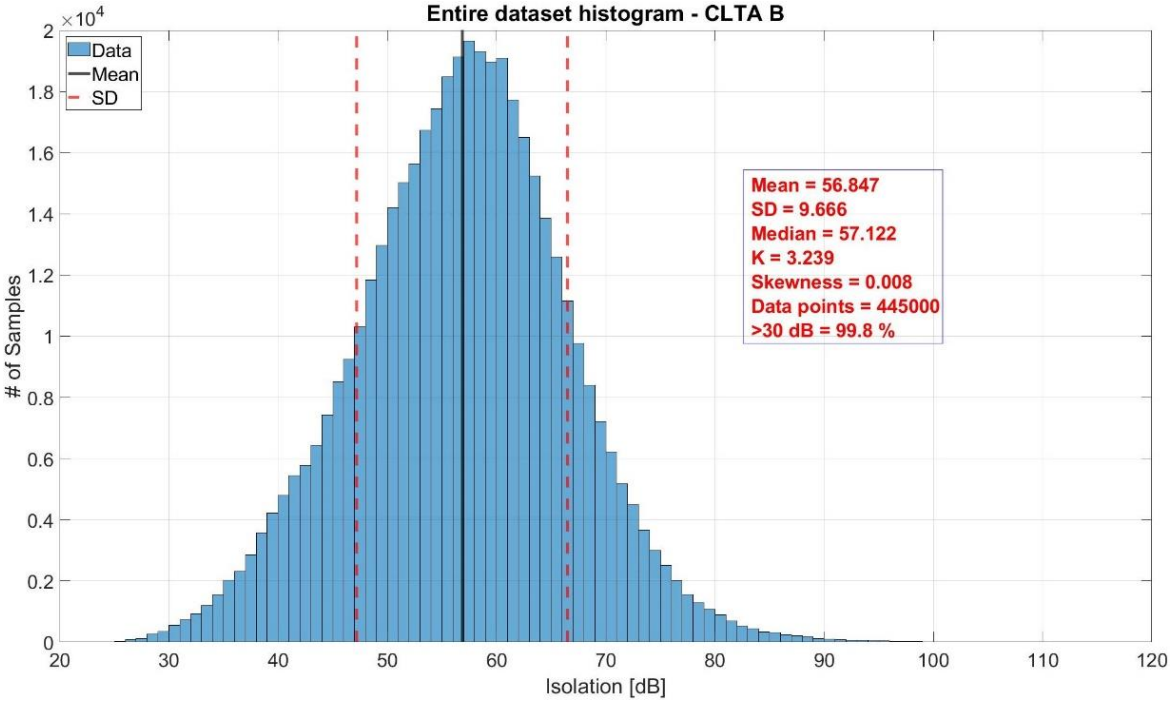


Figure 32. Entire dataset histogram for CLTA B.

In the histograms of Figure 24 and Figure 32 there is a "long tail" of data on the high isolation side which is causing skewness especially in the CLTA A data. These high isolation points can be observed in the frequency sweeps, an example of which is shown in Figure 33. Several points along the sweeps were observed where the S21 drops 20-40 dB between frequency points, meaning the isolation increases by that amount. It is evident in the histograms of smaller subsets later in this section that skewness is almost always positive due to these outliers. This brings to question how useful or interesting analysing the skewness of the data is. Noise cancellation or data filtering could have been potentially justified to dampen or remove the effect of these deep isolation points.

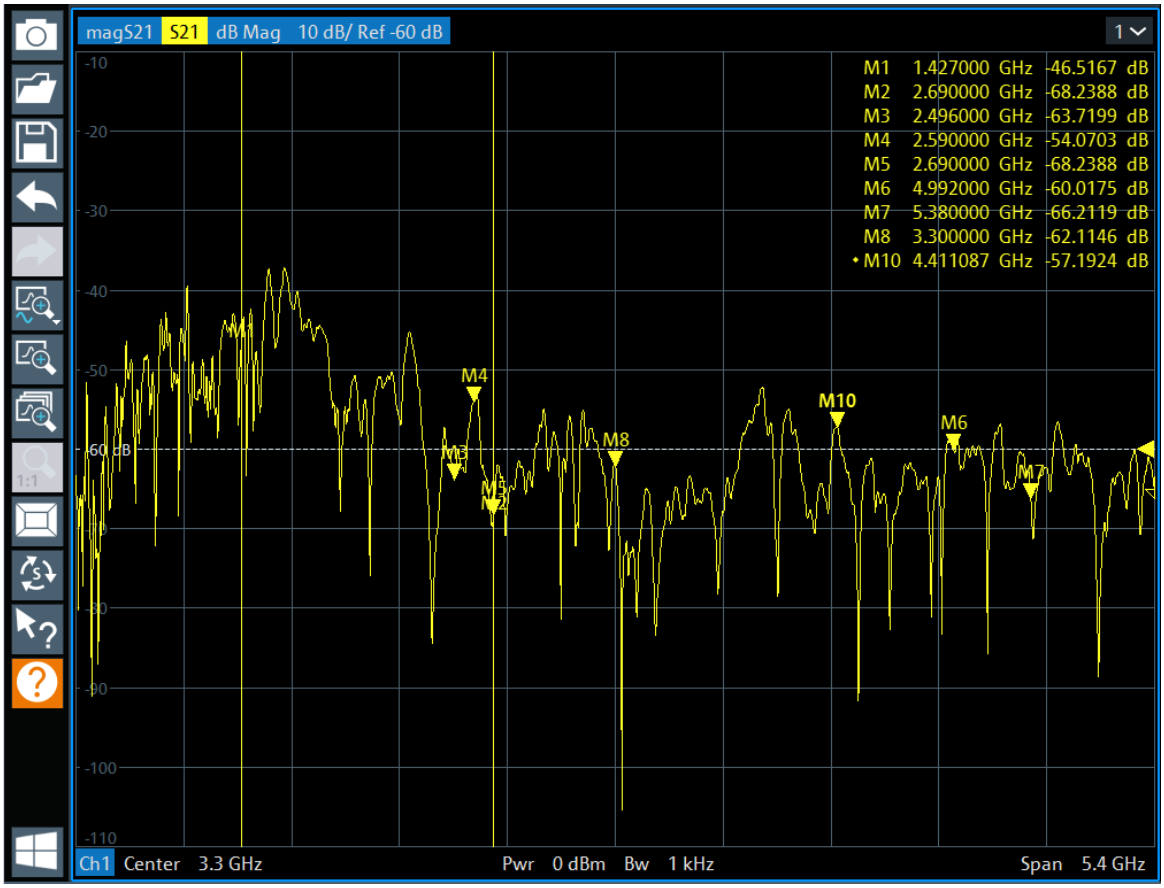


Figure 33. Example of high isolation dips in the frequency sweep.

The CLTA A data for RET angle 7° is split into subsets by Vivaldi rotation angle and polarity in Appendix 3 Figure 59. Mpol polarity has around 1 dB lower mean isolation on compared to Ppol. In line with the observation mentioned in Section 6.2.1, the Vivaldi rotation angle 0° exhibits the lowest mean isolation followed closely by angle 45°. Angle 90° has 1.7-2.3 dB higher mean isolation compared to the other two rotations. The same data subsets for CLTA B shown in Appendix 3 Figure 60 don't exhibit as clear differences between Vivaldi rotation angles or polarities. Distributions between datasets deviate very marginally with biggest difference being Mpol at Vivaldi rotation 90° having 0.6 dB higher isolation compared to 0° and 45°. It is fair to conclude that CLTA B isolation's sensitivity to the Vivaldi rotation angle is nearly negligible compared to CLTA A.

The higher isolation at 90° is partly explained with the Vivaldi HPBW being narrower in the direction of the CLTA antenna in that rotation angle at lower frequencies. This is shown in the 1.7 GHz CST simulation results in Figure 34, where the elevation cut is in the direction of the CLTA at Vivaldi rotation 90°. The beamwidth in the orientation of the CLTA antenna is nearly halved at Vivaldi rotation 90° compared to rotation 0°. As a result, at the 90° rotation the Vivaldi antenna couples to a shorter part of the CLTA antenna with high gain compared to rotation 0°.

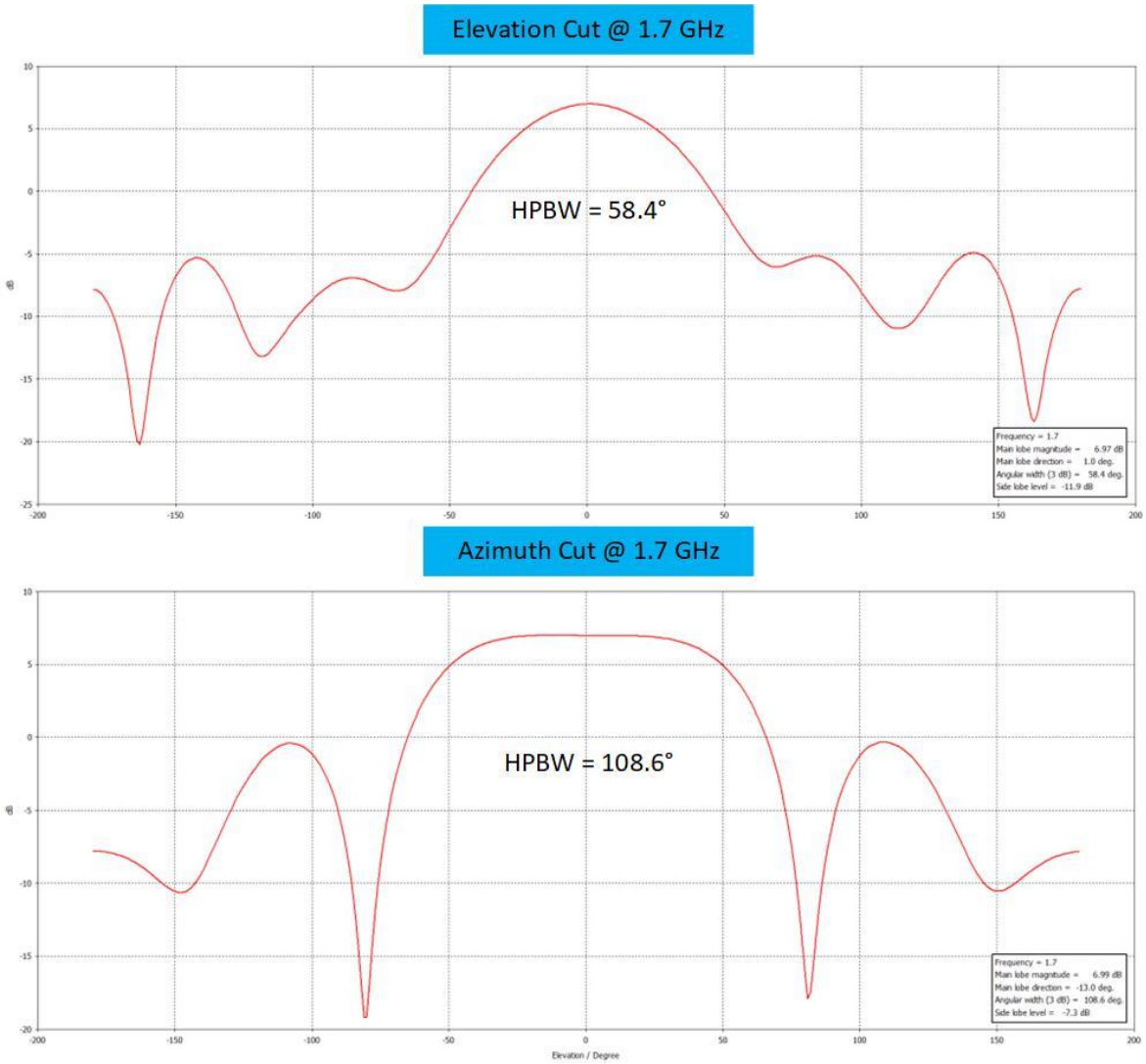


Figure 34. Comparison of Vivaldi azimuth and elevation HPBW at 1.7 GHz frequency.

At 3.3 GHz it is already observed in Figure 35 that the HPBW in both azimuth and elevation directions are nearly identical. This means the difference between Vivaldi rotations 90° and 0° should be lesser at higher frequencies. However, this effect is not observed in the CLTA B results which don't seem to be affected by the Vivaldi rotation in a significant way.

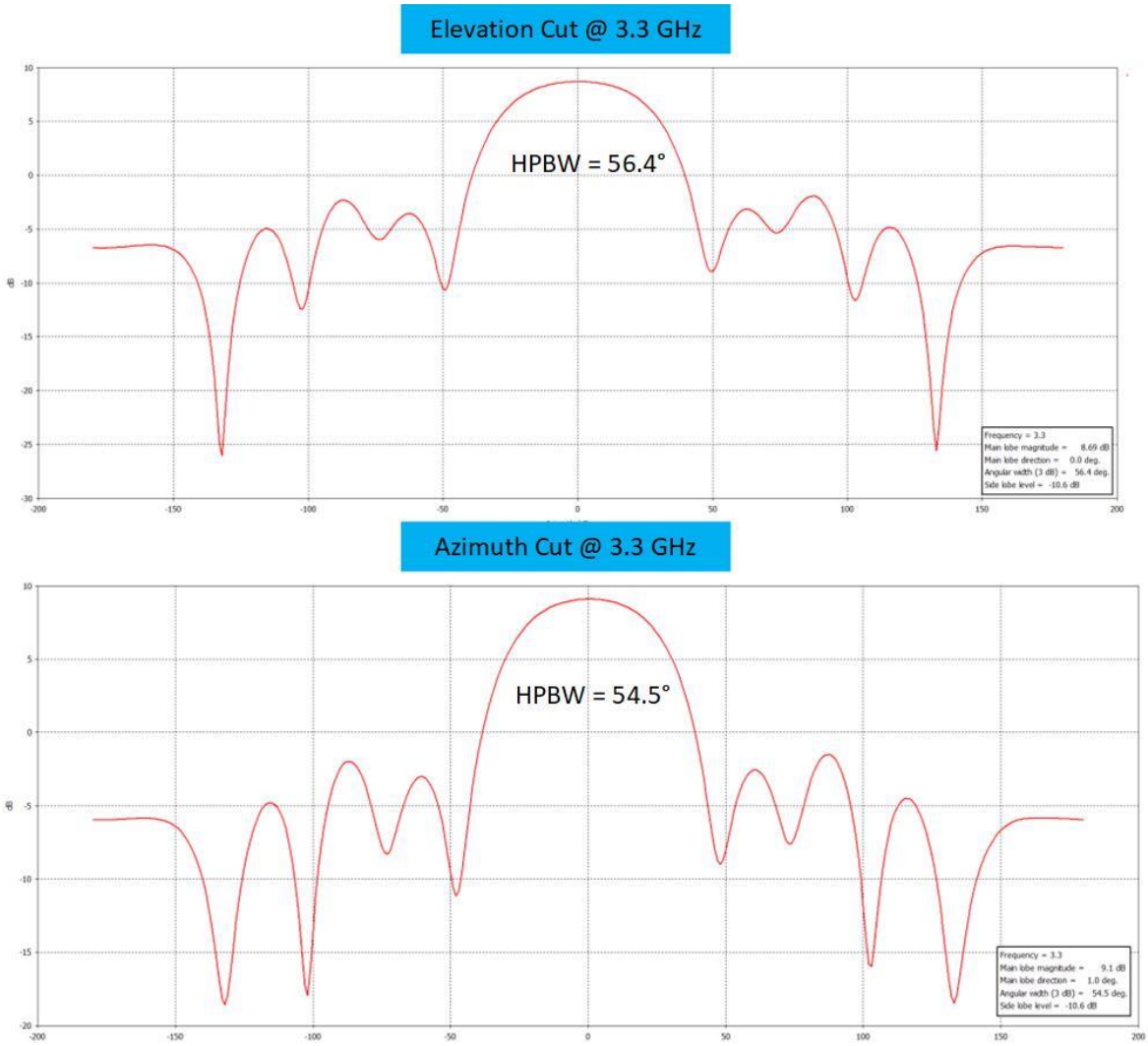


Figure 35. Comparison of Vivaldi azimuth and elevation HPBW at 3.3 GHz frequency.

In Figure 36 the per polarity data of CLTA A is split into three frequency subsets between 1 GHz and 4 GHz. The mean isolation for Mpol/Ppol drops by 3.7/5.3 dB from the 2002 – 3000 MHz frequency range to 1000 – 2000 MHz range. Compared to the 3002 – 4000 MHz frequency range the distributions are more spread indicated by lower K and higher Standard Deviation (SD). The biggest bins of data in the 1000 – 2000 MHz range are below the mean. It could be possible that the two lower frequency distributions are close to splitting into two different distributions with how spread the form is. By splitting the subsets further based on for example Vivaldi position, rotation or CLTA antenna in question it could be possible to separate these two distributions. A long "tail" of outliers on the high isolation side can be seen that increase the skewness, especially on the Mpol data.

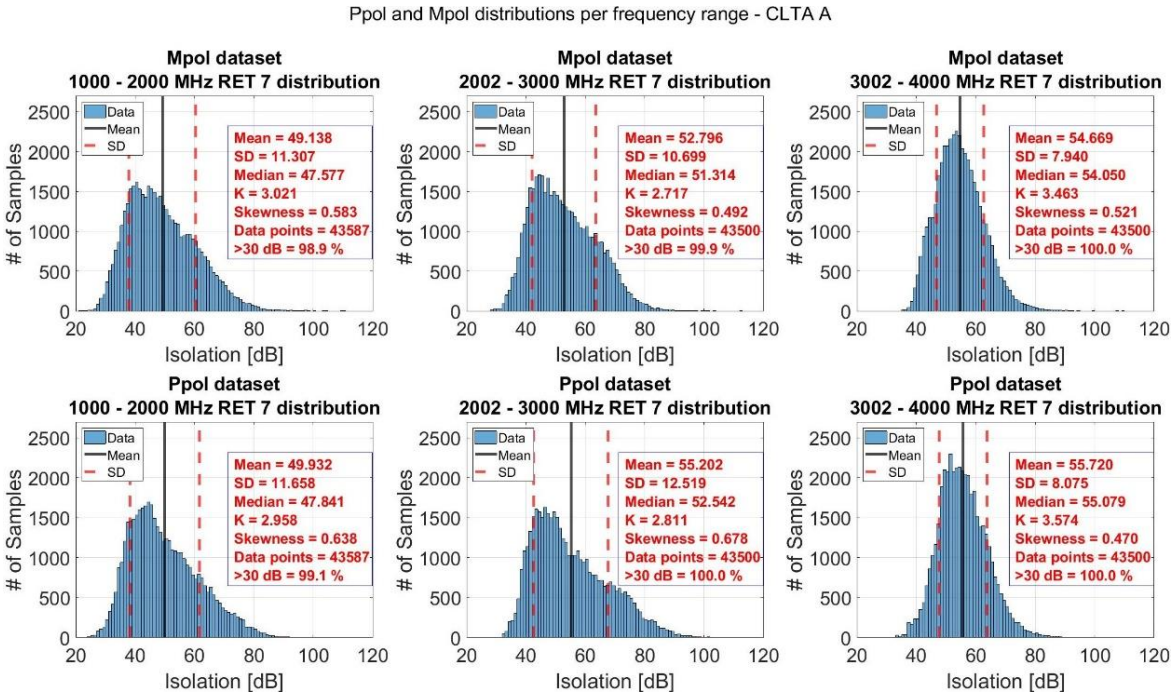


Figure 36. CLTA A below 4 GHz frequency subsets per polarity.

In the higher frequency ranges shown in Appendix 4 Figure 61 the differences between subset distributions are not as noticeable as below 4 GHz. However, the trend seems to be that the distribution gets narrower and mean isolation is higher at higher frequencies. This makes sense when considering that the operation frequencies of all CLTA A antennas except p1 are below 2690 MHz so the lowest isolation points would be below 3 GHz.

In the CLTA B below 4 GHz subsets shown in Appendix 4 Figure 62 the differences between frequency subsets are very similar to CLTA A. The mean isolation is 1-2 dB higher in the 1000 – 2000 MHz range but the increase in Mpol/Ppol mean isolation going to the 2002 – 3000 MHz range is significantly higher at 7.0/7.6 dB. The higher frequency CLTA B datasets in Appendix 4 Figure 63 exhibit the same behaviour as was observed with CLTA A. Here too the main effect is that the distributions get narrower at higher frequencies. The differences between subsets are even smaller compared to CLTA A, which is likely due to all CLTA B antenna operating frequencies being below 2690 MHz. The difference between polarities is lower compared to CLTA A.

These frequency subsets were further broken down per CLTA antenna. From these subsets some highlights are presented here and in Appendix 5. The per antenna distributions for CLTA A at the 1000 – 2000 MHz range are presented in Figure 37. The frequency range in each plot's title is the operating frequency range of that antenna. It is worth noting that in these subsets the amount of data points is starting to get quite low compared to previous figures. The low-band antennas also have more data points due to having more measurement points and the y-axis is scaled accordingly. Biggest outlier is the high-band antenna p1 with 7.1-12.5 dB lower mean isolation compared to other antennas and comparatively narrow distribution with low SD and high K values. It is unexpected that the CLTA A antenna with the highest operation frequency has such low isolation at the bottom of the measured frequency range and outside its operation frequency. This would suggest that high frequency antennas can still be more susceptible to interference from a co-located low frequency antenna than antennas transmitting at the same or higher frequency. The distributions of the other antennas have higher spread and are more skewed with biggest groups of data below the mean. The shape of the distribution for antenna

Lb1 could suggest that it consists of two separate distributions. It could be that the large groups of low isolation points are from the frequency range where the measurement range 1000 – 2000 MHz and Lb1 operation frequency 1695 – 2200 MHz interject. In the positional results in Figure 22, the Lb1 antenna exhibits lower isolation towards the bottom end of the antenna as well.

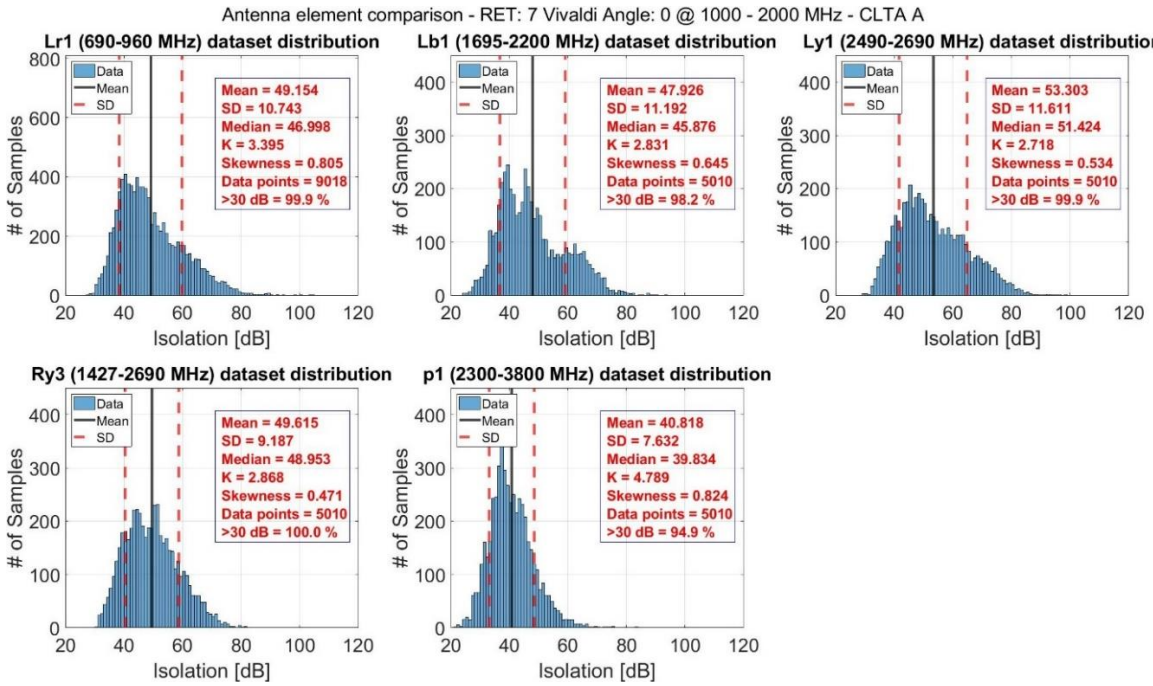


Figure 37. Per antenna isolation histograms for CLTA A at 1000 – 2000 MHz frequency range.

Same subsets of data for CLTA B are shown in Figure 38. There is not as much variance in the mean isolation between antennas compared to CLTA A, but the data sets are more spread. Especially antennas R1 and Y1 have large groups of data below the mean and what looks like a smaller separate distribution around the 65 dB isolation point. The operating frequencies of these antennas do not interject with the 1000 – 2000 MHz measurement frequency and the positional results in Figure 30 are mostly symmetrical. The groups of high isolation points could be due to the measurement frequency being outside of both antennas' operating range, but the lower isolations are more difficult to explain from this analysis.

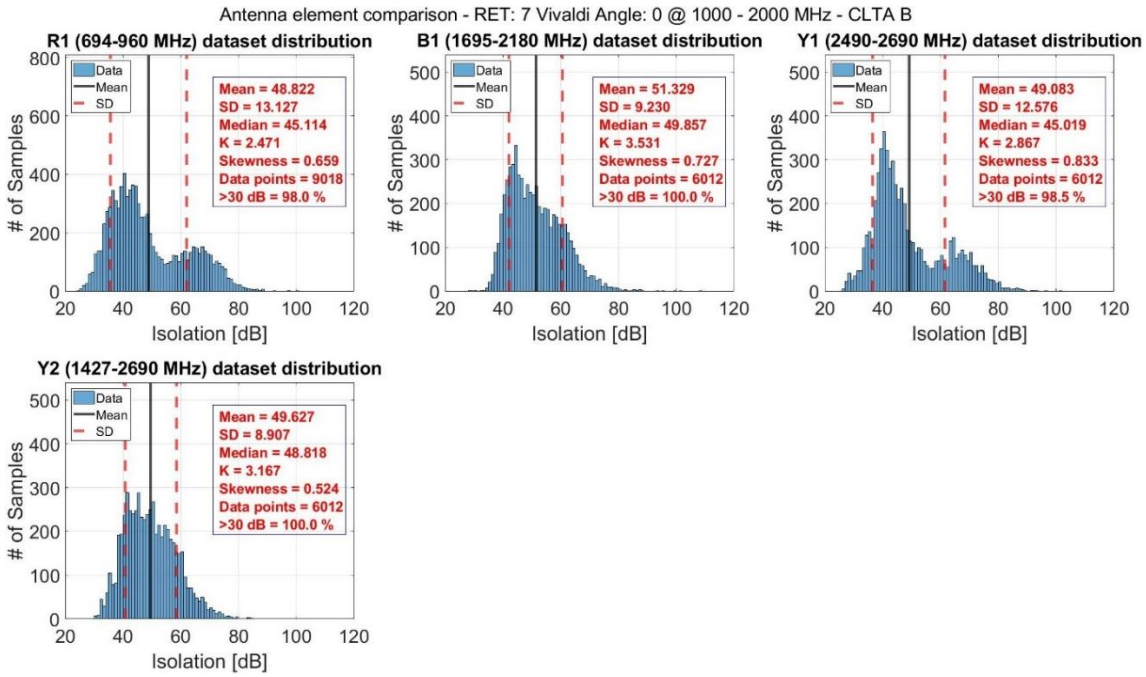


Figure 38. Per antenna isolation histograms for CLTA B at 1000 – 2000 MHz frequency range.

In the next frequency range for CLTA A antennas shown in Appendix 5 Figure 64 the mean isolations are higher, and distributions are getting narrower. This aligns with the earlier observations from per polarity frequency range subsets. Something of note is that Ry3 distribution seems to be a mix of Lb1 and Ly1 distributions, which cover most of the Ry3 frequency range separately. For CLTA B distributions in Appendix 5 Figure 65 for the same frequency range similar effects are seen as with CLTA A. The deviations across all data sets have decreased noticeably as was prevalent with CLTA A. The mean isolations for R1, Y1 and Y2 have increased significantly while for B1 it has stayed the same.

To summarize the effect of frequency, the statistical characteristics as a function of frequency subset for CLTA A and CLTA B are shown in Figure 39 and Figure 40 respectively. For mean and median isolation the trend for most antennas is that it increases at higher frequencies and the differences between antennas become smaller. At the same time the standard deviation can be high at low frequencies but decreases at higher frequencies as the distributions become narrower. Quite clearly above 4 GHz the distributions of antennas are converging and less sensitive to frequency while below 4 GHz the differences are larger, and sensitivity is higher. Between the two CLTAs, the CLTA B antennas seem to converge in pairs even at lower frequencies and statistical characteristics are flatter or changing more linearly with frequency.

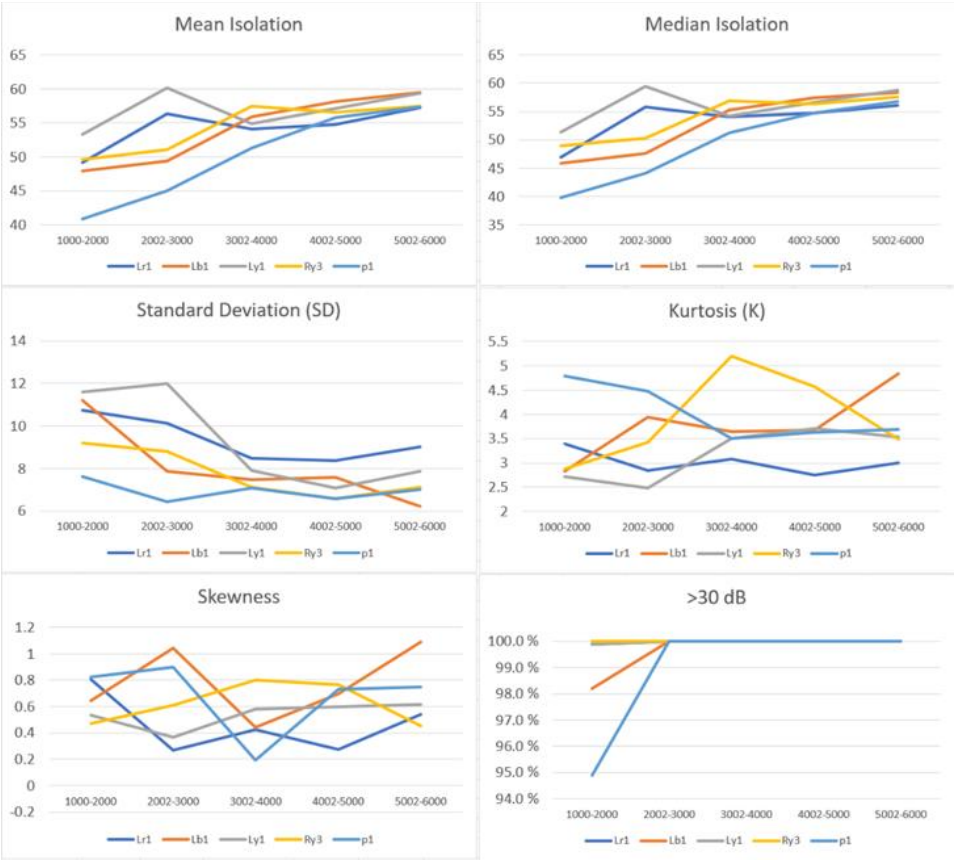


Figure 39. Statistical characteristics of CLTA A frequency subsets per antenna.


Figure 40. Statistical characteristics of CLTA B frequency subsets per antenna.

As distribution narrows and number of outliers becomes smaller, kurtosis should also increase. This can be seen somewhat in CLTA B data, but not clearly with CLTA A where only antenna Lb1 follows said trend. Regardless, it can be seen in SD and visually that the bulk of the data around the mean is getting narrower at higher frequencies. As is seen from equations (3) and (4) kurtosis is affected by distance from the mean in the $4^{th}$ power and skewness in the $3^{rd}$ power. Therefore, the "long tail" of high isolation outlier data points in both CLTA A and B datasets have a large effect on these characteristics compared to the rest of the data closer to the mean. Without these high isolation outliers the kurtosis and skewness would be more indicative of distribution changes withing the bulk of the data, but as such they are skewed by the outliers.

## 5.3 Co-location measurement

At the end of the isolation measurement the time allocated for the measurements was extended from 5.9.2021 to 8.9.2021 as it turned out R&D schedule allowed for it. As a result, the measurements were paused for the weekend and preparations for the co-location spurious emissions measurement were started after. The preparations took an extra day due to some mistakes and practicalities in for example the assembling and installation of the CLTA supports shown in Figure 41. More care should have been taken in measuring and calculating the adjustable bracket positions and heights for the mechanical alignment between the DUT and both CLTAs. The practical assembly and installation issues were less surprising, considering this was the first time they had been used and noting any practicalities were one of the goals. In the initial bring-up of the DUT, the two NR40 carriers were activated with 37 dBm power per carrier instead of the allowed 33.9 dBm value. Due to this mistake a few hours were spent checking via the DUT software interface that all power amplifiers are reporting expected levels power. No abnormalities were found and DUT was transmitting expected power levels.

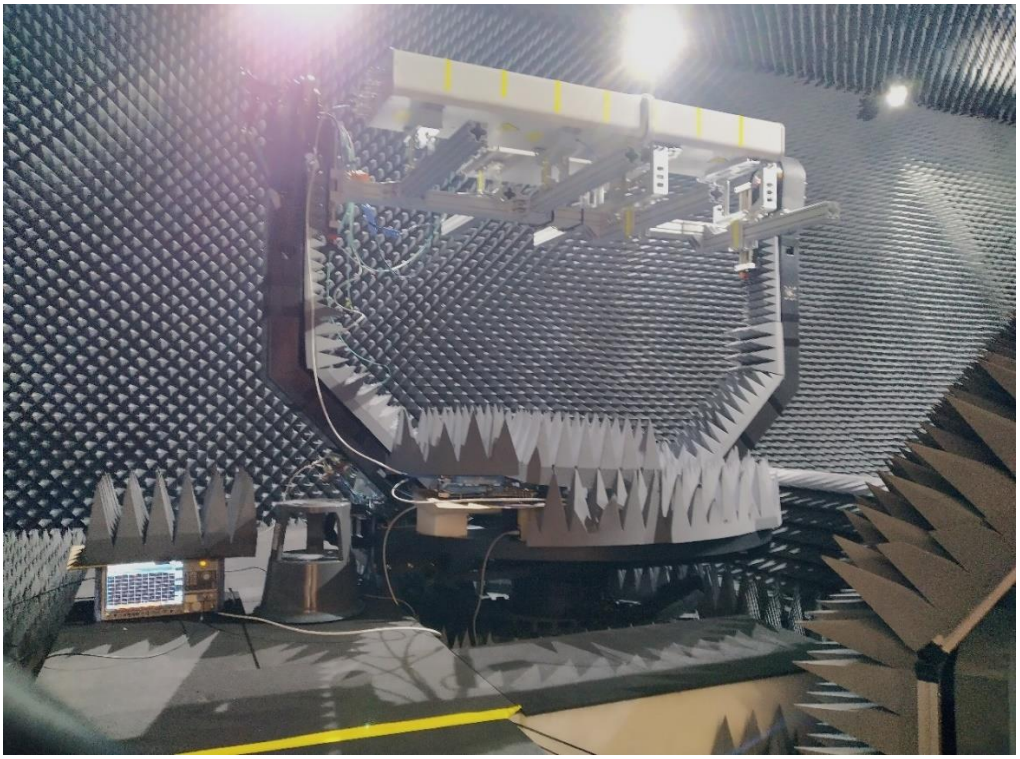

Figure 41. The full co-location spurious emissions measurement setup for CLTA B.

Once all the mechanical preparations were done and the DUT was operational the reference measurements were started where the DUT was powered down. When measuring CLTA B antenna Y2 it was seen that there were some interference sources within the chamber. One of them was a Local Management Interface (LMI) device commonly used to interface with the DUT that created emissions shown in Figure 42. The LMI device was not strictly required for the measurements, so it was powered down and the affected Y2 results were re-measured. Another source of interference is the 2.4 GHz Wi-Fi signal leaking into the chamber most likely through one of the ethernet cables connected to the inlet panel of the chamber. These interference sources had not been documented in the anechoic chamber before and the findings were important both for further development of the environment and future measurements. Note that in Figure 42 the 90 dB raised spectrum in band n41 frequency range is due to offset in calibration caused by diplex filter response and not any actual rise in noise power or carrier at the spectrum analyzer input.

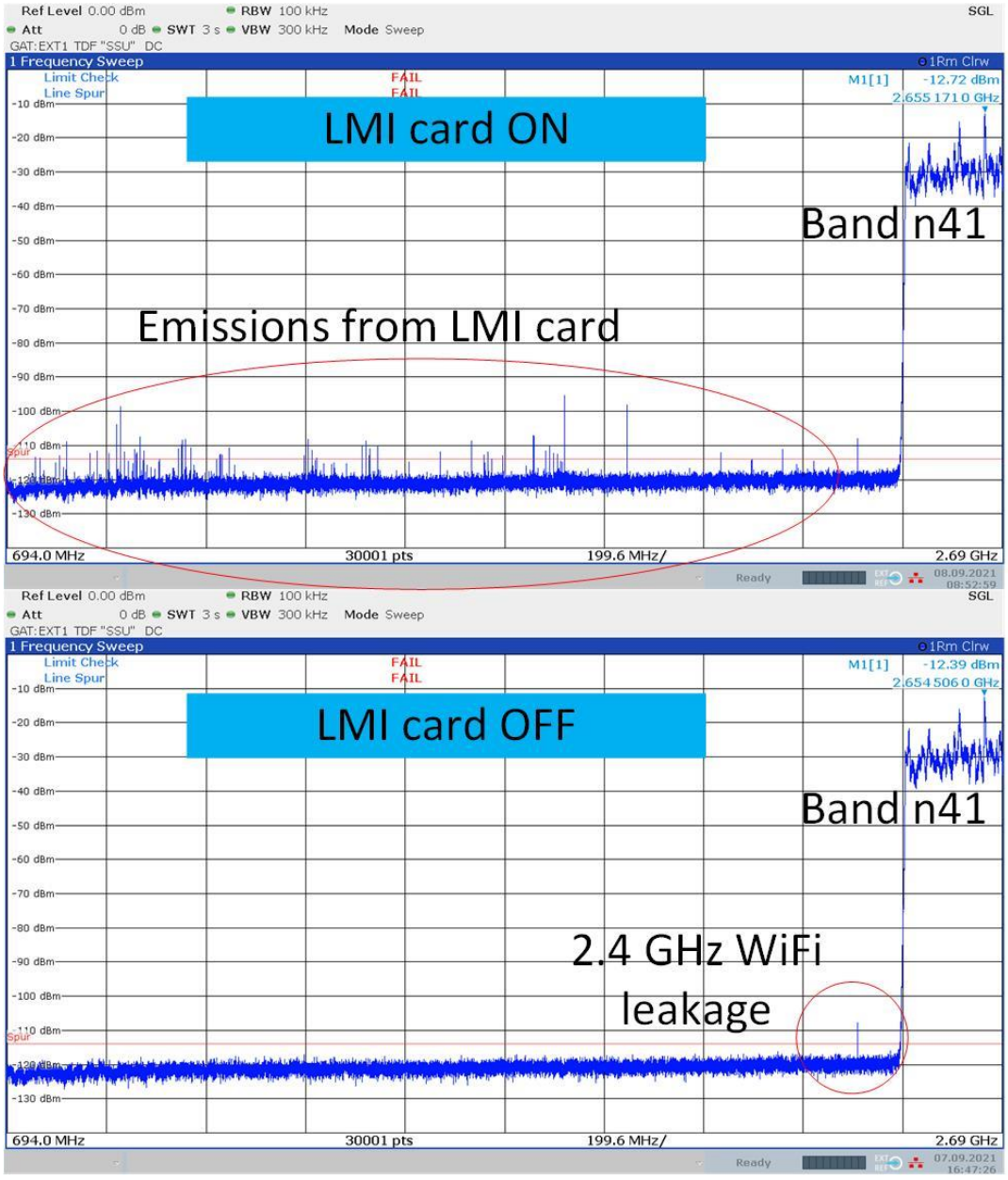


Figure 42. Reference measurement with LMI card.

Another abnormality in the reference measurements was that with CLTA A p1 Ant4 the noise level for both polarities rise in the 3300 – 3800 MHz range shown in Figure 43. As discussed in Section 5.6.2 the spurious emissions are analysed from the sum of polarities. The limit for this frequency range in [4] is -113.7 dBm and the reference measurement fails to meet this requirement by 1.1 dBm at 3371 MHz. The noise characteristics of the FSW spectrum analyzer, external diplex filter and LNA are different at higher frequencies, which is the likely source for the increased noise. Through enabling noise cancellation on the FSW these p1 Ant4 reference measurement fails could have been potentially avoided. This observation could not be verified with CLTA B as none of its antennas operate above 2690 MHz.

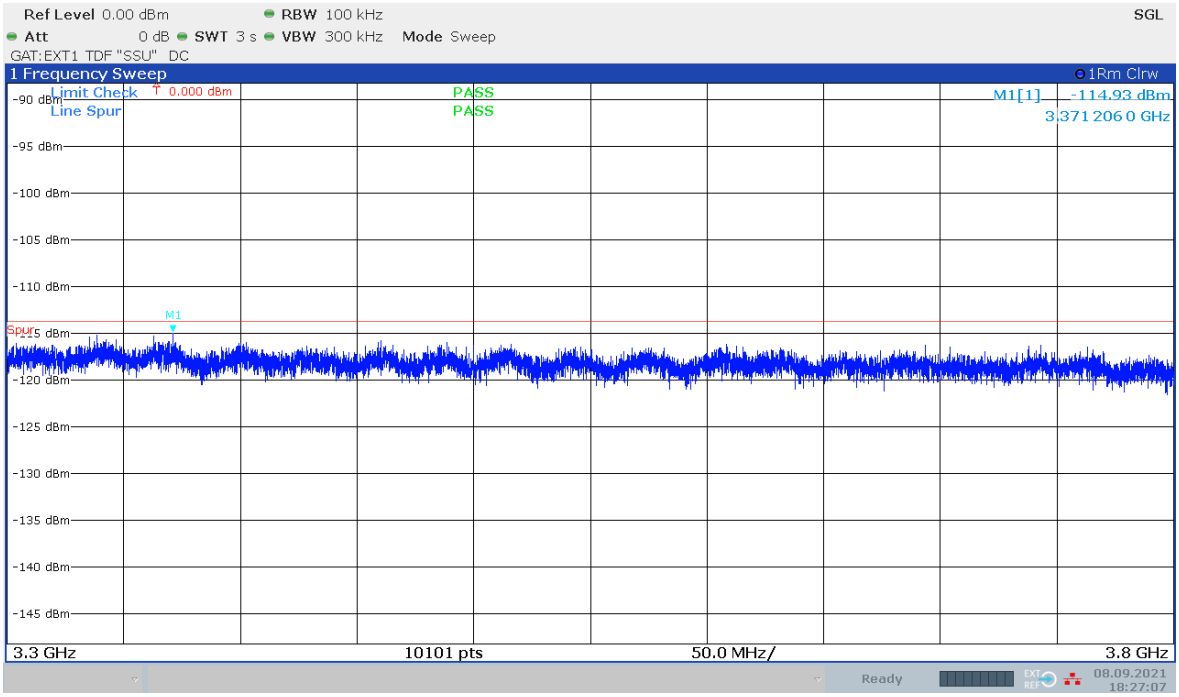

Figure 43. Noise level in CLTA A p1 Ant4 Mpol in frequency range 3300 – 3800 MHz.

Once the reference measurements were done for both CLTAs the 3GPP defined measurements were started. The default RET angle of 7° was used and the DUT was configured to transmit carrier configuration 2xNR40 at full power with beam target direction at azimuth 0° and elevation 6°. Finally in contrast to the 3GPP defined measurements a kind of worst-case measurement was done where DUT beam would be steered towards the CLTA with the hypothesis that it would make the emissions worse. For measuring the CLTA A antenna Ry3 it would have been required to switch positions with the DUT since Ry3 is on the opposite edge of the CLTA than the other measured antennas. To save time and see how the DUT couples with an element on the opposite edge of the victim antenna, this positional switch was not done.

During and after the isolation measurement the results for different RET angles were analysed so that a worst-case RET angle could be determined for each CLTA antenna. These worst-case RET angles listed in Table 13 would then be used in the third part of the spurious emissions measurement along with DUT beam steering towards the CLTA. Using these select RET angles as opposed to doing all measurements at three different RET angles would save time as the measurement campaign was already on a tight schedule. It was accepted that a lot more time would have been required for exhaustive data on the effect of CLTA RET angle.

Table 13. Worst-case RET angles based on isolation measurements

**CLTA A**

| Antenna | Worst-case RET angle based on Vivaldi&CLTA isolation measurements |
|---|---|
| R1 | RET12 |
| B1 | RET7 |
| Y1* | RET7 |
| Y2 | RET2 |

*Antenna operates in DUT band (n41), so it was not used for measurement of co-location spurious emission.

**CLTA B**

| Antenna | Worst-case RET angle based on Vivaldi&CLTA isolation measurements |
|---|---|
| Lr1 | RET10 |
| Lb1 | RET7 |
| Ly1 | RET12 |
| p1 Ant4 | RET12 |
| Ry3 | RET12 |

### *5.3.1 Results*

All the required frequencies in [4] excluding the ones listed in Table 10 were measured with applicable CLTA antennas for each of the two supported polarities. A Python script was used to calculate the polarity combined measurement result as described in Section 5.6.2. From the combined results the highest power result was analysed against the [4] limits via Excel. In this section, only the worst results are displayed and discussed. Even though each frequency range only needs to be measured with one antenna, the frequencies were measured with all applicable antennas for comparison purposes. Some bands are also listed twice in [4] so they were also measured twice.

The reference measurement results for CLTA A antennas are shown in Figure 44 where the most relevant results are highlighted. The reasons for all the five fails were discussed in the previous section. The antenna p1 Ant4 seems to be significantly more susceptible to the Wi-Fi interference compared to antenna Ry3. Considering Ry3 is on the opposite edge of the CLTA compared to p1 Ant4, the probable explanation is that the cable where the Wi-Fi is leaking from is somewhere near the DUT. The Wi-Fi signal is also 6 dB higher in the Ppol of Ry3 compared to Mpol, while for p1 Ant4 Ppol the same difference is 3 dB. The heightened noise in the 3300 – 3800 MHz range can be seen in the intersecting ranges 3400 – 3600 MHz and 3410 – 3490 MHz where the margin to the limit is only 0.2 dB.

| Ant Element | BottomFreq[MHz] | TopFreq[MHz] | MaxSpur[dBm] | MaxSpurFreq[MHz] | Limit | vs Limit | PASS/FAIL | Notes |
|---|---|---|---|---|---|---|---|---|
| p1 | 2300 | 2400 | -101.6700091 | 2400 | -113.9 | 12.229991 | FAIL | WIFI leaking into chamber |
| p1 | 2300 | 2400 | -101.8266784 | 2400 | -113.9 | 12.073322 | FAIL | WIFI leaking into chamber |
| Ry3 | 2300 | 2400 | -110.9634272 | 2400 | -113.9 | 2.9365728 | FAIL | WIFI leaking into chamber |
| Ry3 | 2300 | 2400 | -110.9937558 | 2400 | -113.9 | 2.9062442 | FAIL | WIFI leaking into chamber |
| p1 | 3300 | 3800 | -112.6065405 | 3371.188119 | -113.7 | 1.0934595 | FAIL | |
| p1 | 3400 | 3600 | -113.9008409 | 3462.285714 | -113.7 | -0.200841 | PASS | |
| p1 | 3410 | 3490 | -113.9115917 | 3462.914286 | -113.7 | -0.211592 | PASS | |
| Ry3 | 1710 | 1785 | -116.372267 | 1749.964286 | -115.9 | -0.472267 | PASS | |
| p1 | 3550 | 3700 | -114.2768702 | 3605.142857 | -113.7 | -0.57687 | PASS | |
| p1 | 3600 | 3800 | -114.3336282 | 3633.047619 | -113.7 | -0.633628 | PASS | |
| Lb1 | 1710 | 1785 | -116.6160832 | 1749.928571 | -115.9 | -0.716083 | PASS | |
| Lr1 | 824 | 849 | -116.7511687 | 825.0016026 | -115.9 | -0.851169 | PASS | |
| Ry3 | 1850 | 1910 | -116.7971452 | 1909.134615 | -115.9 | -0.897145 | PASS | |
| Lb1 | 1850 | 1910 | -116.8468222 | 1863.557692 | -115.9 | -0.946822 | PASS | |
| Lr1 | 876 | 915 | -117.2319332 | 890.9375 | -115.9 | -1.331933 | PASS | |
| Lr1 | 788 | 798 | -115.9688856 | 791.9903846 | -113.9 | -2.068886 | PASS | |

Figure 44. CLTA A reference measurement results.

Same reference results for CLTA B are presented in Figure 45. The Wi-Fi leakage only causes two fails since the 2400 MHz frequency is only measured with antenna Y2. With the low-band antenna R1 there is enough noise around 826 MHz frequency that it is on the edge of the -115.9 dBm limit.

| Ant Eleme | BottomFreq[MH | TopFreq[MH | MaxSpur[dBr | MaxSpurFreq[MI | Limit | vs Limit | PASS/FA | Note |
|---|---|---|---|---|---|---|---|---|
| Y2 | 2300 | 2400 | -104.1586842 | 2400 | -113.9 | 9.7413158 | FAIL | WIFI leaking into chamber |
| Y2 | 2300 | 2400 | -104.3783127 | 2400 | -113.9 | 9.5216873 | FAIL | WIFI leaking into chamber |
| R1 | 824 | 849 | -115.9355048 | 825.8830128 | -115.9 | -0.035505 | PASS | |
| R1 | 876 | 915 | -116.4599848 | 900 | -115.9 | -0.559985 | PASS | |
| R1 | 698 | 728 | -114.7017268 | 699.2019231 | -113.9 | -0.801727 | PASS | |
| B1 | 1710 | 1785 | -116.8910407 | 1736.964286 | -115.9 | -0.991041 | PASS | |
| Y2 | 1710 | 1785 | -116.9151196 | 1747.035714 | -115.9 | -1.01512 | PASS | |
| B1 | 1850 | 1910 | -116.9393948 | 1908.653846 | -115.9 | -1.039395 | PASS | |
| Y2 | 1850 | 1910 | -117.0278592 | 1856.923077 | -115.9 | -1.127859 | PASS | |
| R1 | 698 | 716 | -115.2267477 | 698.5192308 | -113.9 | -1.326748 | PASS | |
| R1 | 703 | 803 | -115.5311471 | 703.3809524 | -113.9 | -1.631147 | PASS | |
| R1 | 807 | 824 | -115.6533235 | 822.6378205 | -113.9 | -1.753323 | PASS | |
| R1 | 814 | 849 | -115.8119966 | 823.4230769 | -113.9 | -1.911997 | PASS | |
| R1 | 815 | 830 | -115.8235587 | 824.9278846 | -113.9 | -1.923559 | PASS | |
| R1 | 777 | 787 | -115.8999572 | 782.9134615 | -113.9 | -1.999957 | PASS | |
| R1 | 830 | 845 | -115.9309716 | 832.5 | -113.9 | -2.030972 | PASS | |

Figure 45. CLTA B reference measurement results.

CLTA A results from the measurement where the DUT is transmitting a boresight beam are shown in Figure 46. All the five (5) fail cases from the reference measurement are still present along with seven (7) additional ones. Surprisingly the 3400 – 3600 MHz range is passing with a 0.4 dB margin whereas before the margin was 0.2 dB, so the DUT does not seem to be causing any additional noise in that frequency range. Below 900 MHz there are several substantial fail results with some emissions even higher than the Wi-Fi interference. Around 1750 MHz there is a 0.18 dB fail in the 1710 – 1785 MHz range, but the same emission seems to be absent in the other highlighted frequency ranges that include said frequency. It is likely to be some momentary interference from the DUT or for example a commercial network on 1800 band momentarily leaking into the chamber.

| Ant Eleme | BottomFreq[MH | TopFreq[MH | MaxSpur[dBr | MaxSpurFreq[MI | Limit | vs Limit | PASS/FA | Notes |
|---|---|---|---|---|---|---|---|---|
| Lr1 | 703 | 803 | -98.70283971 | 750 | -113.9 | 15.19716 | FAIL | |
| Lr1 | 703 | 748 | -100.1835818 | 737.3269231 | -113.9 | 13.716418 | FAIL | |
| Lr1 | 703 | 748 | -100.1966556 | 737.3269231 | -113.9 | 13.703344 | FAIL | |
| p1 | 2300 | 2400 | -102.3741771 | 2400 | -113.9 | 11.525823 | FAIL | WIFI leaking into chamber |
| p1 | 2300 | 2400 | -102.4048493 | 2400 | -113.9 | 11.495151 | FAIL | WIFI leaking into chamber |
| Lr1 | 832 | 862 | -102.645849 | 860.1730769 | -113.9 | 11.254151 | FAIL | |
| Lr1 | 832 | 862 | -102.6836757 | 860.1730769 | -113.9 | 11.216324 | FAIL | |
| Ry3 | 2300 | 2400 | -111.4953525 | 2400 | -113.9 | 2.4046475 | FAIL | WIFI leaking into chamber |
| Ry3 | 2300 | 2400 | -111.5656567 | 2400 | -113.9 | 2.3343433 | FAIL | WIFI leaking into chamber |
| p1 | 3300 | 3800 | -112.7154839 | 3370.148515 | -113.7 | 0.9845161 | FAIL | |
| Lr1 | 698 | 728 | -113.1534205 | 721.9423077 | -113.9 | 0.7465795 | FAIL | |
| Ry3 | 1710 | 1785 | -115.7237207 | 1749.964286 | -115.9 | 0.1762793 | FAIL | |
| p1 | 3550 | 3700 | -114.0080777 | 3573.714286 | -113.7 | -0.308078 | PASS | |
| p1 | 3410 | 3490 | -114.106169 | 3427.942857 | -113.7 | -0.406169 | PASS | |
| p1 | 3400 | 3600 | -114.1275603 | 3513.809524 | -113.7 | -0.42756 | PASS | |
| p1 | 3600 | 3800 | -114.1449318 | 3631.142857 | -113.7 | -0.444932 | PASS | |
| Lb1 | 1710 | 1785 | -116.698106 | 1749.964286 | -115.9 | -0.798106 | PASS | |
| Lr1 | 824 | 849 | -116.7558211 | 831.6923077 | -115.9 | -0.855821 | PASS | |
| Ry3 | 1850 | 1910 | -116.8484329 | 1870.673077 | -115.9 | -0.948433 | PASS | |
| Lb1 | 1850 | 1910 | -116.8860507 | 1909.230769 | -115.9 | -0.986051 | PASS | |
| Lr1 | 824 | 849 | -116.8948941 | 830.25 | -115.9 | -0.994894 | PASS | |
| Lr1 | 704 | 716 | -114.9852492 | 714.25 | -113.9 | -1.085249 | PASS | |
| Lr1 | 876 | 915 | -117.1951039 | 891 | -115.9 | -1.295104 | PASS | |
| Lr1 | 698 | 716 | -115.2039337 | 714.2692308 | -113.9 | -1.303934 | PASS | |
| Lr1 | 699 | 716 | -115.4578442 | 714.2291667 | -113.9 | -1.557844 | PASS | |
| Lr1 | 788 | 798 | -115.6921813 | 792.0064103 | -113.9 | -1.792181 | PASS | |
| Ry3 | 1710 | 1785 | -116.0763141 | 1749.964286 | -113.9 | -2.176314 | PASS | |
| Ry3 | 1710 | 1770 | -116.1651775 | 1750 | -113.9 | -2.265178 | PASS | |
| Ry3 | 1710 | 1785 | -116.1677889 | 1749.964286 | -113.9 | -2.267789 | PASS | |
| Ry3 | 1710 | 1755 | -116.1992099 | 1750.024038 | -113.9 | -2.29921 | PASS | |
| Lr1 | 777 | 787 | -116.4012303 | 777.0480769 | -113.9 | -2.50123 | PASS | |
| Ry3 | 1710 | 1780 | -116.4031702 | 1749.966667 | -113.9 | -2.50317 | PASS | |
| Ry3 | 1710 | 1780 | -116.4148624 | 1749.966667 | -113.9 | -2.514862 | PASS | |
| p1 | 2305 | 2315 | -116.4317365 | 2312.596154 | -113.9 | -2.531736 | PASS | |
| Lb1 | 1749.9 | 1784.9 | -116.5300078 | 1749.95609 | -113.9 | -2.630008 | PASS | |

Figure 46. CLTA A spurious emission results for DUT beam direction azimuth 0° and elevation 6°.

Taking a closer look at the 703 – 803 MHz frequency range in Figure 47 shows that there are two large emissions at 750 MHz and 737 MHz along with a raised noise floor around them. On the Ppol side the two emissions are 4-5 dB lower. These emissions could be frequency components from an oscillator or clock signal within the DUT that is leaking to the space around it. For $f_1$ = 737 MHz and $f_2$ = 750 MHz, the 2nd and 3rd order intermodulation (IM) products are calculated as [20]

$$2nd\ harmonics:\ 2f_1 = \mathbf{1474\ MHz}, 2f_2 = 1500\ \text{MHz}$$
$$2nd\ order\ difference\ frequency: f_2 - f_1 = 13\ \text{MHz}$$
$$2nd\ order\ sum\ frequency: f_1 + f_2 = \mathbf{1487\ MHz}$$
$$3rd\ harmonics:\ 3f_1 = 2211\ \text{MHz}, 3f_2 = 2250\ \text{MHz}$$
$$3rd\ order\ difference\ frequency: 2f_1 - f_2 = \mathbf{724\ MHz}, 2f_2 - f_1 = \mathbf{763\ MHz}$$
$$3rd\ order\ sum\ frequency: 2f_1 + f_2 = 2224\ \text{MHz}, 2f_2 + f_1 = 2237\ \text{MHz}.$$

In above equations the frequencies in bold are close to those of observed emissions with one or both CLTAs. Smaller emissions can be seen somewhat periodically across the frequency range every ~8 MHz. Such periodicity could mean that they are frequency components of an 8 MHz clock signal leaking through from the DUT. These periodic emissions will be clearer in the third part of these measurements.

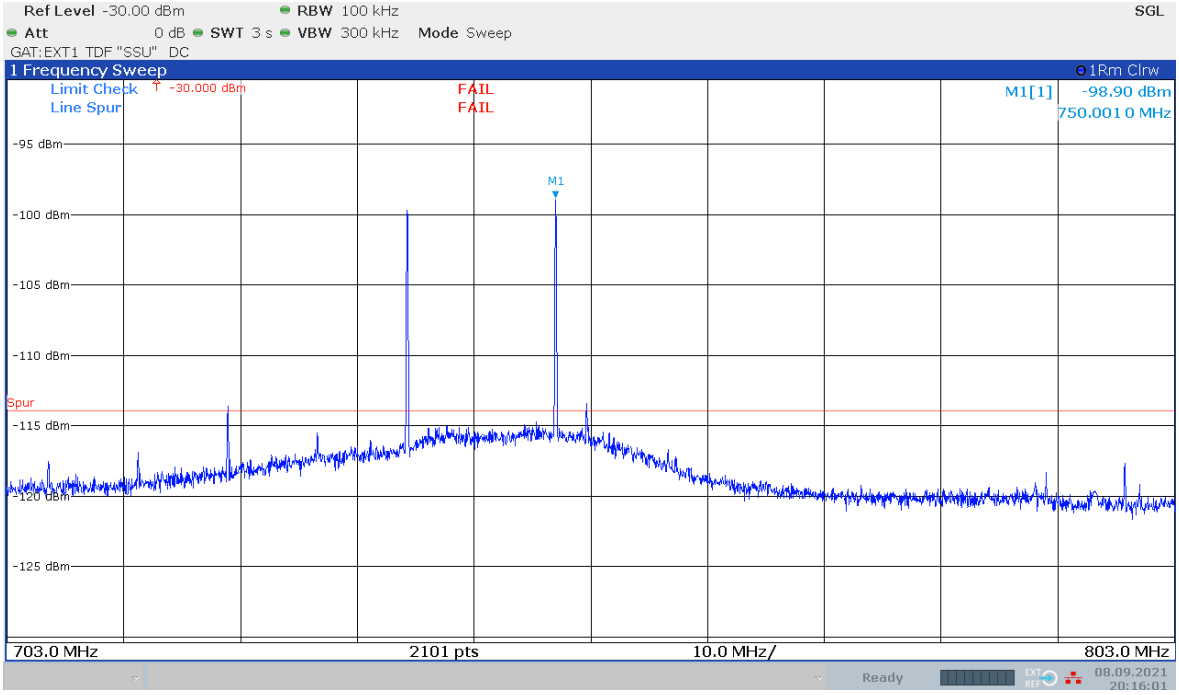


Figure 47. CLTA A antenna Lr1 Mpol 703 – 803 MHz frequency sweep.

Two additional emissions at 860 MHz and 850 MHz are shown in Figure 48. The latter emission is only visible in Mpol side, so it is possibly a temporary emission from the DUT or outside the chamber. The larger 860 MHz leakage could be from a similar source as the 750 MHz and 737 MHz emissions discussed earlier.

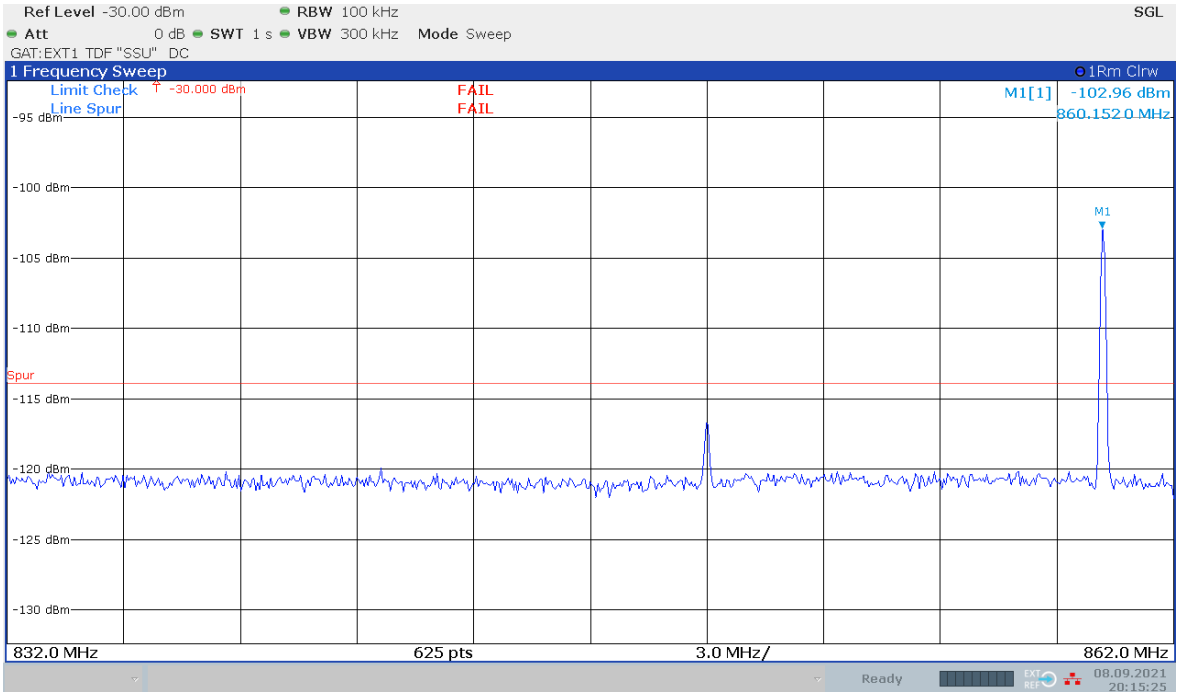


Figure 48. CLTA A antenna Lr1 Mpol 832 – 862 MHz frequency sweep.

Same boresight beam results for CLTA B are shown in Figure 49. In addition to the two (2) fails from the Wi-Fi leakage, there are 11 additional fails. The emissions that were perceived with CLTA A at 722 MHz, 737 MHz, 750 MHz, 860 MHz, and 1750 MHz can be seen in CLTA B results as well. Overall the emissions are more evenly distributed between polarities, whereas with CLTA B the Mpol polarity seemed more susceptible to most of them. The amplitude of the emission at 1750 MHz is changing between measurements as was observed with CLTA A and it results in a 0.6 dB fail -result with antenna B1. Above 3 GHz results could not be verified as no such antenna was measured for CLTA B. There are some additional emissions that were not picked up by CLTA A at frequencies 791 MHz, 826 MHz, 1475 MHz, 1909 MHz. In the 824 – 849 MHz range the reference measurement only had 0.04 dB margin to the -115.9 dBm limit at 826 MHz, so it could be that a re-test would result in a pass -result due to randomness of noise.

| Ant Eleme | BottomFreq[MH | TopFreq[MH | MaxSpur[dBr | MaxSpurFreq[MI | Limit | vs Limit | PASS/FA | Notes |
|---|---|---|---|---|---|---|---|---|
| R1 | 703 | 803 | -99.08034485 | 737.2857143 | -113.9 | 14.819655 | FAIL | |
| R1 | 703 | 748 | -99.71637185 | 737.3269231 | -113.9 | 14.183628 | FAIL | |
| R1 | 703 | 748 | -99.93793846 | 737.3269231 | -113.9 | 13.962062 | FAIL | |
| Y2 | 2300 | 2400 | -102.3466052 | 2400 | -113.9 | 11.553395 | FAIL | WIFI leaking into chamber |
| Y2 | 2300 | 2400 | -102.5372116 | 2400 | -113.9 | 11.362788 | FAIL | WIFI leaking into chamber |
| R1 | 832 | 862 | -106.206657 | 860.1730769 | -113.9 | 7.693343 | FAIL | |
| R1 | 832 | 862 | -106.3983907 | 860.1730769 | -113.9 | 7.5016093 | FAIL | |
| R1 | 788 | 798 | -112.156833 | 791.0288462 | -113.9 | 1.743167 | FAIL | |
| Y2 | 1432 | 1517 | -112.7810911 | 1474.580952 | -113.9 | 1.1189089 | FAIL | |
| B1 | 1710 | 1785 | -115.2985331 | 1750 | -115.9 | 0.6014669 | FAIL | |
| R1 | 698 | 728 | -113.5113347 | 721.8942308 | -113.9 | 0.3886653 | FAIL | |
| B1 | 1850 | 1910 | -115.766629 | 1909.038462 | -115.9 | 0.133371 | FAIL | |
| R1 | 824 | 849 | -115.7977229 | 826.2435897 | -115.9 | 0.1022771 | FAIL | |
| Y2 | 1710 | 1785 | -116.0024018 | 1750 | -115.9 | -0.102402 | PASS | |
| R1 | 876 | 915 | -116.828139 | 891 | -115.9 | -0.928139 | PASS | |
| Y2 | 1850 | 1910 | -116.8542945 | 1865.769231 | -115.9 | -0.954295 | PASS | |
| B1 | 1710 | 1780 | -115.0200297 | 1749.966667 | -113.9 | -1.12003 | PASS | |
| R1 | 704 | 716 | -115.0892416 | 714.25 | -113.9 | -1.189242 | PASS | |
| R1 | 699 | 716 | -115.2125132 | 714.2564103 | -113.9 | -1.312513 | PASS | |
| B1 | 1710 | 1770 | -115.2470221 | 1750 | -113.9 | -1.347022 | PASS | |
| R1 | 698 | 716 | -115.3424105 | 714.2692308 | -113.9 | -1.44241 | PASS | |
| B1 | 1710 | 1780 | -115.3537879 | 1749.966667 | -113.9 | -1.453788 | PASS | |
| B1 | 1749.9 | 1784.9 | -115.3636689 | 1749.95609 | -113.9 | -1.463669 | PASS | |
| B1 | 1710 | 1785 | -115.4989289 | 1749.964286 | -113.9 | -1.598929 | PASS | |
| R1 | 777 | 787 | -115.5848915 | 777.3685897 | -113.9 | -1.684892 | PASS | |
| B1 | 1710 | 1785 | -115.5877424 | 1749.964286 | -113.9 | -1.687742 | PASS | |
| B1 | 1900 | 1920 | -115.6642344 | 1908.942308 | -113.9 | -1.764234 | PASS | |
| B1 | 1850 | 1915 | -115.6780637 | 1913.947619 | -113.9 | -1.778064 | PASS | |
| B1 | 1910 | 1930 | -115.6838699 | 1910.032051 | -113.9 | -1.78387 | PASS | |
| B1 | 1880 | 1920 | -115.7325199 | 1915.512821 | -113.9 | -1.83252 | PASS | |
| R1 | 814 | 849 | -115.7340589 | 821.3477564 | -113.9 | -1.834059 | PASS | |
| B1 | 1850 | 1910 | -115.7976687 | 1907.980769 | -113.9 | -1.897669 | PASS | |
| B1 | 1850 | 1910 | -115.8027973 | 1909.326923 | -113.9 | -1.902797 | PASS | |
| R1 | 807 | 824 | -115.8080998 | 814.0833333 | -113.9 | -1.9081 | PASS | |
| B1 | 1880 | 1920 | -115.8199546 | 1905.961538 | -113.9 | -1.919955 | PASS | |
| R1 | 815 | 830 | -115.8865145 | 821.5384615 | -113.9 | -1.986515 | PASS | |
| Y2 | 1710 | 1780 | -115.9475587 | 1750 | -113.9 | -2.047559 | PASS | |
| Y2 | 1710 | 1780 | -115.9829366 | 1750 | -113.9 | -2.082937 | PASS | |
| Y2 | 1749.9 | 1784.9 | -116.0220857 | 1749.95609 | -113.9 | -2.122086 | PASS | |
| B1 | 1710 | 1755 | -116.0316088 | 1750.024038 | -113.9 | -2.131609 | PASS | |
| Y2 | 1710 | 1785 | -116.0652406 | 1749.964286 | -113.9 | -2.165241 | PASS | |

Figure 49. CLTA B spurious emission results for DUT beam direction azimuth 0° and elevation 6°.

The 737 MHz and 750 MHz emissions measured with CLTA B antenna R1 are shown in Figure 50. For CLTA B the +45pol is more susceptible to these emissions, whereas with CLTA A it was Mpol. In the datasheets for both multiband antennas there was no definition for polarity orientation, so it could be that the physical orientation of CLTA B +45pol and CLTA A Ppol are opposites. There are also additional emissions at frequencies 759MHz, 791 MHz and 799 MHz that were not visible or not as clearly visible with CLTA A. The emission at 791 MHz is resulting in an additional fail -result in the 788 – 798 MHz frequency range.

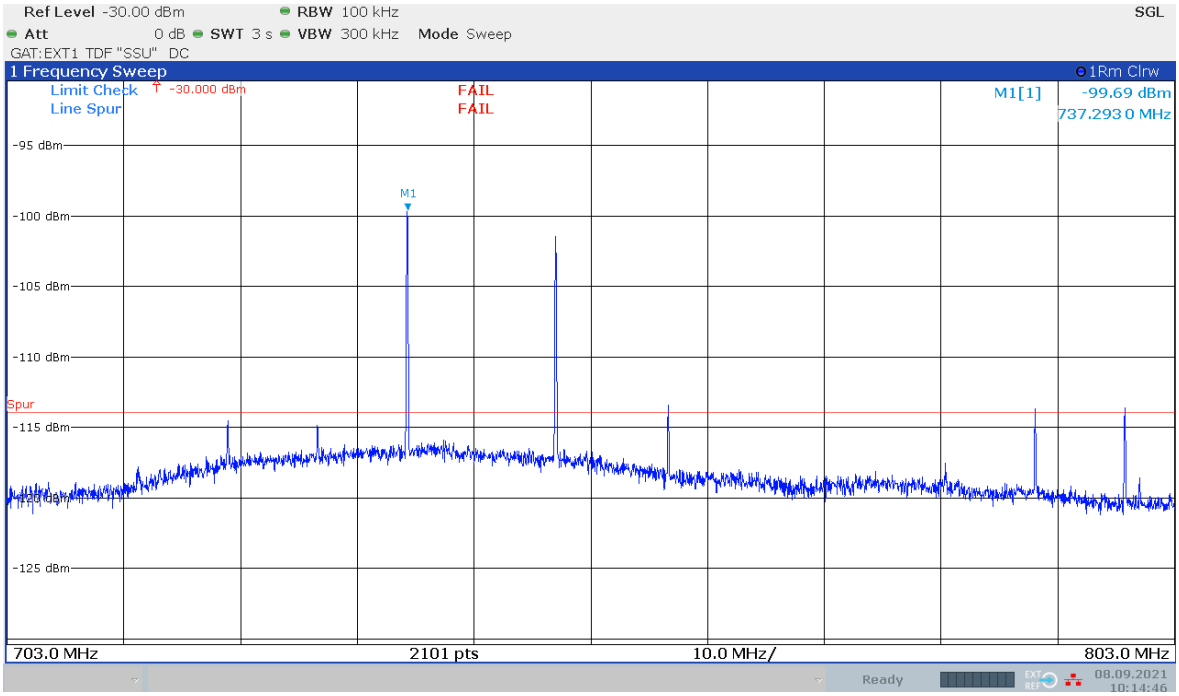


Figure 50. CLTA B antenna R1 +45pol 703 – 803 MHz frequency sweep.

For +45pol of CLTA B antenna B1 results in Figure 51 the noise level rises by 1-2 dB above 1900 MHz and then drops again quite sharply at 1919 MHz. This is not visible in CLTA A results, in CLTA B antenna Y2 results or antenna B1 -45pol results. It is however consistent to all antenna B1 +45pol results from this frequency range, so the rise in noise level is consistent for that polarity of the antenna and not temporary. It could be that the +45pol of B1 is in a physical position within CLTA B where it is susceptible to additional noise in that frequency range or there was some issue with the +45pol antenna connector.

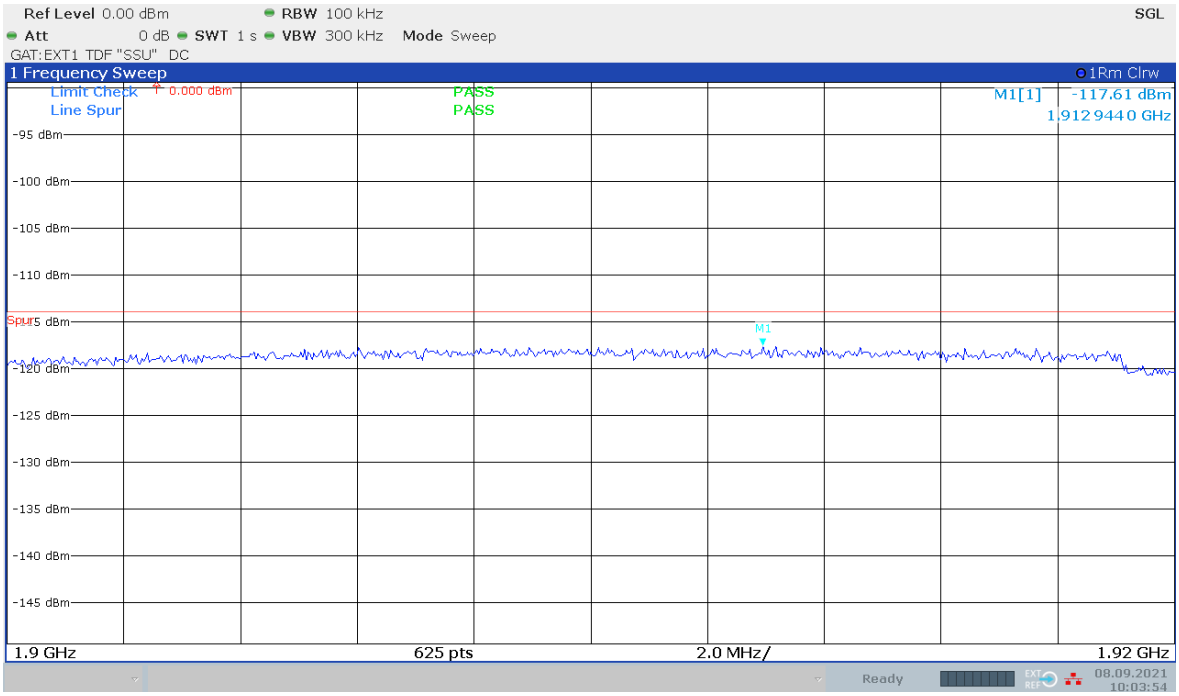


Figure 51. CLTA B antenna B1 +45pol 1900 – 1920 MHz frequency sweep.

The 1475 MHz emission shown in Figure 52 is picked up by both polarities of antenna Y2 and was not visible in CLTA A antenna Ry3 results. It matches the 2nd harmonic frequency of the 737 MHz emission which was calculated earlier in CLTA A results. Considering it is also seen in trial measurement results done before the reference measurements, it is unlikely to be a temporary interference. Based on Figure 11 the Y2 antenna is closer to the centre of CLTA B while Ry3 is on the edge of CLTA A that is further away from the DUT, which is the likely reason why this emission was not visible with CLTA A.

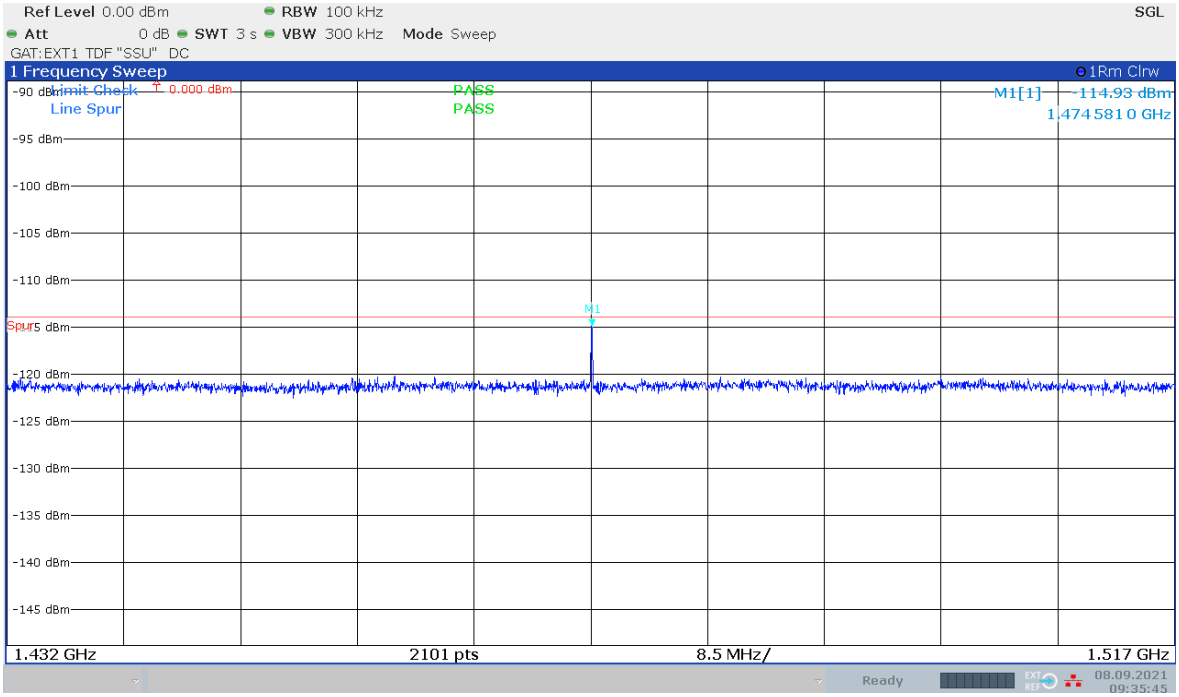


Figure 52. CLTA B antenna Y2 -45pol 1432 – 1517 MHz frequency sweep.

## 5.4 Additional measurements

The third and final spurious emission measurement was not required by the 3GPP specification but was done with a "worst-case" configuration that could hypothetically lead to worse spurious emissions results. The Table 13 RET angles used were chosen based on results of the isolation measurement and it was theorized that steering the beam 50° towards the CLTA would also increase gain of the emissions towards the CLTA antennas.

The CLTA A results in Figure 53 show that the total number of fail -results has gone down by three (3) compared to the boresight beam measurements in Figure 46. These three previous fail results were all from antenna Ry3: two of them from the Wi-Fi leakage and one minor fail at 1750 MHz frequency. Since the Wi-Fi signal is likely leaking from a cable close to the DUT, the change in beamforming should not have an effect. Thus the 3 dB drop in the 2.4 GHz interference is likely related to the change in Ry3 RET angle from 7° to 12°. There are no new fail results that weren't detected with the boresight beam.

| Ant Eleme | BottomFreq[MH | TopFreq[MH | MaxSpur[dBr | MaxSpurFreq[MI | Limit | vs Limit | PASS/FA | Notes |
|---|---|---|---|---|---|---|---|---|
| Lr1 | 703 | 803 | -97.54678734 | 750 | -113.9 | 16.353213 | FAIL | |
| Lr1 | 703 | 748 | -99.31573643 | 737.3269231 | -113.9 | 14.584264 | FAIL | |
| Lr1 | 703 | 748 | -99.35717881 | 737.3269231 | -113.9 | 14.542821 | FAIL | |
| Lr1 | 832 | 862 | -102.0282854 | 860.1730769 | -113.9 | 11.871715 | FAIL | |
| Lr1 | 832 | 862 | -102.1160978 | 860.1730769 | -113.9 | 11.783902 | FAIL | |
| p1 | 2300 | 2400 | -105.7607654 | 2400 | -113.9 | 8.1392346 | FAIL | WIFI leaking into chamber |
| p1 | 2300 | 2400 | -105.7616782 | 2400 | -113.9 | 8.1383218 | FAIL | WIFI leaking into chamber |
| Lr1 | 698 | 728 | -112.5495595 | 721.9423077 | -113.9 | 1.3504405 | FAIL | |
| p1 | 3300 | 3800 | -112.5819874 | 3340.742574 | -113.7 | 1.1180126 | FAIL | |
| Lr1 | 698 | 716 | -113.9988073 | 699.9903846 | -113.9 | -0.098807 | PASS | |
| Lr1 | 699 | 716 | -114.1429592 | 699.9807692 | -113.9 | -0.242959 | PASS | |
| Ry3 | 1626.5 | 1660.5 | -114.1446884 | 1633.419872 | -113.9 | -0.244688 | PASS | |
| p1 | 3410 | 3490 | -114.0369351 | 3462.72381 | -113.7 | -0.336935 | PASS | |
| p1 | 3400 | 3600 | -114.1319524 | 3400.285714 | -113.7 | -0.431952 | PASS | |
| p1 | 3550 | 3700 | -114.2859173 | 3573.642857 | -113.7 | -0.585917 | PASS | |
| Lb1 | 1710 | 1785 | -116.4880511 | 1750 | -115.9 | -0.588051 | PASS | |
| Lr1 | 824 | 849 | -116.557564 | 824.9615385 | -115.9 | -0.657564 | PASS | |
| Lr1 | 704 | 716 | -114.6106495 | 714.25 | -113.9 | -0.710649 | PASS | |
| Lb1 | 1850 | 1910 | -116.6580599 | 1906.923077 | -115.9 | -0.75806 | PASS | |
| p1 | 3600 | 3800 | -114.4813675 | 3607.428571 | -113.7 | -0.781368 | PASS | |
| Ry3 | 1850 | 1910 | -116.8213918 | 1866.25 | -115.9 | -0.921392 | PASS | |
| Ry3 | 1710 | 1785 | -116.9242211 | 1750 | -115.9 | -1.024221 | PASS | |
| Lr1 | 876 | 915 | -117.1233394 | 881.9375 | -115.9 | -1.223339 | PASS | |
| Lr1 | 788 | 798 | -115.2242407 | 791.9903846 | -113.9 | -1.324241 | PASS | |
| Ry3 | 2300 | 2400 | -115.4167684 | 2400 | -113.9 | -1.516768 | PASS | WIFI leaking into chamber |
| Ry3 | 2300 | 2400 | -115.4524584 | 2400 | -113.9 | -1.552458 | PASS | WIFI leaking into chamber |
| Lb1 | 1710 | 1780 | -116.3738721 | 1749.966667 | -113.9 | -2.473872 | PASS | |

Figure 53. CLTA A spurious emission results for DUT beam direction azimuth 50° and elevation 6°.

The emissions for 703 – 803 MHz range measured with CLTA A antenna Lr1 are shown in Figure 54. Compared to boresight beam results the two main emissions are around 1 dB higher with the beam turned towards CLTA A and antenna Lr1 at RET angle 10° instead of 7°. In the rest of the results, the main changes are 1-2 dB increases is noise floor and some minor changes in emission magnitudes between polarities. It is fair to say beam direction and RET angle influence these emissions, even if it isn't a drastic change.

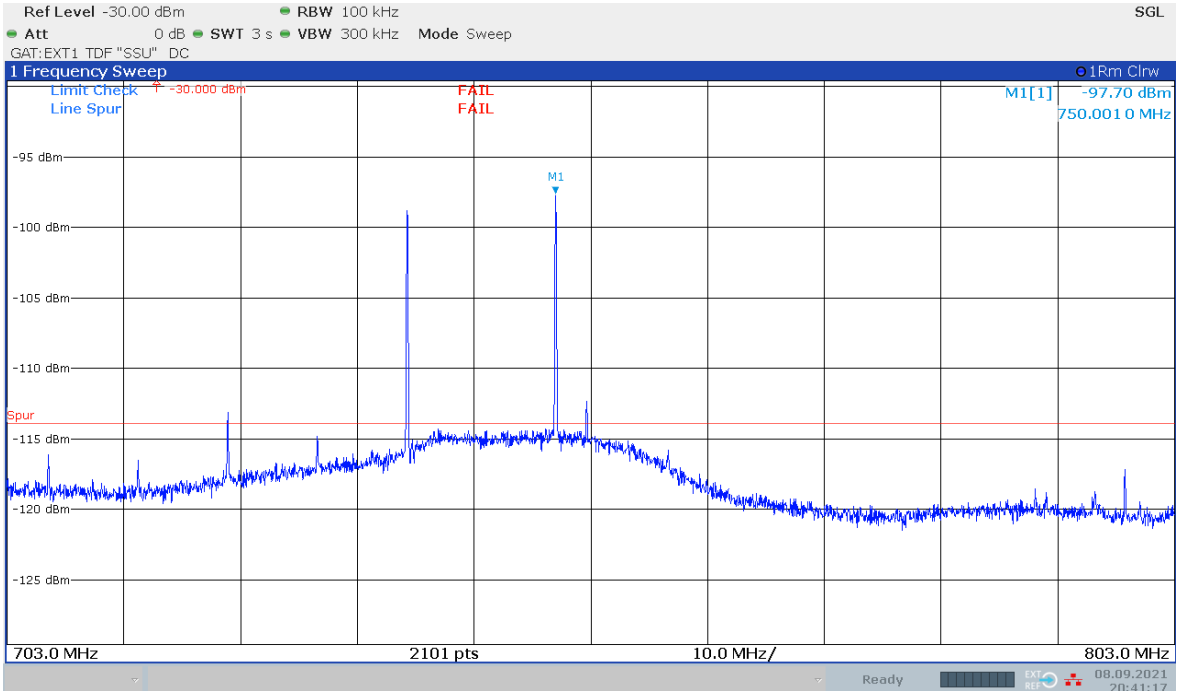


Figure 54. CLTA A antenna Lr1 Mpol 703 – 803 MHz frequency sweep.

The CLTA B results in Figure 55 show three new fail -results and one new pass -result compared to boresight beam results. The fail -result for antenna B1 1850 – 1910 MHz measurement range is gone due to the noise floor no longer being raised in 1900 – 1919 MHz frequency range.

| Ant Eleme | BottomFreq[MH | TopFreq[MH | MaxSpur[dBm] | MaxSpurFreq[M | Limit | vs Limit | PASS/FA | Note |
|---|---|---|---|---|---|---|---|---|
| R1 | 703 | 803 | -99.60390802 | 750 | -113.9 | 14.296092 | FAIL | |
| Y2 | 2300 | 2400 | -104.2852472 | 2400 | -113.9 | 9.6147528 | FAIL | WIFI leaking into chamber |
| Y2 | 2300 | 2400 | -104.2916517 | 2400 | -113.9 | 9.6083483 | FAIL | WIFI leaking into chamber |
| R1 | 703 | 748 | -104.6840962 | 737.3269231 | -113.9 | 9.2159038 | FAIL | |
| R1 | 703 | 748 | -104.7670542 | 737.3269231 | -113.9 | 9.1329458 | FAIL | |
| R1 | 832 | 862 | -105.682346 | 860.1730769 | -113.9 | 8.217654 | FAIL | |
| R1 | 832 | 862 | -105.8927864 | 860.1730769 | -113.9 | 8.0072136 | FAIL | |
| R1 | 698 | 728 | -106.2918665 | 721.9423077 | -113.9 | 7.6081335 | FAIL | |
| R1 | 704 | 716 | -108.2064724 | 714.25 | -113.9 | 5.6935276 | FAIL | |
| R1 | 698 | 716 | -108.6628035 | 714.2692308 | -113.9 | 5.2371965 | FAIL | |
| R1 | 699 | 716 | -108.7358041 | 714.2564103 | -113.9 | 5.1641959 | FAIL | |
| Y2 | 1432 | 1517 | -110.2459921 | 1474.540476 | -113.9 | 3.6540079 | FAIL | |
| R1 | 788 | 798 | -112.1734953 | 791.0288462 | -113.9 | 1.7265047 | FAIL | |
| R1 | 824 | 849 | -115.3002007 | 831.2115385 | -115.9 | 0.5997993 | FAIL | |
| B1 | 1710 | 1785 | -115.6274831 | 1749.964286 | -115.9 | 0.2725169 | FAIL | |
| Y2 | 1710 | 1785 | -116.2835653 | 1749.964286 | -115.9 | -0.383565 | PASS | |
| R1 | 876 | 915 | -116.6046811 | 876.25 | -115.9 | -0.704681 | PASS | |
| Y2 | 1850 | 1910 | -116.9028956 | 1908.365385 | -115.9 | -1.002896 | PASS | |
| B1 | 1850 | 1910 | -116.9849108 | 1864.038462 | -115.9 | -1.084911 | PASS | |
| R1 | 777 | 787 | -115.2839646 | 779.3237179 | -113.9 | -1.383965 | PASS | |
| R1 | 814 | 849 | -115.3137734 | 822.974359 | -113.9 | -1.413773 | PASS | |
| R1 | 815 | 830 | -115.3273703 | 827.7644231 | -113.9 | -1.42737 | PASS | |
| R1 | 807 | 824 | -115.3791108 | 814.0833333 | -113.9 | -1.479111 | PASS | |
| R1 | 824 | 849 | -115.4115254 | 831.4919872 | -113.9 | -1.511525 | PASS | |
| R1 | 824 | 849 | -115.4213172 | 830.3701923 | -113.9 | -1.521317 | PASS | |
| Y2 | 1710 | 1780 | -115.6959978 | 1749.966667 | -113.9 | -1.795998 | PASS | |
| R1 | 830 | 845 | -115.7074597 | 830.3125 | -113.9 | -1.80746 | PASS | |
| B1 | 1710 | 1785 | -115.7197006 | 1749.964286 | -113.9 | -1.819701 | PASS | |
| Y2 | 1710 | 1780 | -115.8233517 | 1749.966667 | -113.9 | -1.923352 | PASS | |
| B1 | 1710 | 1785 | -115.8902265 | 1749.964286 | -113.9 | -1.990226 | PASS | |

Figure 55. CLTA B spurious emission results for DUT beam direction azimuth 50° and elevation 6°.

In the 703 – 803 MHz frequency sweep for CLTA B antenna B1 +45pol shown in Figure 56 the 737 MHz and 750 MHz emissions have dropped in magnitude compared to boresight beam results. However, the smaller emissions are stronger and there are more of them evenly distributed like harmonics of an 8 MHz clock signal. These additional emissions on the lower half of the measurement range are causing fail -results in the 698 – 716 MHz and 704 – 716 MHz ranges. This effect was not present with CLTA A antenna Lr1, so it seems different CLTAs can be more sensitive to certain emissions. It could in theory also be DUT boot specific, as it was depowered between switching from CLTA A to CLTA B.

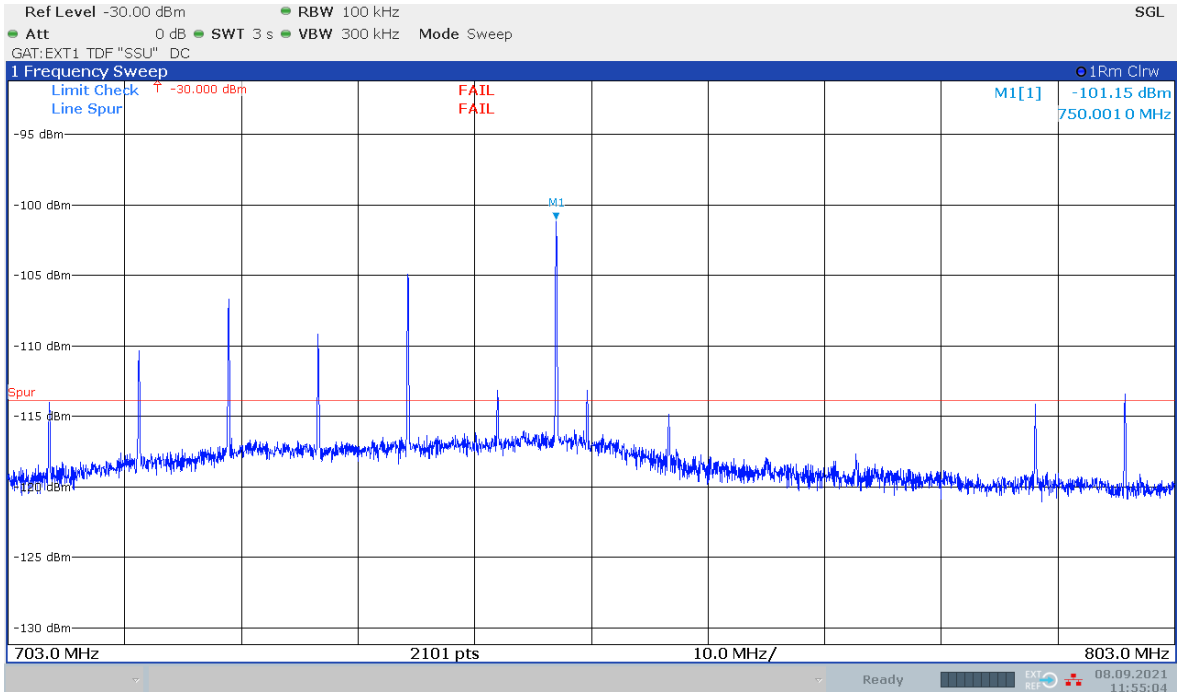


Figure 56. CLTA B antenna R1 +45pol 703 – 803 MHz frequency sweep.

In the 698 – 728 MHz sweep in **Error! Reference source not found.** the emission at 699 MHz would suggest that the N×8 MHz emissions continue even below 700 MHz. It is likely these harmonics continue periodically all the way down to the hypothetical fundamental 8 MHz signal, but it would need to be measured with a low-frequency antenna to make sure.

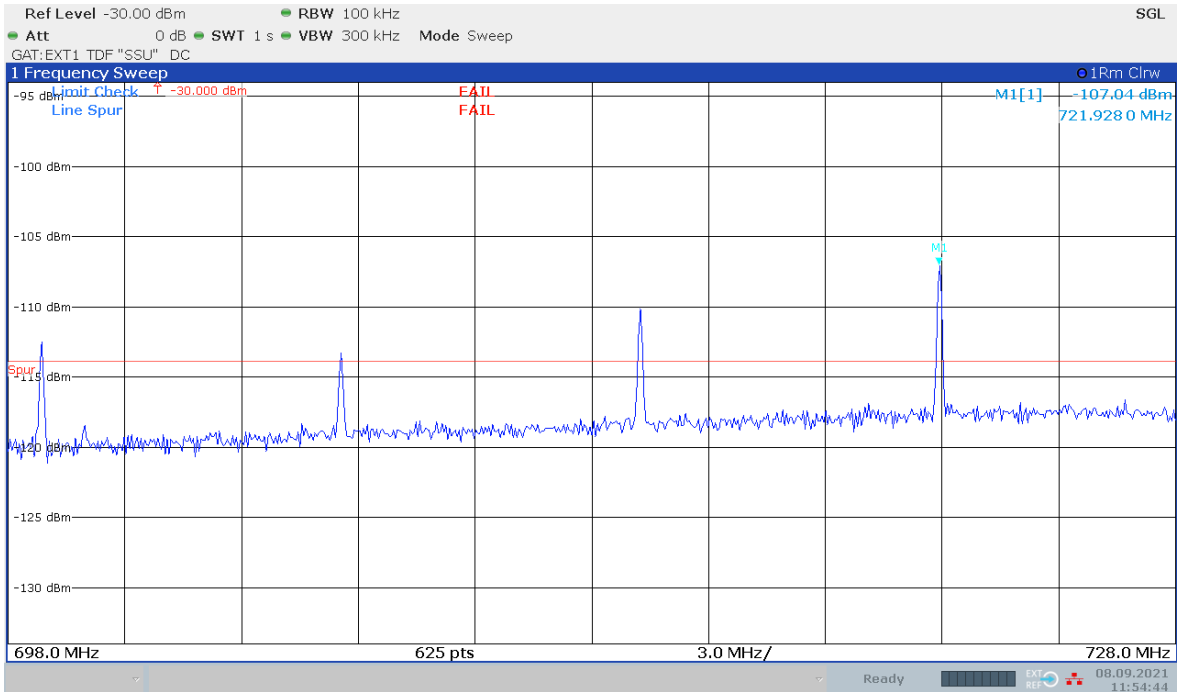


Figure 57. CLTA B antenna R1 +45pol 698 – 728 MHz frequency sweep.

# 6 DISCUSSION

In the CLTA datasheets it was given that the maximum VSWR for all ports is 1.5, which is equal to a return loss of 14 dB. From Figure 19 we could see that the Vivaldi antenna's VSWR is below 1.8 for most of the measured frequency range and 2.5 at worst near 1 GHz. For the isolation measurement the specified return losses for the antennas suggest around 1 dB loss, but it could also be higher due to impedance mismatches. The Vivaldi has finite radiation efficiency, so not all the power delivered to the Vivaldi is transmitted which also increases the isolation results. The radiation efficiency and antenna gain of the Vivaldi could have been better accounted for, but the latter may be complicated to account for as a near-field transformation would be required. In the 3GPP definitions for CLTA path calibration [24], it is required to separately measure the reflection coefficient $\Gamma_{\mathrm{ANT}}$ at the CLTA antenna's connector with a network analyser or equivalent equipment. The result is then combined with other losses $L$ in the test setup to obtain the total path loss $L_{tot} = L + 10\log(1 - |\Gamma_{\mathrm{ANT}}|^2)$ for calibration of the CLTA path. In future implementations of co-location measurements, the reflection coefficient of CLTA antennas should be accounted for in calibration.

The mechanical preparations regarding the positioner CLTA supports could be made easier through re-design. Measuring of the required distances between support beams, positions for the adjustable brackets and their height proved time consuming. This process could be made easier by taping or carving scales and markings to the poles and brackets, which would lessen the need for use of a tape measure and help with accuracy. Once either the CLTA or DUT was lifted and attached on to the supports, adjustments to their positions could not be easily made without detaching and lifting them off the supports. Adding lubricant to the tracks of the t-slot nuts or some mechanical solution like spring retracted wheels could help with being able to glide the brackets and poles into position even with the CLTA or DUT attached. A more holistic approach would be to redesign the supports or the positioner main pole itself according to the principle in Figure 58. This way there would be no need to adjust the attachment points to the main pole and attachments solutions valid for the main pole would be also valid for the side poles. It would however add more weight and require a stronger motor for the positioner, which did not have enough specified torque to rotate both the DUT and CLTA even with the design used. While the positioner was not required for the spurious emissions measurements, the main enabler for future measurement of OTA transmitter intermodulation requirements would be upgrading the motor. For future implementation of said co-location test case exploring and gaining experience in attachment solutions was an important step.

Considering all the physical preparations and distance measurements required for changing from CLTA to another, there was clear benefit to choosing multi-band CLTAs over multiple single-band ones. This could be developed further by having all multi-band CLTA antenna ports connected to an RF switch. The switch would route the antenna under testing to the measurement device and terminate all other ports. This way through test automation control of the switch all the ports in the CLTA could be measured in sequence without having to go into the chamber to physically move the measurement cable and measurement time would. Implementation of such a solution would require some effort due to complexities introduced like CLTAs having different amount of antenna ports. An RF switch with so many ports and requirement of low noise figure can also be expensive.

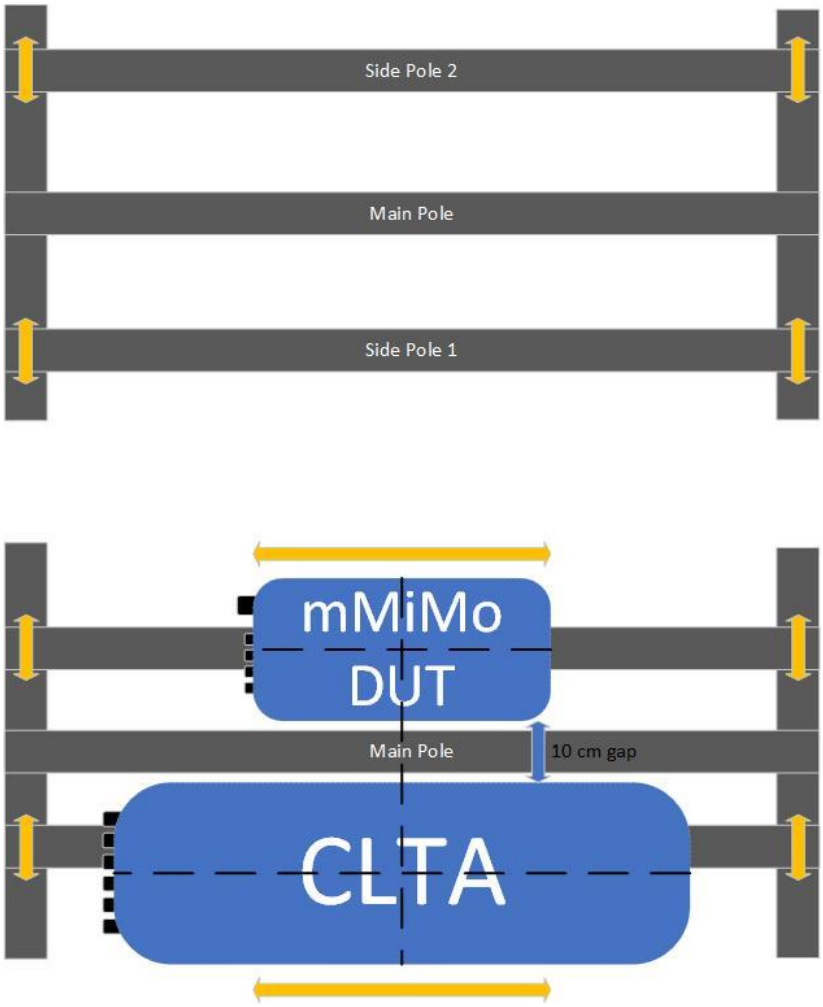


Figure 58. Potential re-design for CLTA supports.

In [4] and [15] it is required that "the vertical radiating regions" of the CLTA and DUT are aligned with the accuracies given in Table 8. In this thesis the multi-band CLTA radome centre was aligned to the DUT instead of the individual CLTA antenna centre. If the latter were done, it would have increased the measurement time as the CLTA would have needed to be moved around more. If the "radiating regions" refers to the radiating elements under the CLTA radome, then sufficiently accurate information of antenna placements would be required from the manufacturer or through taking apart the CLTA. As mentioned in Section 5.2.2, such information was not available from the antenna manufacturer's datasheets. It was seen that some emissions picked up by CLTA B were not seen when measuring with CLTA A. Knowing this, manufacturers could be tempted to use CLTAs that are less susceptible to interference. This proves problematic for definitively verifying conformance to co-location requirements and could be used as justification for a stricter definition for the CLTA or manufacturing of dedicated CLTAs. At the same time from the perspective of adhering to the on-site scenario being mimicked, it makes sense to have the CLTA be a "typical" passive base station antenna instead of something designed specifically for measurement purposes.

In the S21 results of the isolation measurement the single frequency points with high isolation could have been filtered out so that they wouldn't affect the analysis of the data. For transparency this would be best done as a separate analysis of the data and justified by the goal of finding a worst-case isolation between two base station antennas. Another option would have been to use averaging in either the measurement or post-processing of the data to dampen any

sharp changes in isolation. The division into subsets could have been done in a different order as well and taken further. Since there was a clear split between distributions above and below 4 GHz, it might have been helpful to split the data into frequency subsets earlier and then by Vivaldi rotation, RET angle and other parameters.

As has been mentioned in this thesis, more data on the RET angle would have been a welcome addition. A parameter that wasn't explored or validated was the gap between DUT and CLTA, which could have been changed instead of keeping it at the required 10 cm. A lot of the spurious emissions and lowest isolation results were at or below 1 GHz and the Vivaldi antenna was not designed for use below 1.7 GHz. The beamform of the Vivaldi antenna changed at lower frequencies as was seen in Figure 34 and Figure 35, so naturally the isolation's sensitivity to Vivaldi rotation would change with frequency. Curiously, this was not the case with CLTA B, where it seemed like Vivaldi rotation had little to no effect on isolation even at lower frequencies. For these reasons it could have proven beneficial to have a separate measurement antenna for frequencies below 1.7 GHz down to for example 400 MHz where lowest frequency GSM bands operate. A fundamental CST simulation was planned and modelled for isolation of two single column antennas, yet it could not be included due to resource restrictions and need to limit the scope of the thesis. Overall, the isolation measurement and studying of the related phenomena could have been its own separate study that also included the CST simulation to provide a comprehensive understanding on the subject.

The co-location spurious emission results had several fail results for the selected DUT, which is not as surprising when considering 3GPP has no such requirements for the selected DUT's BS type 1-H. It does however justify the addition of these test cases and requiring them for future BS type 1-O products that will be installed in already crowded urban sites. The bulk of the emissions for this DUT operating on the n41 band were at frequencies below its operating band. This means already deployed BS equipment of previous generations operating at lower frequencies than the future 5G radios could be more likely to be victims of interference from said 5G equipment than the other way around. However, 3GPP does not specify different beam steering configurations to be used in co-location spurious emissions testing or what RET angles should be used on the CLTA. As beam steering is a main feature with current and future 5G radios, measuring unwanted emissions with just a single beam steering configuration does not necessarily give a full picture of emissions that can be expected on-site. Even with the limited exploration the effects in this study it was seen that these factors do affect emissions and noise received by the CLTA antennas. In future studies they should be inspected more to definitively evaluate whether additions regarding DUT vertical and horizontal beam steering along with CLTA RET angle should be added to the 3GPP co-location test cases. Yet these additions would also multiply the amount of measurement content required to verify conformance to co-location requirements when the required effort is already considerable with current specifications.

# 7 SUMMARY

Purpose of this thesis was to evaluate and implement the 3GPP specified co-location test case for measuring spurious emissions in an OTA test environment. Key developments and changes in 5G compared to 4G were given as motivation for why co-location testing is important. Descriptions the co-location tests themselves were given, starting with describing the real site scenario and circumstances that the test case is emulating. Brief introduction into 3GPP defined base station types were discussed and synapses for each of the co-location test cases and requirements were given.

Next, the test setup and planning were discussed in detail. The CATR measurement environment and chosen DUT were described. Power budget considerations and calculations for measurement setups were presented to give an idea of the requirements for the measurement setup and components within it. Test plans for measurement execution were laid out to define their scope and present general considerations regarding them. The planned seven-day time table was presented and the step-by-step plan for execution of both measurements were given. The methods used for gathering the measurement data along with categorizing, analysing, and visualizing it are discussed.

In the sixth chapter, the preparations leading up to the measurements were described, including calibration of the measurement setups and preliminary measurements. The execution of planned tests was described, the results were presented and discussed. Problems that arose were laid out and decisions made during the measurements were explained. The visualized results for both CLTAs were presented, observations were made and results of the CLTAs were compared. There were some differences in how the isolation behaved between the CLTAs. Based on the isolation measurement results, some changes in focus were made to the co-location spurious emission measurements to save time. The results from the reference measurement revealed some noise sources within the test environment. The results from the 3GPP specified measurement and the following “worst-case” measurement were displayed per CLTA. The potential sources for the emissions were discussed and it turned out there were some differences between CLTAs when it came to picking up specific emissions or their magnitude. The “worst-case” scenario measurement showed that beamforming and Remote Electrical Tilt angle influence emissions, but the effect wasn’t the same for both CLTAs.

Finally, potential improvements that could be made to future implementations of the measurements done in this thesis were discussed. Topics for future studies were given, particularly regarding the effect of Remote Electrical Tilt angles and beamforming when it comes to unwanted emissions in a co-location scenario.

# 8 REFERENCES


[1] Remmert H. (read 6.6.2022) 2G, 3G, 4G LTE Network Shutdown Updates. URL: https://www.digi.com/blog/post/2g-3g-4g-lte-network-shutdown-updates

[2] De Luca S. (read 6.6.2022) New benchmark on switching off 2G and 3G networks in Europe. URL: https://www.cullen-international.com/news/2021/07/New-benchmark-on-switching-off-2G-and-3G-networks-in-Europe.html

[3] 3GPP. (read 1.2.2021) About 3rd Generation Partnership Project. URL: https://www.3gpp.org/about-3gpp

[4] 3rd Generation Partnership Project (2020) Technical Specification Group Radio Access Network; NR; Base Station (BS) conformance testing Part 2: Radiated conformance testing (Release 17). 3GPP TS 38.141-2, 347 p.

[5] 3GPP (read 14.6.2022) Long Term Evolution. URL: https://www.3gpp.org/technologies/keywords-acronyms/98-lte

[6] Khan, M., Bashir S. & Habib A. (2014) Semi Round Robin Pairing and Scheduling in Uplink Virtual Multiple Input Multiple Output (VMIMO) communications. Journal of Space Technology 4, p.61-66.

[7] 3rd Generation Partnership Project (2019) Technical Specification Group Services and System Aspects; Release 15 Description; Summary of Rel-15 Work Items (Release 15). 3GPP TR 21.915, 118 p.

[8] Shafi M. et al. (2017) 5G: A Tutorial Overview of Standards, Trials, Challenges, Deployment, and Practice. IEEE Journal on Selected Areas in Communications, Vol. 35, No. 6, pp. 1201-1221.

[9] G. Barb & M. Otesteanu. (2020) 4G/5G: A Comparative Study and Overview on What to Expect from 5G. In: 43rd International Conference on Telecommunications and Signal Processing (TSP), July 07-09, Milan, Italy, p. 37-40, doi: 10.1109/TSP49548.2020.9163402.

[10] 3rd Generation Partnership Project (2022) Technical Specification Group Radio Access Network; Evolved Universal Terrestrial Radio Access (E-UTRA); Base Station (BS) radio transmission and reception (Release 17). 3GPP TS 36.104, 293 p.

[11] 3rd Generation Partnership Project (2022) Technical Specification Group Radio Access Network; NR; User Equipment (UE) radio transmission and reception; Part1: Range 1 Standalone (Release 17). 3GPP TS 38.101-1, 582 p.

[12] Ni Yunfeng, Liang Jiahao, Shi Xiaohong & Ban Dongdong. (2019) Research on Key Technology in 5G Mobile Communication Network. In: 2019 International Conference on Intelligent Transportation, Big Data & Smart City (ICITBS), January 12-13, Changsha, China, p. 199-201, doi: 10.1109/ICITBS.2019.00054.

[13] H. A. Salman, G. Aldabbagh, Z. Taha & L. F. Ibrahim. (2015) Topological Planning and Design of Heterogeneous Mobile Networks in Dense Areas. In: International Conference on Computational Science and Computational Intelligence (CSCI), December 07-09, Las Vegas, NV, USA, p. 709-714, doi: 10.1109/CSCI.2015.151.

[14] A. Sukarno, A. Hikmaturokhman & D. Rachmawaty. (2020) Comparison of 5G NR Planning in Mid-Band and High-Band in Jababeka Industrial Estate. In: IEEE International Conference on Communication, Networks and Satellite (Comnetsat), December 17-18, Batam, Indonesia, p. 12-17, doi: 10.1109/Comnetsat50391.2020.9329000.

[15] 3rd Generation Partnership Project (2021) Technical Specification Group Radio Access Network; NR; Base Station (BS) radio transmission and reception (Release 17). 3GPP TS 38.104, 305 p.

[16] International Telecommunication Union (2012) Rec. ITU-R SM.329-7 1 RECOMMENDATION ITU-R SM.329-7 SPURIOUS EMISSIONS (Question ITU-R 55/1) (1951-1953-1956-1959-1963-1966-1970-1978-1982-1986-1990-1997). ITU-R SM.329-12, 23 p.

[17] Antenna Interface Standards Group (2018) Antenna Port Colour Coding Standard AISG-APC (V3.2.1). URL: https://aisg.org.uk/files/AISG-Antenna-Port-Color-Coding-v3.2.1.pdf

[18] 3rd Generation Partnership Project (2020) Technical Specification Group Radio Access Network; Evolved Universal Terrestrial Radio Access (E-UTRA) and Universal Terrestrial Radio Access (UTRA); Radio Frequency (RF) requirement background for Active Antenna System (AAS) Base Station (BS) radiated requirements (Release 15). 3GPP TR 37.843, 84 p.

[19] 3rd Generation Partnership Project (1999) TSG-RAN Working Group 4 (Radio) Meeting #8. TSGR4#8(99)631, 8p. URL: ftp://www.3gpp.org/tsg_ran/WG4_Radio/TSGR4_08/Docs/PDFs/r4-99631.pdf

[20] Pozar D. M. (2012) Microwave engineering (4th Edition), Wiley, New Jersey, USA, 736 p.

[21] L3Harris Narda-MITEQ. (read March 2022) AFS and JS series Amplifiers datasheet. URL: https://www.everythingrf.com/products/microwave-rf-amplifiers/miteq/567-74-afs3-00100600-13-10p-4

[22] Rohde & Schawrz. (read March 2022) R&S®ZNL Vector Network Analyzer - Specifications URL: https://scdn.rohde-schwarz.com/ur/pws/dl_downloads/dl_common_library/dl_brochures_and_datasheets/pdf_1/ZNL_dat-sw_en_3607-1071-22_v0600.pdf

[23] 3rd Generation Partnership Project (2022) Technical Specification Group Radio Access Network; NR; Base Station (BS) conformance testing Part 1: Conducted conformance testing (Release 17). 3GPP TS 38.141-1, 326 p.

[24] 3rd Generation Partnership Project (2022) Technical Specification Group Radio Access Network; Radio Frequency (RF) conformance testing background for radiated Base Station (BS) requirements (Release 17). 3GPP TR 37.941, 329p.

# 9 APPENDICES

Appendix 1 MATLAB script for analysing CLTA & Vivaldi isolation measurement results

Appendix 2 Python script for summing measurement results

Appendix 3 Additional isolation measurement results for different Vivaldi angles

Appendix 4 Additional isolation measurement results for different frequency subsets

Appendix 5 Additional isolation measurement results per CLTA antenna frequency subset

# Appendix 1 MATLAB script for analysing CLTA & Vivaldi isolation measurement results

```
%This script was created to run statistical analysis for co-location isolation
%measurements. It is done by processing s1p -files containing S21 results measured
%between measurement antenna and DUT antenna. Angle/phase values of the
%files are ignored, as only magnitude was of interest in the measurement.
%It is assumed that every file has the same frequency sweep range.

%The measurement antenna (referred to as Vivaldi) is moved to different
%positions along the vertical edge of the DUT antenna. In each position the
%Vivaldi is also rotated to different angles.
%The different position for each measurement and angle of the Vivaldi are
%assumed to be contained within the file name of the s1p -file.
%In the middle point of each element results for different mechanical tilt angles (RET
%angles) are also provided and analyzed in this script.


%% %%%%%%%%%%%%%%%%%%%%%%%%%%%%%% SETUP %%%%%%%%%%%%%%%%%%%%%%%%%%%%%%%%

clear;
close all;

% Filepath to the results folder where it branches off to different antenna
% results. Take care that filepath to s1p files per each element's polarity is e.g:
% C:\Users\kotikump\Documents\DI measurement results\Meas_results\Preliminary Vivaldi
measurement results\CLTA A\Lb1_1695_2200\Mpol
dataRoot = 'C:\Users\kotikump\Documents\DI measurement results\Meas_results\Preliminary
Vivaldi measurement results';

% Folder names for each DUT antenna's results, names of antenna elements
% and their frequency ranges which make up the element specific folder
% name.
Ant1='CLTA A';
elementsAnt1 = {'Lr1'; 'Lb1'; 'Ly1'; 'Ry3'; 'p1'};
frequenciesAnt1 = [690 960; 1695 2200; 2490 2690; 1427 2690; 2300 3800];
elementLengthsAnt1 = [2100; 1050; 1050; 1050; 1050]; % Length of antenna elements
elementPositionAnt1 = {'Left'; 'TopL'; 'TopL'; 'TopR'; 'BottomL'}; % Position of antenna
elements as viewed from radome side
defaultRETAnt1 = 7;

Ant2='CLTA B';
elementsAnt2 = {'R1'; 'B1'; 'Y1'; 'Y2'};
frequenciesAnt2 = [694 960; 1695 2180; 2490 2690; 1427 2690];
elementLengthsAnt2 = [2090; 1045; 1045; 1045]; % Length of antenna elements
elementPositionAnt2 = {'Left'; 'BottomL'; 'BottomL'; 'BottomL'}; % Position of antenna
elements as viewed from radome side
defaultRETAnt2 = 7;

measPoints = 2700;
freqStep = 2;   % Frequency step between measurement points in MHz


%%%%%%%%%% CHOOSE ANTENNA HERE %%%%%%%%%%
measAnt = Ant1;
%measAnt = Ant2;

if measAnt == Ant1
    antName = Ant1;
    antennaElements = elementsAnt1;
    elementFreqs = frequenciesAnt1;
    elementLengths = elementLengthsAnt1;
    elementPositions = elementPositionAnt1;
    defaultRET = defaultRETAnt1;
    [elementCount,n] = size(elementsAnt1);

elseif measAnt == Ant2
    antName = Ant2;
    antennaElements = elementsAnt2;
    elementFreqs = frequenciesAnt2;
    elementLengths = elementLengthsAnt2;
    elementPositions = elementPositionAnt2;
    defaultRET = defaultRETAnt2;
    [elementCount,n] = size(elementsAnt2);
```

```
end


% Initialize Minus polarity (-45deg)
MpolelementData = cell(elementCount, n); % Cell matrix for per element measurement data
MpolFilelist = cell(elementCount,n);
MpolFileCount = zeros(elementCount,1);
MpolmeasAngles = cell(elementCount,n);
MpolNormPositions = cell(elementCount,n);
MpolRETAngles = cell(elementCount,n);
% Initialize Plus polarity (+45deg)
PpolelementData = cell(elementCount, n);
PpolFilelist = cell(elementCount,n);
PpolFileCount = zeros(elementCount,1);
PpolmeasAngles = cell(elementCount,n);
PpolNormPositions = cell(elementCount,n);
PpolRETAngles = cell(elementCount,n);

%% %%%%%%%%%%%%%%%%%%%%%%%% READ DATA %%%%%%%%%%%%%%%%%%%%%%%%%%%%%%%%

% Cell matrices which will contain results for both polarities
n = 2;
maxIsolation = cell(elementCount,n);
minIsolation = cell(elementCount,n);
avgIsolation = cell(elementCount,n);

% Get list of files for each element and initialize arrays for Angle and
% Position values.
for e = 1:elementCount

    [MpolFilelist{e}, PpolFilelist{e}] = GetFileList(dataRoot, measAnt, antennaElements,
elementFreqs,e);

    %Initialize cell arrays for Vivaldi angles and Vivaldi positions
    fileCount = size(MpolFilelist{e});
    MpolFileCount(e) = fileCount(1);
    MpolmeasAngles{e}=ones(1, MpolFileCount(e));
    %MpolmeasPositions{e}=ones(1, MpolFileCount(e));
    MpolNormPositions{e}=ones(1, MpolFileCount(e));
    MpolRETAngles{e}=ones(1, MpolFileCount(e));
    maxIsolation{e,1} = zeros(MpolFileCount(e),2);
    minIsolation{e,1} = zeros(MpolFileCount(e),2);
    avgIsolation{e,1} = zeros(MpolFileCount(e),1);

    fileCount = size(PpolFilelist{e});
    PpolFileCount(e) = fileCount(1);
    PpolmeasAngles{e}=ones(1, PpolFileCount(e));
    %PpolmeasPositions{e}=ones(1, PpolFileCount(e));
    PpolNormPositions{e}=ones(1, PpolFileCount(e));
    PpolRETAngles{e}=ones(1, PpolFileCount(e));
    maxIsolation{e,2} = zeros(PpolFileCount(e),2);
    minIsolation{e,2} = zeros(PpolFileCount(e),2);
    avgIsolation{e,2} = zeros(PpolFileCount(e),1);


end


% Matrixes for analysis results
% 3D matrix since each value will have a corresponding frequency
analysisArguments = {'Magnitude','Frequency','Position','Angle','RET','Polarity'};
%m = max([max(MpolFileCount), max(PpolFileCount)]);
n = size(analysisArguments);


for e = 1:elementCount

    % Per element (m) arrays for Vivaldi angles and positions along vertical
    % edge of CLTA for each measurement point (x)

    M = zeros(measPoints, 2); % Initilialize per element data matrix
    P = zeros(measPoints, 2); % Initilialize per element data matrix


    for f = 1:MpolFileCount(e)
```

```
        [filePath, MpolmeasAngles{e}(f), MpolNormPositions{e}(f), MpolRETAngles{e}(f)] =
GetMeasInfo(MpolFilelist, e, f, defaultRET, elementPositions, elementLengths);
        % Read data file and extract per element data into matrix
        fid = fopen(filePath);
        M = getElementData(M,fid,5,f);
        fclose(fid);
    end
    % Add data matrices for each element into cell array
    MpolelementData{e} = M;

    for f = 1:PpolFileCount(e)

        [filePath, PpolmeasAngles{e}(f), PpolNormPositions{e}(f), PpolRETAngles{e}(f)] =
GetMeasInfo(PpolFilelist, e, f, defaultRET, elementPositions, elementLengths);
        fid = fopen(filePath);
        P = getElementData(P,fid,5,f);
        fclose(fid);

    end

    PpolelementData{e} = P;

end

% First column is frequency in every cell, rest are data for different meas
% points
frequencyPoints = MpolelementData{1}(:,1);
% Cut out sub-1GHz points, since Vivaldi is not matched there:
fPoints = (frequencyPoints >= 1e9);
frequencyPoints = frequencyPoints(fPoints);
measPoints = max(size(frequencyPoints));

%% %%%%%%%%%%%%%%%%%%%%%%%% ANALYZE DATA %%%%%%%%%%%%%%%%%%%%%%%%%%%%%%


% Find min/max/avg values for all the frequency sweeps along with the
% Vivaldi positions, angles, RET angles and frequencies that they happen at
dataPoints = zeros(measPoints,1);

MpolDataCount = measPoints*MpolFileCount;
PpolDataCount = measPoints*PpolFileCount;
TotalDataCount = sum(measPoints*MpolFileCount)+sum(measPoints*PpolFileCount);

AllMpolData = zeros(sum(MpolDataCount),1);
AllPpolData = zeros(sum(PpolDataCount),1);
AllData = zeros(TotalDataCount,1);

for e = 1:elementCount

    for f = 1:MpolFileCount(e)

        dataPoints = MpolelementData{e}(:,f+1);
        dataPoints = dataPoints(fPoints);
        Angle = MpolmeasAngles{e}(f);
        Position = MpolNormPositions{e}(f);
        [maxIsolation{e,1}(f,1),maxIsolation{e,1}(f,2)] =
getMaximum(dataPoints,frequencyPoints);
        [minIsolation{e,1}(f,1),minIsolation{e,1}(f,2)] =
getMinimum(dataPoints,frequencyPoints);
        avgIsolation{e,1}(f,1) = getMean(dataPoints);

        idx = find(AllMpolData==0,1,'first'):1:(find(AllMpolData==0,1,'first')+measPoints-1);
        AllMpolData(idx) = (-1)*dataPoints;

    end

    for f = 1:PpolFileCount(e)

        dataPoints = PpolelementData{e}(:,f+1);
        dataPoints = dataPoints(fPoints);
        Angle = PpolmeasAngles{e}(f);
        Position = PpolNormPositions{e}(f);
        [maxIsolation{e,2}(f,1),maxIsolation{e,2}(f,2)] =
getMaximum(dataPoints,frequencyPoints);
```

```
        [minIsolation{e,2}(f,1),minIsolation{e,2}(f,2)] =
getMinimum(dataPoints,frequencyPoints);
        avgIsolation{e,2}(f,1) = getMean(dataPoints);

        idx = find(AllPpolData==0,1,'first'):1:(find(AllPpolData==0,1,'first')+measPoints-1);
        AllPpolData(idx) = (-1)*dataPoints;

    end

end

AllData(1:end) = [AllMpolData;AllPpolData];


%% %%%%%%%%%%%%%%%%%%%%%%%%%% PLOT DATA %%%%%%%%%%%%%%%%%%%%%%%%%%%%%%%%%%
%% % MIN/MAX/AVG LINEPLOTS %%%
f1 = figure;
f2 = figure;
f3 = figure;
f4 = figure;
f5 = figure;
f6 = figure;
f7 = figure;

markers = {'+','o','*','.','x','s','d','^','v','>','<','p','h'};
lines = {'-','--',':','-.'};
colors = {'r','g','b','c','m','y','k','w'};



Polarities = {'Mpol','Ppol'};
% datatypes = {'Max','Min','Average'};
datatypes = {'Min','Average'};
m = size(datatypes)*elementCount;
m = m(2);
Legend0 = strings(2,m);
Legend45 = strings(2,m);
Legend90 = strings(2,m);

xAxisLable1 = ['(Position of Vivaldi along element',newline,'vertical
edge)',newline,'/',newline,'(Antenna element size)',newline,'[m/m]'];
yAxisLable1 = 'Isolation [dB]';
% Axis limits:
xL = [round(min(MpolNormPositions{2}),2) round(max(MpolNormPositions{2}),2)];
yL = [15 70];

n = 1;  % Plots in vertical direction of figure
m = 6;  % Plots in horizontal direction of figure

NormPositions = [MpolNormPositions, PpolNormPositions];
measAngles = [MpolmeasAngles, PpolmeasAngles];
measRETAngles = [MpolRETAngles, PpolRETAngles];

defaultRETminIso = zeros(2,elementCount);
minRETminIso = zeros(2,elementCount);
maxRETminIso = zeros(2,elementCount);

defaultRETavgIso = zeros(2,elementCount);
minRETavgIso = zeros(2,elementCount);
maxRETavgIso = zeros(2,elementCount);

for p = 1:2

    for e = 1:elementCount

%         legendIndex = [3*e-2,3*e-1,3*e]; %Max included
        legendIndex = [3*e-2,2*e-1,2*e];  %Min & Avg only

        Positions = NormPositions{e,p};
        Angles = measAngles{e,p};
        RETAngles = measRETAngles{e,p};

        %%% PLOT (MAX/)MIN/AVG ISOLATION AS FUNCTION OF VIVALDI POSITION %%%
        %%% PER VIVALDI ANGLE AND CLTA POLARITY                      %%%
```

```
        %Plot Vivaldi Angle 0deg RET7 results
        figure(f1)
        Angle = 0;
        RET = defaultRET;

        subplot(n,m,p)
        hold on
        title('Vivaldi 0deg RET7 '+string(Polarities{p}))
        xlim(xL)
        xticks(xL(1):0.25:xL(2))
        ylim(yL)
        xlabel(xAxisLable1)
        ylabel(yAxisLable1)

%         datatype = 'Max';
%         Legend0(p,legendIndex(1)) = string(antennaElements{e})+' '+datatype;
%         [results,sortedPositions,sortedAngles,sortedRETAngles,sortedfreqs] =
sortData(maxIsolation(:,p), datatype, Positions, Angles, RETAngles, e);
%         [y,ii,line] = formLineData(results, datatype, sortedAngles, sortedRETAngles,
markers, lines, colors, Angle, RET, e);
%         plot(Positions(ii),(-1)*y,line) % Plot max

        datatype = 'Min';
%        Legend0(p,legendIndex(2)) = string(antennaElements{e})+' '+datatype+'
'+elementFreqs(e,1)+'-'+elementFreqs(e,2)+"MHz";
        Legend0(p,legendIndex(2)) = string(antennaElements{e})+' '+datatype;
        [results,sortedPositions,sortedAngles,sortedRETAngles,sortedfreqs] =
sortData(minIsolation(:,p), datatype, Positions, Angles, RETAngles, e);
        [y,ii,line] = formLineData(results, datatype, sortedAngles, sortedRETAngles, markers,
lines, colors, Angle, RET, e);
        plot(sortedPositions(ii),(-1)*y,line) % Plot min 0deg

        datatype = 'Average';
%        Legend0(p,legendIndex(3)) = string(antennaElements{e})+' '+datatype+'
'+elementFreqs(e,1)+'-'+elementFreqs(e,2)+"MHz";
        Legend0(p,legendIndex(3)) = string(antennaElements{e})+' '+datatype;
        [results,sortedPositions,sortedAngles,sortedRETAngles,sortedfreqs] =
sortData(avgIsolation(:,p), datatype, Positions, Angles, RETAngles, e);
        [y,ii,line] = formLineData(results, datatype, sortedAngles, sortedRETAngles, markers,
lines, colors, Angle, RET, e);
        plot(sortedPositions(ii),(-1)*y,line) % Plot min 0deg


        %Plot Vivaldi Angle 45deg RET7 results
        Angle = 45;
        RET = defaultRET;

        subplot(n,m,p+2)
        hold on
        title('Vivaldi 45deg RET7 '+string(Polarities{p}))
        xlim(xL)
        xticks(xL(1):0.25:xL(2))
        ylim(yL)
        xlabel(xAxisLable1)
        ylabel(yAxisLable1)

        datatype = 'Min';
        Legend45(p,legendIndex(2)) = string(antennaElements{e})+' '+datatype;
        [results,sortedPositions,sortedAngles,sortedRETAngles,sortedfreqs] =
sortData(minIsolation(:,p), datatype, Positions, Angles, RETAngles, e);
        [y,ii,line] = formLineData(results, datatype, sortedAngles, sortedRETAngles, markers,
lines, colors, Angle, RET, e);
        plot(sortedPositions(ii),(-1)*y,line) % Plot min 45deg

        datatype = 'Average';
        Legend45(p,legendIndex(3)) = string(antennaElements{e})+' '+datatype;
        [results,sortedPositions,sortedAngles,sortedRETAngles,sortedfreqs] =
sortData(avgIsolation(:,p), datatype, Positions, Angles, RETAngles, e);
        [y,ii,line] = formLineData(results, datatype, sortedAngles, sortedRETAngles, markers,
lines, colors, Angle, RET, e);
        plot(sortedPositions(ii),(-1)*y,line) % Plot mean 45deg


        %Plot Vivaldi Angle 90deg RET7 results
        Angle = 90;
```

```
        RET = defaultRET;

        subplot(n,m,p+4)
        hold on
        title('Vivaldi 90deg RET7 '+string(Polarities{p}))
        xlim(xL)
        xticks(xL(1):0.25:xL(2))
        ylim(yL)
        xlabel(xAxisLable1)
        ylabel(yAxisLable1)

        datatype = 'Min';
        Legend90(p,legendIndex(2)) = string(antennaElements{e})+' '+datatype;
        [results,sortedPositions,sortedAngles,sortedRETAngles,sortedfreqs] =
sortData(minIsolation(:,p), datatype, Positions, Angles, RETAngles, e);
        [y,ii,line] = formLineData(results, datatype, sortedAngles, sortedRETAngles, markers,
lines, colors, Angle, RET, e);
        plot(sortedPositions(ii),(-1)*y,line) % Plot min 90deg

        datatype = 'Average';
        Legend90(p,legendIndex(3)) = string(antennaElements{e})+' '+datatype;
        [results,sortedPositions,sortedAngles,sortedRETAngles,sortedfreqs] =
sortData(avgIsolation(:,p), datatype, Positions, Angles, RETAngles, e);
        [y,ii,line] = formLineData(results, datatype, sortedAngles, sortedRETAngles, markers,
lines, colors, Angle, RET, e);
        plot(sortedPositions(ii),(-1)*y,line) % Plot mean 90deg

        %%% PLOT MIN&AVG ISOLATIONS FOR DIFFERENT RET ANGLES PER POLARITY %%%
        %%% CENTER POINT OF AE, PER POLARITY ACROSS ALL ANTENNA ELEMENTS  %%%

        minRET = min(RETAngles);
        maxRET = max(RETAngles);

        %Gather results for default RET angle
        Angle = 0;
        RET = defaultRET;
        Position = 0.5;
        [midDiff,idx] = min(abs(sortedPositions-Position)); %find position closest to middle
of antenna
        %disp(midDiff) %debug
        Position = sortedPositions(idx);

        datatype = 'Min';
        [results,sortedPositions,sortedAngles,sortedRETAngles,sortedfreqs] =
sortData(minIsolation(:,p), datatype, Positions, Angles, RETAngles, e);
        [y,~,~] = formLineData(results, datatype, sortedAngles, sortedRETAngles, markers,
lines, colors, Angle, RET, e, Position, sortedPositions);
        defaultRETminIso(p,e) = y;

        datatype = 'Average';
        [results,sortedPositions,sortedAngles,sortedRETAngles,sortedfreqs] =
sortData(avgIsolation(:,p), datatype, Positions, Angles, RETAngles, e);
        [y,~,~] = formLineData(results, datatype, sortedAngles, sortedRETAngles, markers,
lines, colors, Angle, RET, e, Position, sortedPositions);
        defaultRETavgIso(p,e) = y;

        %Gather results for minimum RET angle
        Angle = 0;
        RET = minRET;

        datatype = 'Min';
        [results,sortedPositions,sortedAngles,sortedRETAngles,sortedfreqs] =
sortData(minIsolation(:,p), datatype, Positions, Angles, RETAngles, e);
        [y,~,~] = formLineData(results, datatype, sortedAngles, sortedRETAngles, markers,
lines, colors, Angle, RET, e);
        minRETminIso(p,e) = y;

        datatype = 'Average';
        [results,sortedPositions,sortedAngles,sortedRETAngles,sortedfreqs] =
sortData(avgIsolation(:,p), datatype, Positions, Angles, RETAngles, e);
        [y,~,~] = formLineData(results, datatype, sortedAngles, sortedRETAngles, markers,
lines, colors, Angle, RET, e, Position, sortedPositions);
        minRETavgIso(p,e) = y;

        %Gather results for maximum RET angle
```

```
        Angle = 0;
        RET = maxRET;

        datatype = 'Min';
        [results,sortedPositions,sortedAngles,sortedRETAngles,sortedfreqs] =
sortData(minIsolation(:,p), datatype, Positions, Angles, RETAngles, e);
        [y,~,~] = formLineData(results, datatype, sortedAngles, sortedRETAngles, markers,
lines, colors, Angle, RET, e);
        maxRETminIso(p,e) = y;

        datatype = 'Average';
        [results,sortedPositions,sortedAngles,sortedRETAngles,sortedfreqs] =
sortData(avgIsolation(:,p), datatype, Positions, Angles, RETAngles, e);
        [y,~,~] = formLineData(results, datatype, sortedAngles, sortedRETAngles, markers,
lines, colors, Angle, RET, e, Position, sortedPositions);
        maxRETavgIso(p,e) = y;

    end

end

% Text positions in x-axis
tX = xL(2)-1.0;
mX = xL(2)-0.5;
bX = xL(2)-0.41+xL(1);  %For CLTA A
%
% Text positions in y-axis
tY = 1;
mY = 0.97;
bY = 0.93;
scaleY = 0.3;

% Add legends and markers to subplots:
subplot(n,m,1)
plot([0 0.5 1; 0 0.5 1], [yL;yL;yL]')  % Mark element top, middle and bottom
text([tX mX bX], yL(2)*scaleY*[tY mY bY], {'<Element Top', '<Element Middle', 'Element
Bottom>'})
legend(Legend0(1,:))
grid on
subplot(n,m,2)
plot([0 0.5 1; 0 0.5 1], [yL;yL;yL]')  % Mark element top, middle and bottom
text([tX mX bX], yL(2)*scaleY*[tY mY bY], {'<Element Top', '<Element Middle', 'Element
Bottom>'})
% legend(Legend0(2,:))
grid on
subplot(n,m,3)
plot([0 0.5 1; 0 0.5 1], [yL;yL;yL]')  % Mark element top, middle and bottom
text([tX mX bX], yL(2)*scaleY*[tY mY bY], {'<Element Top', '<Element Middle', 'Element
Bottom>'})
% legend(Legend45(1,:))
grid on
subplot(n,m,4)
plot([0 0.5 1; 0 0.5 1], [yL;yL;yL]')  % Mark element top, middle and bottom
text([tX mX bX], yL(2)*scaleY*[tY mY bY], {'<Element Top', '<Element Middle', 'Element
Bottom>'})
% legend(Legend45(2,:))
grid on
subplot(n,m,5)
plot([0 0.5 1; 0 0.5 1], [yL;yL;yL]')  % Mark element top, middle and bottom
text([tX mX bX], yL(2)*scaleY*[tY mY bY], {'<Element Top', '<Element Middle', 'Element
Bottom>'})
% legend(Legend90(1,:))
grid on
subplot(n,m,6)
plot([0 0.5 1; 0 0.5 1], [yL;yL;yL]')  % Mark element top, middle and bottom
text([tX mX bX], yL(2)*scaleY*[tY mY bY], {'<Element Top', '<Element Middle', 'Element
Bottom>'})
% legend(Legend90(2,:))
grid on

sgtitle(sprintf('Min and Mean Isolations between Vivaldi and %s', antName))
hold off


%% % PLOT BAR GRAPHS FOR RET ANGLES %%%
```

```
figure(f2)
categories = {'MIN_{minRET}','MEAN_{minRET}', 'MIN_{defaultRET}','MEAN_{defaultRET}',
'MIN_{maxRET}', 'MEAN_{maxRET}'};
x = categorical(categories);
x = reordercats(x,categories);


subplot(2,1,1)
hold on
%xAxisLable1 = ['(Position of Vivaldi along antenna element vertical
edge)',newline,'/',newline,'(Antenna element size)',newline,'[m/m]'];
yAxisLable1 = 'Isolation [dB]';
%Mpol RET effect
MINISOminResult = [(-1)*max(minRETminIso(1,:)) (-1)*max(defaultRETminIso(1,:)) (-
1)*max(maxRETminIso(1,:))];
MINISOmaxResult = [(-1)*min(minRETminIso(1,:)) (-1)*min(defaultRETminIso(1,:)) (-
1)*min(maxRETminIso(1,:))];
MINISOdiffResult = MINISOmaxResult - MINISOminResult;

MEANISOminResult = [(-1)*max(minRETavgIso(1,:)) (-1)*max(defaultRETavgIso(1,:)) (-
1)*max(maxRETavgIso(1,:))];
MEANISOmaxResult = [(-1)*min(minRETavgIso(1,:)) (-1)*min(defaultRETavgIso(1,:)) (-
1)*min(maxRETavgIso(1,:))];
MEANISOdiffResult = MEANISOmaxResult - MEANISOminResult;

a = [MINISOminResult; MEANISOminResult];
a = a(:)';
b = [MINISOmaxResult; MEANISOmaxResult];
b = b(:)';
bar(x,b);
bar(x,a);

ylabel(yAxisLable1)
title('Mpol')
grid on
legend('Maximum','Minimum')

subplot(2,1,2)
hold on
%Ppol RET effect
MINISOminResult = [(-1)*max(minRETminIso(2,:)) (-1)*max(defaultRETminIso(2,:)) (-
1)*max(maxRETminIso(2,:))];
MINISOmaxResult = [(-1)*min(minRETminIso(2,:)) (-1)*min(defaultRETminIso(2,:)) (-
1)*min(maxRETminIso(2,:))];
MINISOdiffResult = MINISOmaxResult - MINISOminResult;

MEANISOminResult = [(-1)*max(minRETavgIso(2,:)) (-1)*max(defaultRETavgIso(2,:)) (-
1)*max(maxRETavgIso(2,:))];
MEANISOmaxResult = [(-1)*min(minRETavgIso(2,:)) (-1)*min(defaultRETavgIso(2,:)) (-
1)*min(maxRETavgIso(2,:))];
MEANISOdiffResult = MEANISOmaxResult - MEANISOminResult;

a = [MINISOminResult; MEANISOminResult];
a = a(:)';
b = [MINISOmaxResult; MEANISOmaxResult];
b = b(:)';
bar(x,b)
bar(x,a)
ylabel(yAxisLable1)
title('Ppol')
grid on
legend('Maximum','Minimum')
sgtitle(sprintf('Range of minimum and average isolation per RET angle at element middle - %s',
antName))

%% % PLOT HISTOGRAMS FOR DIFFERENT DATASETS %%%
%% WHOLE DATASET & POLARITY SPECIFIC HISTOGRAMS

xLimits = [20 120];
yLimits = '';

%Entire dataset
figure(f3)
formHistogram(AllData, xLimits, yLimits)
```

```
title(sprintf('Entire dataset histogram - %s', antName))

%%MPol subset vs Ppol subset
figure(f4)
subplot(2,1,1)
formHistogram(AllMpolData, xLimits, yLimits)
title('Mpol dataset')
subplot(2,1,2)
formHistogram(AllPpolData, xLimits, yLimits)
title('Ppol dataset')
sgtitle(sprintf('Histograms per Polarity - %s', antName))

%% VIVALDI ANGLE SUBSETS

figure(f5)
%Vivaldi Angle 0
Angle = 0;
RET = 7;
yLimitsWhole = [0 7000];
yLimitsSP = [0 3500];


subplot(3,3,1)
subset = gatherSubsets(AllData, measPoints, measAngles, measRETAngles, NormPositions,
frequencyPoints, Angle, RET);
formHistogram(subset, xLimits, yLimitsWhole)
title('Whole dataset Angle 0 RET 7 distribution')

subplot(3,3,2)
subset = gatherSubsets(AllMpolData, measPoints, MpolmeasAngles, MpolRETAngles,
MpolNormPositions, frequencyPoints, Angle, RET);
formHistogram(subset, xLimits, yLimitsSP)
title('Mpol Angle 0 RET 7 distribution')

subplot(3,3,3)
subset = gatherSubsets(AllPpolData, measPoints, PpolmeasAngles, PpolRETAngles,
PpolNormPositions, frequencyPoints, Angle, RET);
formHistogram(subset, xLimits, yLimitsSP)
title('Ppol Angle 0 RET 7 distribution')

% %Vivaldi Angle 45
Angle = 45;
RET = 7;
subplot(3,3,4)
subset = gatherSubsets(AllData, measPoints, measAngles, measRETAngles, NormPositions,
frequencyPoints, Angle, RET);
formHistogram(subset, xLimits, yLimitsWhole)
title('Whole dataset Angle 45 RET 7 distribution')

subplot(3,3,5)
subset = gatherSubsets(AllMpolData, measPoints, MpolmeasAngles, MpolRETAngles,
MpolNormPositions, frequencyPoints, Angle, RET);
formHistogram(subset, xLimits, yLimitsSP)
title('Mpol Angle 45 RET 7 distribution')

subplot(3,3,6)
subset = gatherSubsets(AllPpolData, measPoints, PpolmeasAngles, PpolRETAngles,
PpolNormPositions, frequencyPoints, Angle, RET);
formHistogram(subset, xLimits, yLimitsSP)
title('Ppol Angle 45 RET 7 distribution')

% %Vivaldi Angle 90
Angle = 90;
RET = 7;
subplot(3,3,7)
subset = gatherSubsets(AllData, measPoints, measAngles, measRETAngles, NormPositions,
frequencyPoints, Angle, RET);
formHistogram(subset, xLimits, yLimitsWhole)
title('Whole dataset Angle 90 RET 7 distribution')

subplot(3,3,8)
subset = gatherSubsets(AllMpolData, measPoints, MpolmeasAngles, MpolRETAngles,
MpolNormPositions, frequencyPoints, Angle, RET);
formHistogram(subset, xLimits, yLimitsSP)
title('Mpol Angle 90 RET 7 distribution')
```

```
subplot(3,3,9)
subset = gatherSubsets(AllPpolData, measPoints, PpolmeasAngles, PpolRETAngles,
PpolNormPositions, frequencyPoints, Angle, RET);
formHistogram(subset, xLimits, yLimitsSP)
title('Ppol Angle 90 RET 7 distribution')

sgtitle(sprintf('Whole, Mpol and Ppol distributions per Vivaldi Angle - %s', antName))

%% FREQUENCY SUBSETS

figure(f6)
Angle = '';
RET = 7;
yLimits = [0 2700];
% yLimits = [0 1000];
% Polarity = 'Whole';
% data = AllData;
% angles = measAngles;
% RETs = measRETAngles;

%Mpol Dataset

Polarity = 'Mpol';
data = AllMpolData;
angles = MpolmeasAngles;
RETs = MpolRETAngles;

% %
% fStart = 1000;   %MHz
% fStop = 2000;   %MHz
% fPoints = (frequencyPoints >= fStart*1e6) & (frequencyPoints < (fStop+2)*1e6);  % Upper
limit +2MHz to make sure final point is included (might be at e.g. 2000.3MHz)
% subset = gatherSubsets(data, measPoints, angles, RETs, NormPositions, frequencyPoints,
Angle, RET, '', fPoints);
% subplot(2,3,1)
% formHistogram(subset, xLimits, yLimits)
% title(sprintf('%s dataset %d - %d MHz RET %d distribution', Polarity, fStart, fStop, RET))
%
% %
% fStart = 2002;   %MHz
% fStop = 3000;   %MHz
% fPoints = (frequencyPoints >= fStart*1e6) & (frequencyPoints < (fStop+2)*1e6);
% subset = gatherSubsets(data, measPoints, angles, RETs, NormPositions, frequencyPoints,
Angle, RET, '', fPoints);
% subplot(2,3,2)
% formHistogram(subset, xLimits, yLimits)
% title(sprintf('%s dataset %d - %d MHz RET %d distribution', Polarity, fStart, fStop, RET))
%
% %
% fStart = 3002;   %MHz
% fStop = 4000;   %MHz
% fPoints = (frequencyPoints >= fStart*1e6) & (frequencyPoints < (fStop+2)*1e6);
% subset = gatherSubsets(data, measPoints, angles, RETs, NormPositions, frequencyPoints,
Angle, RET, '', fPoints);
% subplot(2,3,3)
% formHistogram(subset, xLimits, yLimits)
% title(sprintf('%s dataset %d - %d MHz RET %d distribution', Polarity, fStart, fStop, RET))

%
fStart = 3002;   %MHz
fStop = 4000;   %MHz
fPoints = (frequencyPoints >= fStart*1e6) & (frequencyPoints < (fStop+2)*1e6);
subset = gatherSubsets(data, measPoints, angles, RETs, NormPositions, frequencyPoints, Angle,
RET, '', fPoints);
subplot(2,3,1)
formHistogram(subset, xLimits, yLimits)
title(sprintf('%s dataset %d - %d MHz RET %d distribution', Polarity, fStart, fStop, RET))

%
fStart = 4002;   %MHz
fStop = 5000;   %MHz
fPoints = (frequencyPoints >= fStart*1e6) & (frequencyPoints < (fStop+2)*1e6);
subset = gatherSubsets(data, measPoints, angles, RETs, NormPositions, frequencyPoints, Angle,
RET, '', fPoints);
```

```
subplot(2,3,2)
formHistogram(subset, xLimits, yLimits)
title(sprintf('%s dataset %d - %d MHz RET %d distribution', Polarity, fStart, fStop, RET))

%
fStart = 5002;   %MHz
fStop = 6000;   %MHz
fPoints = (frequencyPoints >= fStart*1e6) & (frequencyPoints < (fStop+2)*1e6);
subset = gatherSubsets(data, measPoints, angles, RETs, NormPositions, frequencyPoints, Angle,
RET, '', fPoints);
subplot(2,3,3)
formHistogram(subset, xLimits, yLimits)
title(sprintf('%s dataset %d - %d MHz RET %d distribution', Polarity, fStart, fStop, RET))


% Ppol Dataset

Polarity = 'Ppol';
data = AllPpolData;
angles = PpolmeasAngles;
RETs = PpolRETAngles;

% %
% fStart = 1000;   %MHz
% fStop = 2000;   %MHz
% fPoints = (frequencyPoints >= fStart*1e6) & (frequencyPoints < (fStop+2)*1e6);  % Upper
limit +2MHz to make sure final point is included (might be at e.g. 2000.3MHz)
% subset = gatherSubsets(data, measPoints, angles, RETs, NormPositions, frequencyPoints,
Angle, RET, '', fPoints);
% subplot(2,3,4)
% formHistogram(subset, xLimits, yLimits)
% title(sprintf('%s dataset %d - %d MHz RET %d distribution', Polarity, fStart, fStop, RET))
%
% %
% fStart = 2002;   %MHz
% fStop = 3000;   %MHz
% fPoints = (frequencyPoints >= fStart*1e6) & (frequencyPoints < (fStop+2)*1e6);
% subset = gatherSubsets(data, measPoints, angles, RETs, NormPositions, frequencyPoints,
Angle, RET, '', fPoints);
% subplot(2,3,5)
% formHistogram(subset, xLimits, yLimits)
% title(sprintf('%s dataset %d - %d MHz RET %d distribution', Polarity, fStart, fStop, RET))
%
%
% fStart = 3002;   %MHz
% fStop = 4000;   %MHz
% fPoints = (frequencyPoints >= fStart*1e6) & (frequencyPoints < (fStop+2)*1e6);
% subset = gatherSubsets(data, measPoints, angles, RETs, NormPositions, frequencyPoints,
Angle, RET, '', fPoints);
% subplot(2,3,6)
% formHistogram(subset, xLimits, yLimits)
% title(sprintf('%s dataset %d - %d MHz RET %d distribution', Polarity, fStart, fStop, RET))

%
fStart = 3002;   %MHz
fStop = 4000;   %MHz
fPoints = (frequencyPoints >= fStart*1e6) & (frequencyPoints < (fStop+2)*1e6);
subset = gatherSubsets(data, measPoints, angles, RETs, NormPositions, frequencyPoints, Angle,
RET, '', fPoints);
subplot(2,3,4)
formHistogram(subset, xLimits, yLimits)
title(sprintf('%s dataset %d - %d MHz RET %d distribution', Polarity, fStart, fStop, RET))

%
fStart = 4002;   %MHz
fStop = 5000;   %MHz
fPoints = (frequencyPoints >= fStart*1e6) & (frequencyPoints < (fStop+2)*1e6);
subset = gatherSubsets(data, measPoints, angles, RETs, NormPositions, frequencyPoints, Angle,
RET, '', fPoints);
subplot(2,3,5)
formHistogram(subset, xLimits, yLimits)
title(sprintf('%s dataset %d - %d MHz RET %d distribution', Polarity, fStart, fStop, RET))

%
fStart = 5002;   %MHz
```

```
fStop = 6000;   %MHz
fPoints = (frequencyPoints >= fStart*1e6) & (frequencyPoints < (fStop+2)*1e6);
subset = gatherSubsets(data, measPoints, angles, RETs, NormPositions, frequencyPoints, Angle,
RET, '', fPoints);
subplot(2,3,6)
formHistogram(subset, xLimits, yLimits)
title(sprintf('%s dataset %d - %d MHz RET %d distribution', Polarity, fStart, fStop, RET))



if ~isempty(Angle)
    sgtitle(sprintf('Ppol and Mpol distributions per frequency range at Vivaldi Angle %d -
%s', Angle, antName))
else
    sgtitle(sprintf('Ppol and Mpol distributions per frequency range - %s', antName))
end
%% ELEMENT SUBSETS FOR FREQUENCY SUBSET

figure(f7)

Polarity = 'Whole';
Angle = 0;  % Set to empty '' to include all angles
data = AllData;
angles = measAngles;
RETs = measRETAngles;

fStart = 5002;   %MHz
fStop = 6000;   %MHz

for eIdx = 1:max(size(antennaElements))

    if eIdx > 1
        yLimits = [0 450];
    else
        yLimits = [0 900];  % Lowband element has 2x the datapoints
    end
    efreq = elementFreqs(eIdx,:);
    fPoints = (frequencyPoints >= fStart*1e6) & (frequencyPoints < (fStop+2)*1e6);  % Upper
limit +2MHz to make sure final point is included (might be at e.g. 1518.3MHz)
    subset = gatherSubsets(data, measPoints, angles, RETs, NormPositions, frequencyPoints,
Angle, RET, '', fPoints, eIdx);
    subplot(2,3,eIdx)
    formHistogram(subset, xLimits, yLimits)
    title(sprintf('%s (%d-%d MHz) dataset distribution', antennaElements{eIdx}, efreq(1),
efreq(2)))
    %prevSubset = subset;    %DEBUG

end

if ~isempty(Angle)
    sgtitle(sprintf('Antenna element comparison - RET: %d Vivaldi Angle: %d @ %d - %d MHz -
%s', RET, Angle, fStart, fStop, antName))
else
    sgtitle(sprintf('Antenna element comparison - RET: %d @ %d - %d MHz - %s', RET, fStart,
fStop, antName))
end


%% %%%%%%%%%%%%%%%%%%%%%%%%%%%%%%%%%%%%%%%%%%%%%%%%%%%%%%%%%%%%%%%%%%%%%%%%%%%%%%% %%

%%%%%%%%%%%%%%%%%%%%%%%%%%%%%%%% FUNCTIONS %%%%%%%%%%%%%%%%%%%%%%%%%%%%%%%%


function elePath = GetElePath(rootFolder, Antenna, AntElements, AntFreqs, index)
% Form the filepath to wanted antenna element's measurement results.
    eleFolderName =
strcat(AntElements{index},'_',string(AntFreqs(index,1)),'_',string(AntFreqs(index,2)));
    elePath = strcat(rootFolder,'\',Antenna,'\',eleFolderName);

end

function [MpolFilelist,PpolFilelist] = GetFileList(rootFolder, Antenna, Elements, Frequencies,
index)
% Gather filelists for measurement results of both polarities for one
% element.
```

```
    % Filepath to element of Ant1
    elementPath = GetElePath(rootFolder, Antenna, Elements, Frequencies,index);
    % Get filelist of Mpol result files for antenna element
    MpolFilelist=dir(fullfile(elementPath+'\Mpol', '*.s1p'));
    % Get filelist of Ppol result files for antenna element
    PpolFilelist=dir(fullfile(elementPath+'\Ppol', '*.s1p'));


end

function value = extractValue(Filelist, valPos, index, defaultRET)
% From the name of the ith file in Filelist extract value in position
% valPos.
    fileInfo = split(Filelist(index).name, '_');
    if valPos==3 && contains(fileInfo{valPos},'RET')
        value = str2double(regexp(fileInfo{valPos}, '\d*', 'Match'));
    elseif valPos==3
        value = defaultRET;
    else
        value = str2double(regexp(fileInfo{valPos}, '\d*', 'Match'));
    end

end

function [filePath, Angle, normPosition, RETAngle] = GetMeasInfo(Filelist, eleIndex,
fileIndex, defaultRET, elementPositions, elementLengths)

    e = eleIndex;
    f = fileIndex;
    % Form filepath for current data file
    filePath = fullfile(Filelist{e}(f).folder, '\', Filelist{e}(f).name);
    % Extract test antenna angle and position from data file name
    Angle = extractValue(Filelist{e}, 1, f);
    %MpolmeasAngles{e}(f) = Angle;
    Position = extractValue(Filelist{e}, 2, f);
    %MpolmeasPositions{e}(f) = Position;
    RETAngle = extractValue(Filelist{e}, 3, f, defaultRET);
    %MpolRETAngles{e}(f) = RETAngle;

    % Take into account whether element is in top or bottom half of
    % antenna when calculating normalized test antenna position
    if contains(elementPositions(e), 'Bottom')
        normPosition = (Position-elementLengths(e))/elementLengths(e);
    else
        normPosition = Position/elementLengths(e);
    end
    %MpolNormPositions{e}(f) = normPosition;

end

function elementDataMatrix = getElementData(M, fileID, headerLines, index)
% Extract per element data from the given file.
    % If first file, read frequency column. Otherwise read only S21
    % magnitude. Ignore angle column in both cases.
    if index>1
        C = textscan(fileID, '%*f %f %*f', 'HeaderLines', headerLines, 'CollectOutput', true,
'CommentStyle', '{');
        elementDataMatrix = [M cell2mat(C)];
    else
        C = textscan(fileID, '%f %f %*f', 'HeaderLines', headerLines, 'CollectOutput', true,
'CommentStyle', '{');
        elementDataMatrix = cell2mat(C);
    end

end

function [frequency, maximum] = getMaximum(data,frequencyPoints)
% Find frequency sweep maximum magnitude and the frequency at which it occurs
    % Assuming results are S21 data, maximum isolation is the additive
    % inverse of the minimum S21 value
    [maximum, index] = min(data);
    frequency = frequencyPoints(index);

end
```

```
function [frequency, minimum] = getMinimum(data,frequencyPoints)
% Find frequency sweep minimum magnitude and the frequency at which it occurs
    % Assuming results are S21 data, minimum isolation is the additive
    % inverse of the maximum S21 value
    [minimum, index] = max(data);
    frequency = frequencyPoints(index);

end

function avg = getMean(data)
% Find frequency sweep average magnitude
    % Assuming results are S21 data, average isolation is the additive
    % inverse of the average S21 value
    avg = mean(data);
    %frequency = frequencyPoints(index);

end

function [sortedData,sortedPositions,sortedAngles,sortedRETAngles,sortedFreqs] =
sortData(data, datatype, Positions, Angles, RETAngles, eIndex )
% Sort data by ascending position before plotting
    if contains(datatype, 'Average')
        sortedFreqs = [];
        sortedData = data{eIndex}(:,1);
        [sortedPositions,I] = sort(Positions);

    else
        sortedFreqs = data{eIndex}(:,1);
        sortedData = data{eIndex}(:,2);
        % Sort positions in ascending order and re-arrange other
        % parameters and data accordingly
        [sortedPositions,I] = sort(Positions);
        sortedFreqs = sortedFreqs(I);
    end
    sortedData = sortedData(I);
    sortedAngles = Angles(I);
    sortedRETAngles = RETAngles(I);
end

function [y,ii,line] = formLineData(data, datatype, angles, RETs, markers, lines, colors,
Angle, RET, eIndex, Position, positions)
% Return data for wanted Angle, RET and positions.
    ii=find(angles==Angle);
    kk=find(RETs~=RET);
    ii=setdiff(ii,kk);  % Exclude unwanted RET angles
    if exist('Position','var') && exist('positions','var')
        pp = find(positions~=Position);
        ii = setdiff(ii,pp);    % Exclude unwanted positions (if given)
        %disp(fprintf("pp = %d \nii = %d\n", pp, ii)) %debug
    end
    y = data(ii,1); % Return wanted data points
    % Form plot line and markers as string variables
    if contains(datatype,'Average')
        line = string(markers{eIndex})+string(lines{1})+string(colors{eIndex});
    else
        line = string(markers{eIndex})+string(lines{2})+string(colors{eIndex});
    end

end

function formHistogram(data, xLimits, yLimits)
% Process data and form a histogram
% Texbox will show mean, SD, median, kurtosis, skewness, # of datapoints
% and how % of values above 30dB.

    treshold = 30;
    binWidth = 1;

    mu = mean(data);
    sigma = std(data);
    med = median(data);
    k = kurtosis(data);
    sk = skewness(data);
    dp = size(data);
```

```
    dp = dp(1);
    aboveTrsh = sum(data > treshold)/max(size(data))*100;

    h = histogram(data);
    h.BinWidth = binWidth;
    xline(mu, 'Color', 'b', 'LineWidth', 2);
    xline(mu - sigma, 'Color', 'r', 'LineWidth', 2, 'LineStyle', '--');
    xline(mu + sigma, 'Color', 'r', 'LineWidth', 2, 'LineStyle', '--');
    tBox = sprintf(' Mean = %.3f\n SD = %.3f\n Median = %.3f\n K = %.3f\n Skewness = %.3f\n
Data points = %d\n >%d dB = %.1f %%', mu, sigma,med,k,sk,dp,treshold,aboveTrsh);
    % Limit x and y axis, if limits given as arguments and not empty.
    if exist('xLimits','var') && ~isempty(xLimits)
        xlim(xLimits);
    end
    if exist('yLimits','var') && ~isempty(yLimits)
        ylim(yLimits);
    end
    xL=xlim;
    yL=ylim;
    text(xL(2)*0.69, yL(2)*0.63, tBox, 'Color', 'r', 'Fontweight', 'bold', 'FontSize', 12,
'EdgeColor', 'b');
    grid on
    xlabel('Isolation [dB]')
    ylabel('# of Samples')
    legend('Data','Mean','SD','Location','NorthWest')

end

function dataSubset = extractSubset(datas, measPoints, angles, RETs, Positions, Angle, RET,
Position)
% Return desired subset from data of single antenna elemnt based on given
% Vivaldi angle, CLTA RET, position and frequency

    if exist('Angle','var') && ~isempty(Angle)
        idx=find(angles==Angle);
    else
        fileCount = max(size(datas))/measPoints;
        idx = [1:1:fileCount];
    end
    %disp(aidx) %debug
    if exist('RET','var') && ~isempty(RET)
        Ridx=find(RETs~=RET);
        idx = setdiff(idx,Ridx);
    end
    if exist('Position','var') && ~isempty(Position)
        Pidx=find(Positions~=Position);
        idx = setdiff(idx,Pidx);
    end
    %disp(idx) %debug
    idx = idx*measPoints;
    n = size(idx);
    n = n(2);
    dataSubset = zeros(n*measPoints,1);
    for i=1:n
        startIndex = idx(i)-measPoints+1;
        index = find(dataSubset==0,1,'first');
        dataSubset(index:index+measPoints-1) = datas(startIndex:idx(i));
    end

end

function dataSubsets = gatherSubsets(datas, measPoints, angles, RETs, Positions, freqs, Angle,
RET, Position, freqPoints, elementIdx)
% Collect desired subsets from data of all antenna elements based on given
% Vidaldi angle, CLTA RET and position.

    [eles,pols]=size(angles);
    dataStop = 0;
    dataSubsets = [];

    if exist('elementIdx','var') && ~isempty(elementIdx)
        for p = 1:pols
            for e = 1:(elementIdx-1)
                fileCount = size(angles{e,p});
                fileCount = fileCount(2);
```

```
                dataStop = dataStop + fileCount*measPoints;
                dataStart = dataStop - fileCount*measPoints +1;
            end
        end
        for p = 1:pols
%             for e = 1:(elementIdx-1)
%                 fileCount = size(angles{e,p});
%                 fileCount = fileCount(2);
%                 dataStop = dataStop + fileCount*measPoints;
%                 dataStart = dataStop - fileCount*measPoints +1;
%             end
            e = elementIdx;
            fileCount = size(angles{e,p});
            fileCount = fileCount(2);
            dataStop = dataStop + fileCount*measPoints;
            dataStart = dataStop - fileCount*measPoints +1;
            %disp(dataStart)
            %disp(dataStop)

            %disp(fprintf('Start %d Stop %d fileCount %d', dataStart, dataStop, fileCount))
%debug
            data = datas(dataStart:dataStop);
            if exist('Position','var') && ~isempty(Position)
                dataSubset = extractSubset(data, measPoints, angles{e,p}, RETs{e,p},
Positions{e,p}, Angle, RET, Position);
            else
                dataSubset = extractSubset(data, measPoints, angles{e,p}, RETs{e,p},
Positions{e,p}, Angle, RET);
            end

            if exist('freqPoints','var') && ~isempty(freqPoints)
                subsetSize = max(size(dataSubset))/measPoints;
                freqMask = repmat(freqPoints,subsetSize,1);
                dataSubset = dataSubset(freqMask);

            end

            dataSubsets = [dataSubsets; dataSubset];

        end

    else
        for p = 1:pols

            for e = 1:eles
                fileCount = size(angles{e,p});
                fileCount = fileCount(2);
                dataStop = dataStop + fileCount*measPoints;
                dataStart = dataStop - fileCount*measPoints +1;
                %disp(fprintf('Start %d Stop %d fileCount %d', dataStart, dataStop,
fileCount)) %debug
                data = datas(dataStart:dataStop);
                if exist('Position','var') && ~isempty(Position)
                    dataSubset = extractSubset(data, measPoints, angles{e,p}, RETs{e,p},
Positions{e,p}, Angle, RET, Position);
                else
                    dataSubset = extractSubset(data, measPoints, angles{e,p}, RETs{e,p},
Positions{e,p}, Angle, RET);
                end

                if exist('freqPoints','var') && ~isempty(freqPoints)
                    subsetSize = max(size(dataSubset))/measPoints;
                    freqMask = repmat(freqPoints,subsetSize,1);
                    dataSubset = dataSubset(freqMask);

                end

                dataSubsets = [dataSubsets; dataSubset];

            end

        end
    end
end
```

# Appendix 2 Python script for summing measurement results

```
    # This script handles trace data files (.csv) generated by (legacy) T-Gate
when testing OTA co-location spurious emissions.
    # The purpose of the script is to take two files from the same frequency
sweep but different polarity measurements and sum
    # the powers of the two polarities together. The resulting sum results for
each frequency sweep are then stored in a similarly
    # structured .csv file.

    ### USING THE SCRIPT: ###
    # Names of the folders for different polarities containing the wanted trace
data files should be given as command line arguments.
    # The script should be run in the same folder as these two folders are in.
    # If the two folders are named Pol1 and Pol2, the command line argument
should be for example:

    # py SummingResults.py Pol1 Pol2

    # Remember that easiest way to get the folder names on the cmd line is
starting to type the folder name and pressing Tab to cycle through folders in
the cmd path you are in currently.
    # Results from each file pair having the same frequency range in their file
name will be summed and the maximum sum result for each sweep is printed in cmd
and in a csv file
    # named [Folder1Name]_[Folder2Name]_Results.csv (in the above example:
Pol1_Pol2_Results.csv)

    ### TRACE DATA FILES: ###
    # Names of the T-Gate generated trace data files in each folder are e.g.
698.000_716.000_01032021135539.csv
    # The first two numbers are the frequency range of the sweep in MHz and the
third number is a timestamp.
    # If both folders don't have a file with the same frequency range an error
will be raised and the script is terminated prematurely.
    # Having several files with the same exact frequency range in the folders
should be avoided, as it was assumed there is one file per sweep in each folder
when making this script.

    # Script has been tested on Python 3.9.2

    import sys
    import csv
    import os
    import glob
    import math

    def dBmToWatt(dBmValue):
        #Convert value in dBm to Watts
        watts = (10**(float(dBmValue)/10))/1000
        return watts

    def WattTodBm(wattValue):
        #Convert value in Watts to dBm
        dBm = 10*math.log(1000*float(wattValue),10)
        return dBm

    def dBmSumming(dBmValue1, dBmValue2):
        #Sum two dBm values together by converting them to watts, addition and
converting back to dBm.
        WattSum = dBmToWatt(dBmValue1)+dBmToWatt(dBmValue2)
```

```
        dBmSum = WattTodBm(WattSum)
        return dBmSum

    def is_integer(n):
        #Check if string is a number or not
        try:
            float(n)
        except ValueError:
            return False
        else:
            return True

    def get_CurrentWorkingFolderName():
        #Returns name of current working folder where script is being run.
        folderName = os.path.basename(os.getcwd())
        return folderName

    def get_FileList(folderName):
        #Returns list of .csv files in the given folder in operating folder.
        FilePath = './'+folderName+'*/*.csv'
        FileList = glob.glob(FilePath)
        if FileList == []:
            print("No files found in folder:", folderName)
            quit()
        else:
            return FileList

    def get_Contents(csvFile):
        #Reads first column of csv as frequencies and second as measurement
results
        #Returns list of frequencies and list of measurement results

        Frequencies = []
        Values = []
        csvReader = csv.reader(csvFile)

        for row in csvReader:
            Frequencies.append(row[0])
            Values.append(row[1])
        return Frequencies, Values


    def get_FreqRange(filePath):
        #Return a tuple containing the START and STOP frequencies extracted from
the file name.
            freqRange = filePath.split('\\')[2].split('_')
            #Remove time and date value from list
            freqRange.pop(2)

            return tuple(freqRange)

    def find_xpolFile(freqRange, folderFilelist):
        #Based on given frequency range find matching file in other folder
            for file in folderFilelist:
                if "\\" + freqRange[0] + '_' + freqRange[1] + '_' in file:
                    SecondPolarityFileName = file
            try:
                return SecondPolarityFileName
            except:
                print("Could not find matching files in the two folders for
frequency range:",freqRange[0],'-',freqRange[1])
```

```
                quit()

    def find_maxValue(freqList, valueList):
        #Find maximum value in list and return frequency point and said value
        i = 0
        for value in valueList:
            valueList[i] = float(valueList[i])
            i = i+1
        maxValue = max(valueList)
        maxIndex = valueList.index(maxValue)
        maxFreq = float(freqList[maxIndex])/(10**6)
        return str(maxFreq), str(maxValue)

    def find_xpolValue(frequency, xpolFrequencies, xpolValues, filePath):
        #Find value at given frequency from xpol file
        try:
            freqIndex = xpolFrequencies.index(frequency)
        except:
            Range = getFreqRange(filePath)
            print("Could not find a matching frequencies for maximum in
frequency sweep:", Range[0],'-',Range[1])
        xpolValue = xpolValues[freqIndex]
        return xpolValue

    def make_SummedValues(CoPolFrequencies, xPolFrequencies, CoPolValues,
xPolValues, xpolFileName):
        #For each CoPolValue [dBm] at each CoPolFrequency [Hz] find the
xpolValue [dBm] at corresponding xPolFrequency
        #and return the sum of all the values as a list.
        i=0
        sumValues = []
        for freqPoint in CoPolFrequencies:
            copolValue = CoPolValues[i]
            xpolValue =
find_xpolValue(freqPoint,xPolFrequencies,xPolValues,xpolFileName)
            sumValues.append(dBmSumming(copolValue, xpolValue))
            i=i+1
        return sumValues

    ###MAIN LOOP###

    CurrentFolder = get_CurrentWorkingFolderName()
    Folder1 = sys.argv[1]
    Folder2 = sys.argv[2]

    print('Name for polarity #1 folder:', Folder1)
    print('Name for polarity #2 folder:', Folder2)


    Folder1Filelist = get_FileList(Folder1)
    Folder2Filelist = get_FileList(Folder2)

    Results = []

    #Take all copol files in Folder1 and find their matchin xpol files in
Folder2.
    #Then sum results at same exact frequency points and store in Results array.
    for path in Folder1Filelist:
        #Extract frequency range from file name
        FR = get_FreqRange(path)
        #Skip CSV files with names that aren't in the T-Gate trace data format.
```

```
        if is_integer(FR[0]) and is_integer(FR[1]):
            pass
        else:
            print("Skipping .csv file", path,"where frequency range extraction
from file name resulted in non-integer values:\n", FR)
            print("")
            continue
        #Find the path of the matching xpol file in second folder.
        xpolFileName = find_xpolFile(FR, Folder2Filelist)
        #Gather frequency points and dBm values from copol and xpol files.
        with open(path) as copolTraceData:
            Freq1, Val1 = (get_Contents(copolTraceData))
            Freq1.pop(0)
            Val1.pop(0)
        with open(xpolFileName) as xpolTraceData:
            Freq2, Val2 = (get_Contents(xpolTraceData))
            Freq2.pop(0)
            Val2.pop(0)
        #Sum all values at same frequency points.
        sumValues = make_SummedValues(Freq1, Freq2, Val1, Val2, xpolFileName)
        #Find the maximum sum value and it's frequency point.
        maxFreq, maxSumVal = find_maxValue(Freq1, sumValues)
        print("Maximum power with both polarities summed in frequency
range",FR[0],'-',FR[1], ':')
        print("Frequency point  ||","   Total power")
        print(maxFreq, maxSumVal)
        #Store result with corresponding frequency range FR and frequency point
maxFreq.
        Results.append([FR[0],FR[1],maxSumVal,maxFreq])

    #Print results into CSV file
    filename = CurrentFolder+"_"+Folder1+"_"+Folder2+"_Results.csv"
    with open(filename, mode='w', newline='', encoding='utf-8') as resultsFile:
        resultsWriter = csv.writer(resultsFile, dialect='excel-tab',
delimiter=';', quotechar='"', quoting=csv.QUOTE_MINIMAL)
        header =
['BottomFreq[MHz]','TopFreq[MHz]','MaxSpur[dBm]','MaxSpurFreq[MHz]']
        resultsWriter.writerow(header)
        for row in Results:

            resultsWriter.writerow(row)
```

Appendix 3 Additional isolation measurement results for different Vivaldi angles

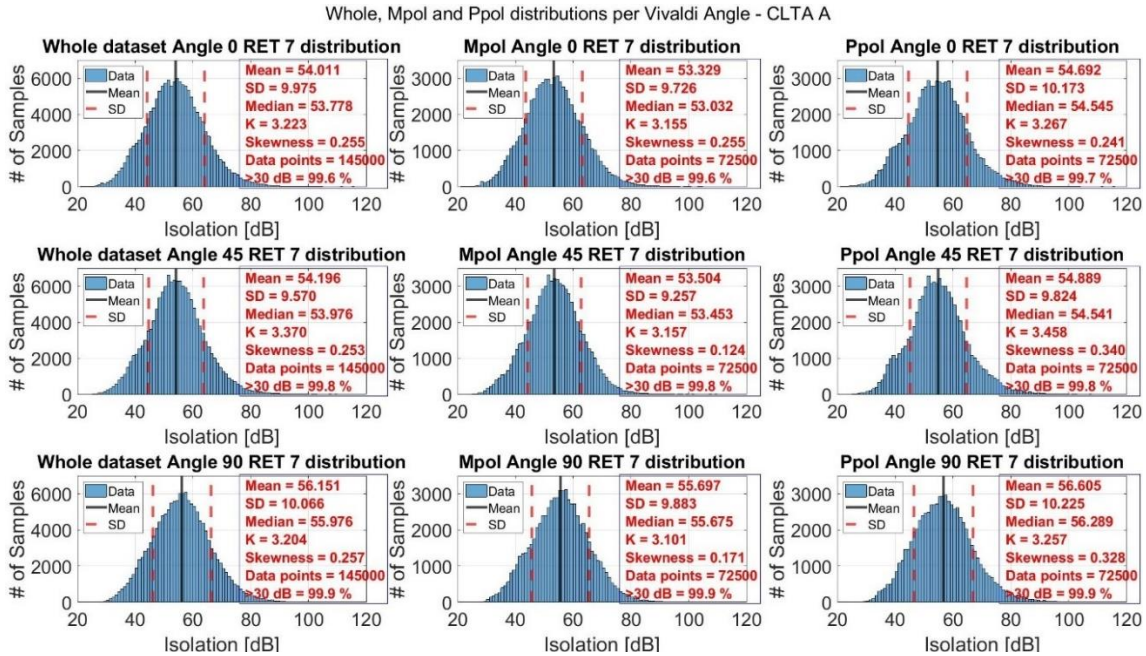


Figure 59. CLTA A histograms for different polarities and Vivaldi rotation angles.

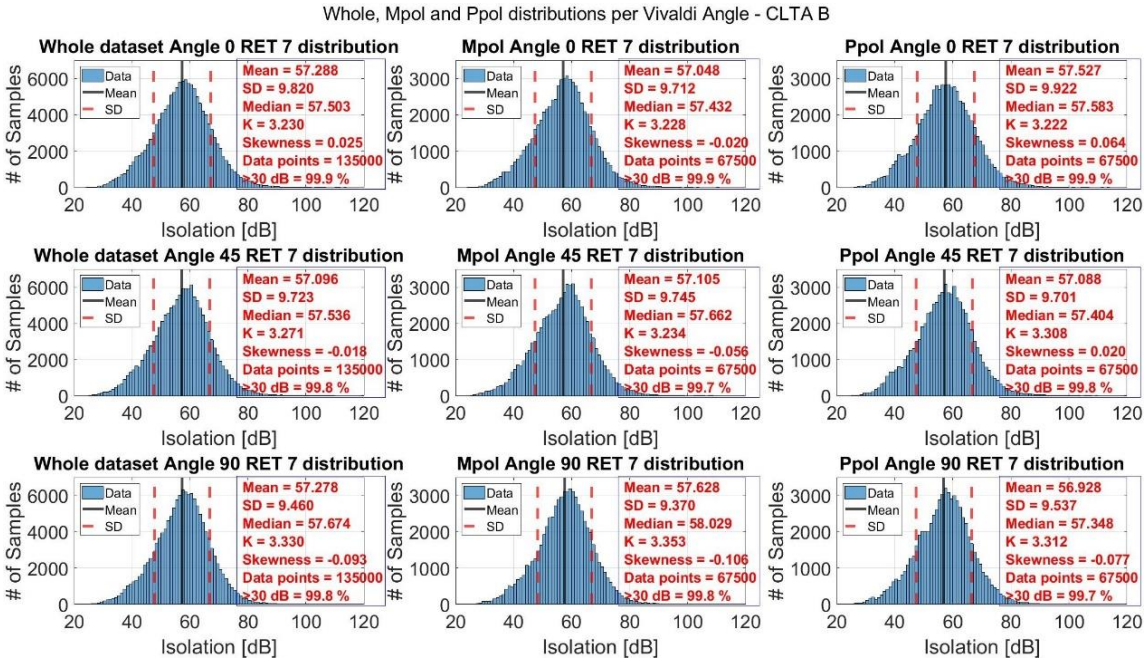


Figure 60. CLTA B histograms for different polarities and Vivaldi rotation angles.

# Appendix 4 Additional isolation measurement results for different frequency subsets

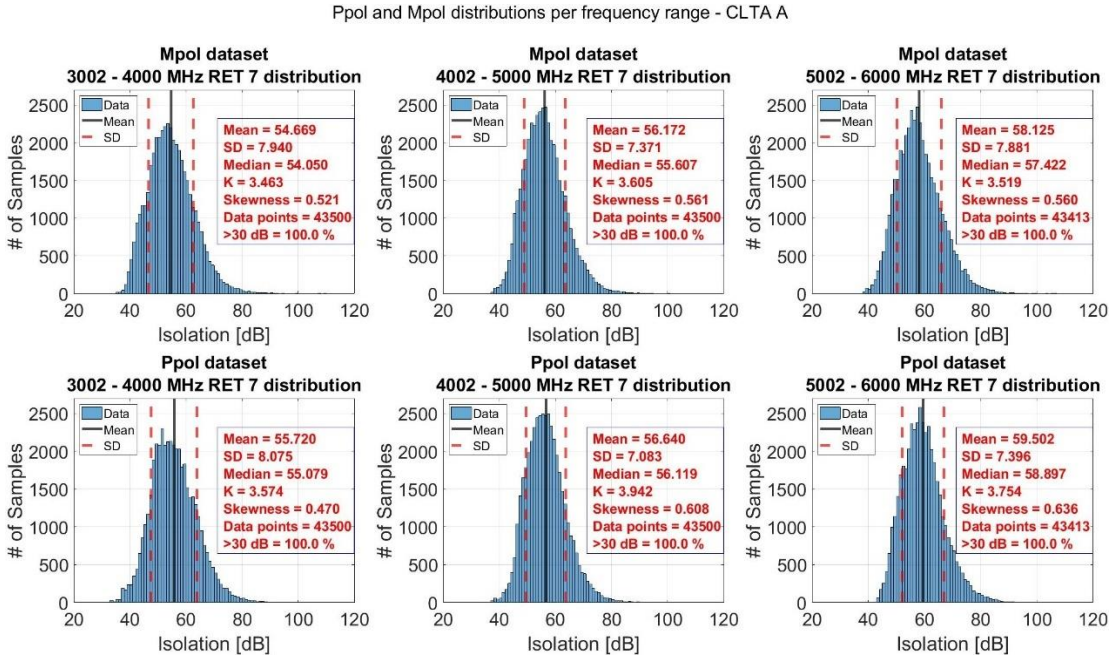


Figure 61. CLTA A above 3 GHz frequency subsets per polarity.

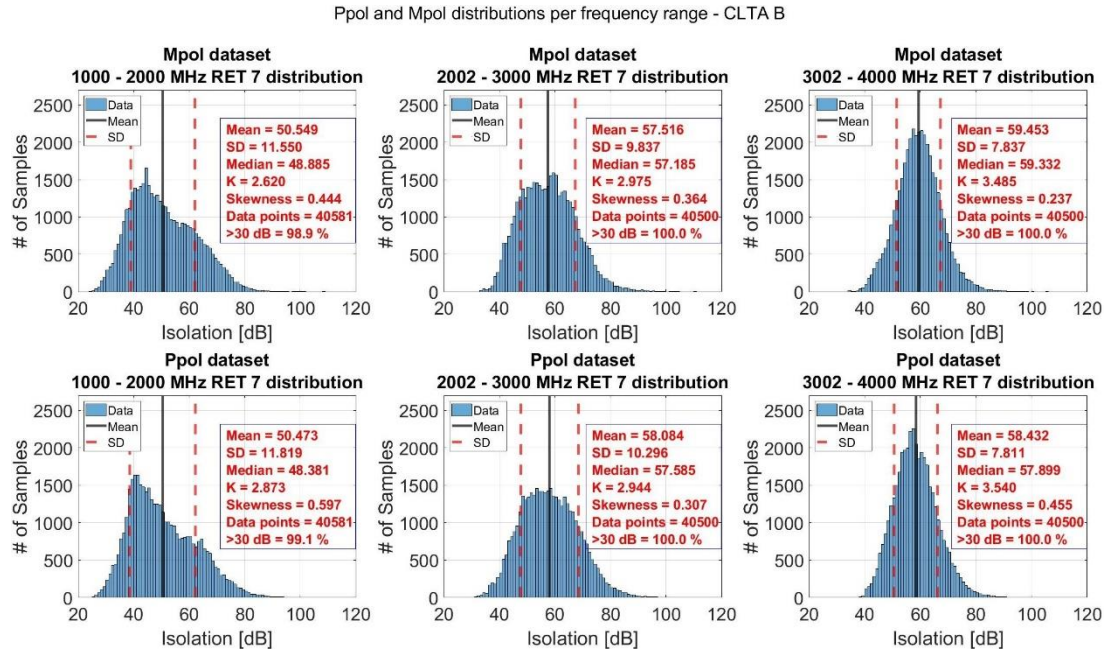


Figure 62. CLTA B below 4 GHz frequency subsets per polarity.

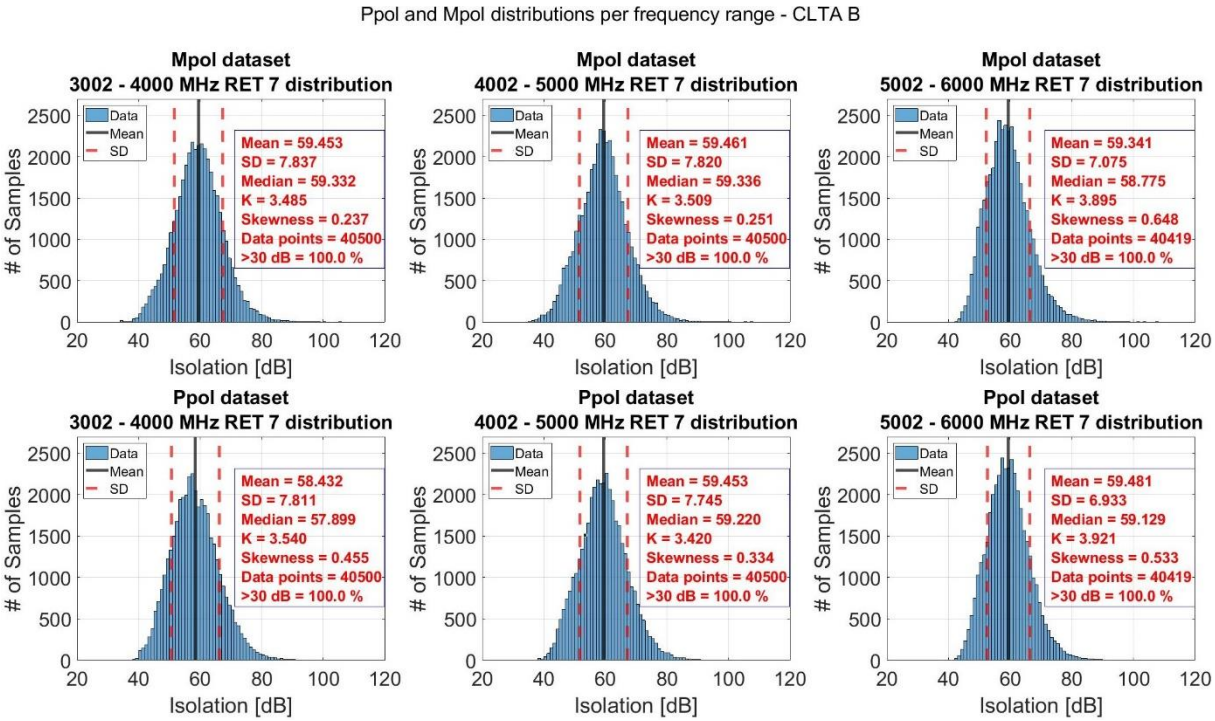


Figure 63. CLTA B above 3 GHz frequency subsets per polarity.

Appendix 5 Additional isolation measurement results per CLTA antenna frequency subset

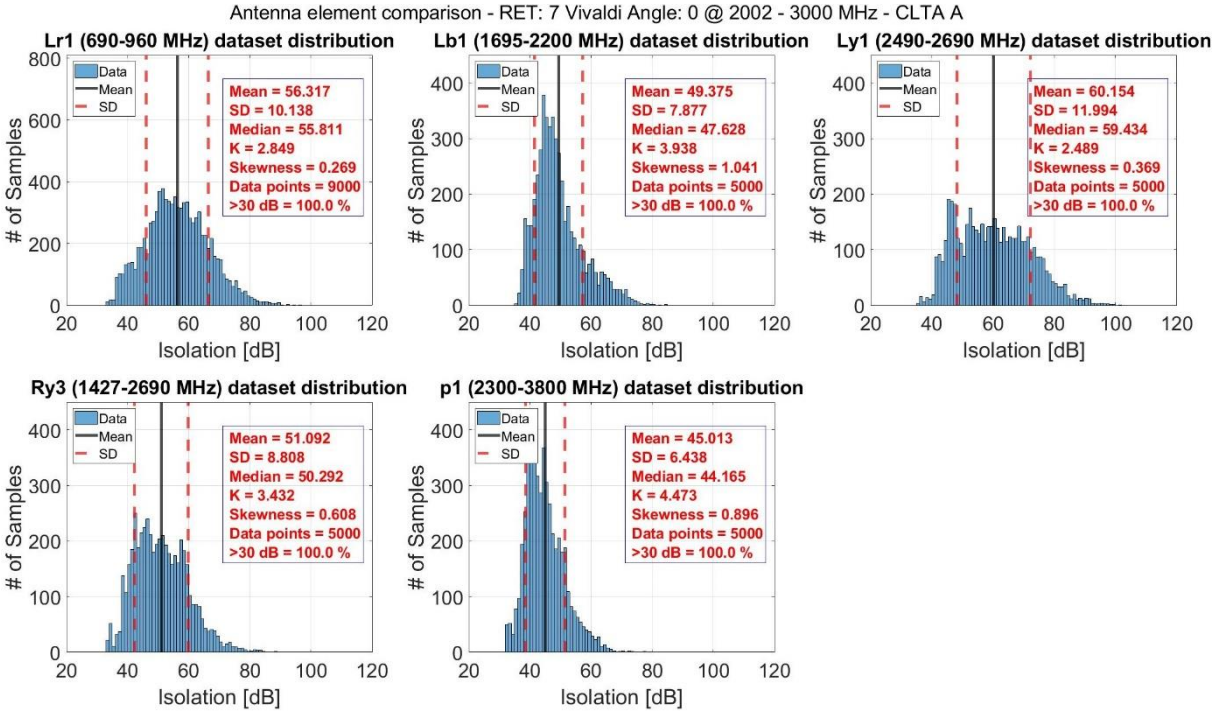


Figure 64. Per antenna isolation histograms for CLTA A at 2002 - 3000 MHz frequency range.

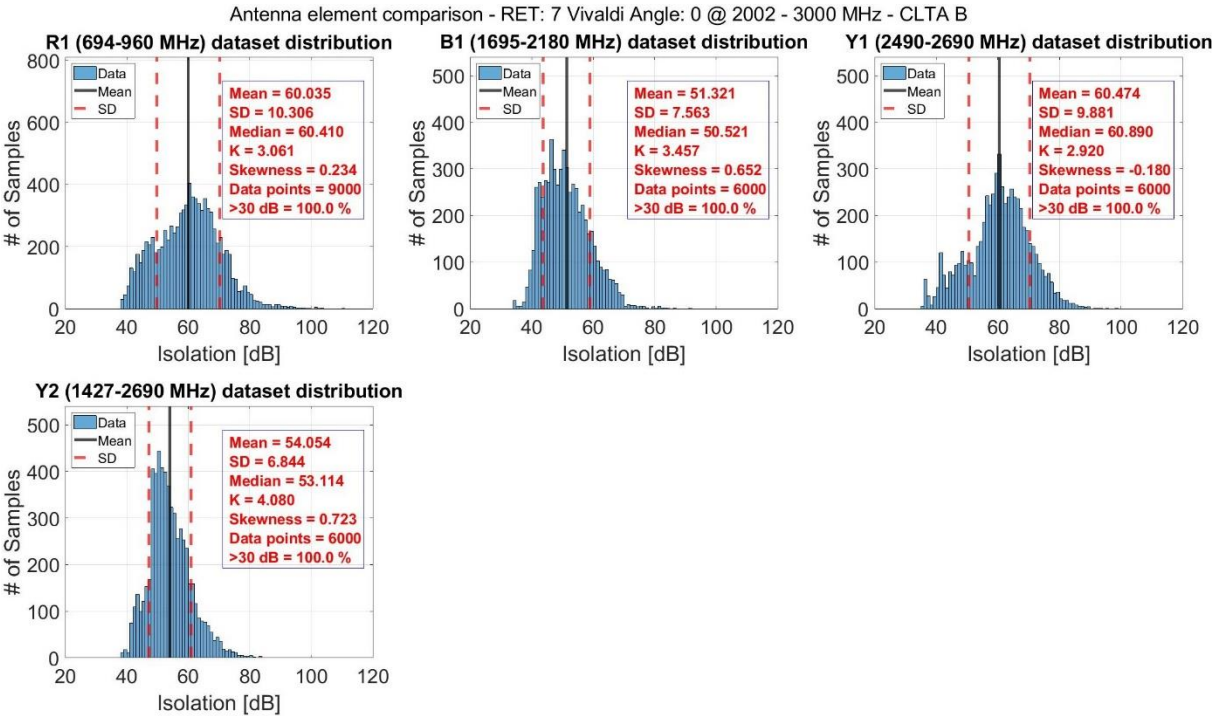


Figure 65. Per antenna isolation histograms for CLTA B at 2002 - 3000 MHz frequency range.